BERICHTE
aus dem Fachbereich Geowissenschaften
der Universität Bremen

No. 181

von Lom-Keil, H.

SEDIMENTARY WAVES ON THE NAMIBIAN CONTINENTAL MARGIN AND IN THE ARGENTINE BASIN - BOTTOM FLOW RECONSTRUCTIONS BASED ON HIGH RESOLUTION ECHOSOUNDER DATA

Berichte, Fachbereich Geowissenschaften, Universität Bremen, No. 181,
126 pages, Bremen 2001

ISSN 0931-0800

Table of Contents

1 Introduction

Bottom currents influence the deposition of particulate matter in many places of the world's oceans. Depending on the strength and direction of the currents, the composition of the settling particles and the already deposited material, the local seafloor topography and the properties of the involved waters, the resulting depositional patterns show a great diversity. Contourites may develop behind the mouths of underwater pathways, where flow velocities quickly decrease after the widening of a passage. Contourites are also typical features beneath boundary currents, which flow along basin margins. Drift deposits, which are several kilometers thick, occur in the Argentine basin and are thought to develop in the center of gyral circulation (e.g. *Kennett*, 1982). Their location may probably be related to the basement or sea floor topography. On smaller scales, deep water obstacles as seamounts frequently produce fluctuations in the velocity field of the surrounding flow, which cause spatial variations in the local accumulation rates. Sedimentary waves or mudwaves are another common current related bedform, which occurs in regions with long term stationary bottom flow as the sediment drifts in the deep basins (e.g. *Klaus and Ledbetter*, 1988), but also at locations where short flow events play a significant role in deposition, e.g. on levees of submarine canyons (e.g. *Normark* et al., 1980).

1.1 Palaeoflow reconstruction – a short outline of methods

To reconstruct deep-sea bottom flows, several methods have been established. Most of them have in common that sediment material, retrieved in isolated sediment cores, is analyzed for specific parameters. Depending on the type of the proxies, estimates of large scale flow patterns and water mass distributions can be made. Direct and to some extent quantitative statements on the local bottom flow are usually not possible with this approach. Such quantitative estimates would be, however, valuable information to understand the reaction of the deep oceans on climatic changes. They may also provide useful boundary information for ocean circulation models.

For the modern ocean, oceanography provides several methods of direct flow measurements, ranging from satellite altimetry to moored current meters and free floating buoys. Recently, also new chemical tracers as CFCs (chlorofluorocarbon) could be used to track the spreading of deep water masses (e.g. *Orsi et al.*, 1999). Bottom photographs,

which document small scaled current related features on the seafloor as ripples are another tool to obtain clues on modern bottom flow patterns (e.g. *Flood and Shor*, 1988).

An indirect method of flow measurement, which is widely accepted, is the analysis of grain size distributions in deposited material (e.g. *Ledbetter*, 1993, *McCave et al.*, 1995). This method is based on the assumption that the settling of particles on the seafloor is influenced by the bottom flow. Fine grained material will be easier transported by the bottom flow than coarse particles and therefore sediments under the influence of strong bottom currents will tend to be coarser than sediments deposited in absence of bottom flows. However, this approach has some drawbacks, which require a careful investigation of the samples and impedes the interpretation. Settling and adhesion of particles on the seafloor not only depends on the grain size, but also on the grain shape. Additionally, particles often settle as small conglomerates, which may break up into individual grains after deposition. Often the source function of the deposited material is poorly known and changes in the sediment composition at the source may appear as changes in the flow velocity on the seafloor. To cope with these problems, the grain size analysis usually is restricted to a well defined subset of the particulate matter, as for example the terrigenous silt fraction (e.g. *Ledbetter*, 1993). Carefully applied, the grain size analysis provides a method not only for reconstruction of modern bottom flow patterns, but also for estimations of the palaeoflow history at selected sites and therefore is a very valuable palaeoceanographic tool.

In this study, a physical approach for the interpretation of current related bedforms is presented. As mentioned above, bottom currents not only influence the composition of the deposited material, but also the bedforms of sedimentary layers. These bedforms and especially their internal structure and associated changes can be analyzed with the help of acoustic methods of appropriate signal frequencies. Acoustic methods allow the study of current related bedforms over large areas and therefore provide information for a complete picture of the bottom flow pattern at a specific site. Suitable models may then be used to quantitatively estimate flow intensities and directions.

1.2 Sedimentary waves and models

A special and very famous form of current related deposition patterns are sedimentary waves. Sedimentary waves are sinusoidal bedforms, which are observed at many places of the world. The known sizes of waves vary from 150 m height and 10 km length to a few

meters height and some 100 m length. Sedimentary waves exist in regions, where bottom flow patterns are stable over long time scales, as on the flanks of the drift deposits in the Argentine Basin, but also in regions, where bottom flow is thought to be superimposed by pulsed short termed events, as on the levees of submarine channels. Their pronounced regularity in space and time makes sedimentary waves appropriate candidates for modeling.

The first model, which proposed the existence of internal waves in a stratified fluid, which passes over a sinusoidal topography, was the lee-wave model of *Flood* (1988). He assumed a mean flow with a given stratification perpendicular to the wave crest and showed that this flow causes sinusoidal perturbations in the velocity field behind the crest, which in turn results in a preferential deposition of particles at specific positions on the wave. Thereby the growth and in particular the migration of sedimentary waves could be explained. However, wave migration perpendicular to the bottom flow, at least perpendicular to the modern flow, is usually not observed. In contrast, waves appear to migrate at arbitrary angles to the prevailing flow direction. To consider this discrepancy, *Blumsack and Weatherly* (1989) proposed an extension to existing theory, which introduced a time variable flow component parallel to the wave crest. Thereby they could explain a wave orientation and migration at specific angles to the flow direction. Especially the wave migration, observed at several sites on the flanks of the Zapiola Drift, could now be handled. The most recent generalization of sedimentary wave theory was put forward by *Hopfauf and Spieß* (2000). Their model takes into account the full, three-dimensional Coriolis vector, which was used as a scalar in earlier models. This allows the consideration of the absolute orientation of the waves and the bottom flow and therefore represents the most complete discussion of mudwave growth and development up to now.

1.3 Sedimentary waves, bottom flow and SFB 261 cruises

During the German long term research project SFB 261 – *Der Südatlantik: Rekonstruktion von Stoffhaushalt und Stromsystemen* several cruises were carried out in the south-eastern Atlantic, where coastal upwelling and the influence of the cold Benguela Current regime reign the near-surface oceanography. Past changes in both systems, which may be induced by climatic changes, are documented in the deposited material. First time during R/V METEOR Cruise M20/2 (*Schulz et al.*, 1992) and later during R/V SONNE Cruise So86 (*Bleil et al.*, 1993), a region of small scaled sinusoidal structures on the

seafloor was observed with the shipboard narrow beam subbottom profiler Parasound on the Namibian continental margin. The available net of high resolution echosounder data was considerably extended during METEOR Cruises M34/1 (*Bleil et al.*, 1996) and M34/2 (*Schulz et al.*, 1996) and these spatial data sets confirmed the initial idea that the observed sinusoidal features could really be extremely small scaled sedimentary waves, maintained by a deep-sea contour current. Sedimentary waves, however, are not the only indications for the presence of a steady deep water flow. Parasound data and also high resolution seismic data collected during Cruise M34/1 (*Bleil et al.*,1996) showed large scale variations in accumulation rates in this region.

As the observed structures are quite small with wave heights of only 5 to 8 m at wave lengths of 300 to 700 m, the first part of this work deals with a careful investigation of the acoustic data. A combination of Parasound echosounder data and Hydrosweep swath sonar data is used to discuss the origin of the observed structures and their relation to an inferred contour current along the continental margin. Additionally, a first effort is made to apply the model of *Hopfauf and Spieß* (2000) to the study area.

In the second part, internal changes of the wave geometry in combination with fluctuations in lateral variations of the accumulation rates are then studied in a combined approach to derive information on the palaeoflow history of the bottom flow at the Namibian continental margin. A seismic line, which was recorded along the crest of the Walvis Ridge provides information on the onset of sedimentary waves growth. A stratigraphic frame, established with the help of DSDP and ODP sites, is linked with the interpretation of model results and used to propose a quantitative estimation of palaeoflow history of the last 5 my.

In 1994 and 2000, R/V METEOR cruises M29/1 (*Segl et al.*, 1994) and M46/3 (*Bleil et al.*, 2000) of the SFB 261 to the south-western Atlantic provided a dense net of Parasound data on the western flank of the Zapiola Drift complex. The Zapiola Drift is known to be covered by the biggest sedimentary waves of the world. Origin and maintenance of the waves have been attributed to a cyclonic bottom flow pattern, which is centered around the drift. This gyre was first described by *Flood and Shor* (1988) after an analysis of bottom photographs in the region. Recent CFC-tracer studies seem to confirm this pattern. However, the history of this flow is poorly known.

The third part of this study presents a detailed analysis of the structure of the sedimentary waves and the implications on the bottom flow on the western Zapiola Drift flank. As already shown for the Namibian continental margin, variations in lateral

accumulation rates here are a secondary indicator for the flow activity. Model results are used to infer the flow direction and strength and a palaeoflow history is proposed for the last 100 ky.

The used mudwave model was developed by *Hopfauf and Spieß* (2000) in parallel to this work. The model results, provided by V. Hopfauf for the boundary conditions, which were determined from the acoustic data, were carefully interpreted and served as an important tool for the quantification of estimates of bottom circulation intensities. The manuscript of *Hopfauf and Spieß* (2000), as accepted by Deep-Sea Research, is attached as an appendix for reference

1.4 A short note on timing

This work was closely coupled to the parallel development of a revised mudwave model (*Hopfauf and Spieß*, 2000). Therefore publication of individual papers of this study had to be postponed until the final acceptance and publication of the model, which was not before November 2000. A publication of parts of this study is planned and the structure and layout of the work reflects these plans..

2 Small scaled sedimentary waves on the Namibian continental slope - Evidence of stationary contour current activity

H. v. Lom, V. Spieß and V. Hopfauf

2.1 Abstract

Narrow beam echosounding data reveals small sinusoidal sedimentary structures on the Namibian continental slope. The structures are restricted to a water depth ranging from 1200 to 1800 meters and show a conspicuous regularity over an extent of 250 km along slope. Their size is varying in length from 250 to 700 m and in height from 5 to 8 m. The geometry of the structures and their location southward of the junction of Walvis Ridge and Namibian continental margin suggest that they are sedimentary waves, formed and maintained by an eastern, southward oriented contour current. Application of an inverse model allows a quantitative estimate of the mean current velocity.

2.2 Introduction

During several cruises of German research vessels to the South Atlantic Ocean, conducted as part of the University of Bremen special research project SFB 261 and as pre-site survey for Ocean Drilling Program (ODP) Leg 175, small scaled sinusoidal structures were observed with the narrow beam sediment echosounder Parasound off the Namibian coast. The structures are situated south of the Walvis Ridge along the South West African continental margin in a water depth of 1200 - 1800 meters (Fig. 2.1). Their wavelengths range from 250 - 700 meters, their heights vary between 5 and 8 meters.

Bremner (1981) already mentioned these structures and proposed to interpret them as a series of parallel troughs formed by downslope-sliding of sediment in a highly fluidized state. On the basis of a dense net of profiles with digitally recorded, high-resolution echosounder data (*Spieß*, 1993) and a precise knowledge of the local bathymetry we now propose to interpret these structures as small scaled sedimentary waves, formed by a contour current.

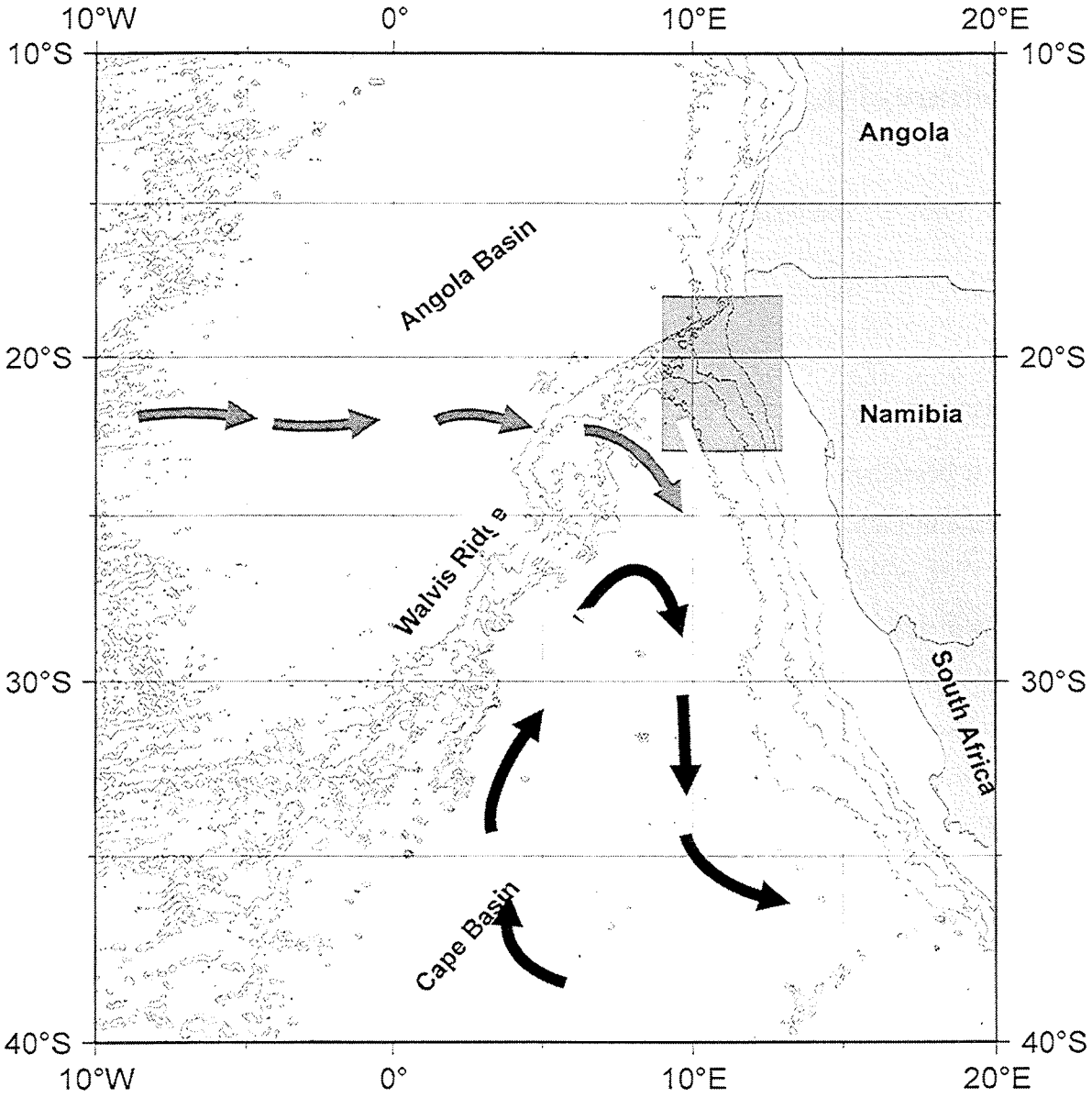

Figure 2.1: Location of the study area on the junction of Walvis Ridge and Namibian continental margin. Isobaths are given in 1000 m intervals after *Smith and Sandwell* (1997). The shaded arrows represent the deep water flow directions as proposed by *Reid* (1989, 1996, ↑) for the AAIW and UCDW, by *Speer et al.* (1995, ↑) for the Namib Col Current and by *Nelson* (1989, ↑) for the deep Cape Basin circulation.

2.2.1 Setting

The Walvis Ridge divides the eastern South Atlantic Ocean into the northern Angola Basin and the southern Cape Basin (Fig. 2.1). To the north the continental margin is characterized by a rough topography with steep slopes and incisions. In contrast, the continental margin south of the Walvis Ridge has smooth slopes with well stratified sediments. The sediments mainly consist of pelagic biogenic material mixed with biogenic particle influx related to upwelling processes. Upwelling occurs all along the southwestern African coast. The associated increase in biological production is basically restricted to the inner shelf and shelf edge (*Summerhayes*, 1983). Terrigenous input is low. Sources of mainly clay and silt input are the river load of the Orange river, distributed to the north by the Benguela Current, and dust input from the Namib desert (*Bornhold*, 1973, *Bremner*, 1975, *Diester-Haass* et al., 1992).

2.2.2 Oceanography

In his detailed description of Atlantic circulation patterns *Reid* (1989) distinguished six major deep water masses in the South Atlantic. The Antarctic Bottom Water (AABW), represented in the South Atlantic by the Weddel Sea Deep Water (WSDW), is the most dense water and fills the deep parts of all basins up to a water depth of 3800 - 4300 m. It is superimposed by the Lower Circumpolar Deep Water (LCDW), ranging from 3000 – 4000 m, the North Atlantic Deep Water (NADW), filling 1000 – 3500 m , and the Upper Circumpolar Deep Water (UCDW) at 1000 – 1500 m. The Circumpolar Water, which is the origin for UCDW and LCDW, covers a wide range of densities in the Southern Ocean part of which is also owned by the NADW. Hence the Circumpolar Water is split into an upper and lower part by the NADW. As shallower deep water masses *Reid* (1989) identifies the Antarctic Intermediate Water (AAIW), in depths of 700 - 1100 m, and above between the AAIW and the thermocline the South Atlantic Central Water (SACW).

The dominant surface water current is the cold Benguela Current, flowing in north-west direction along the South African coast and turning west at 20° S (e.g. *Hart and Currie* ,1960, *Stramma and Peterson*, 1989). Between 15° S and 20° S the Benguela Current converges with the southward flowing tropical Angola Current (*Moroshkin et al.*, 1970).

The knowledge about distribution and transport of deep water masses in the South Atlantic Ocean is mainly based upon the early work of *Wüst and Defant* (1936) and several oceanographic transects recently performed during the South Atlantic Ventilation

Experiment (SAVE, 1987 – 1989) and the World Ocean Circulation Experiment (WOCE, 1991 – 1997). For the eastern boundary of the South Atlantic a southward transport of all water below 400 m was derived (*Reid*, 1989, *Reid*, 1996, *Speer et al.*, 1995, *Roether and Putzka*, 1996). These water masses here are the eastern branch of the southward spreading NADW and an eastern backflow of southern deep water (AAIW and UCDW), which is spreading northward at the western South Atlantic boundary and partly turning to the east in subtropical latitudes (Fig. 2.1). A significant contribution is provided by the Namib Col Current (*Speer et al.*, 1995), which crosses the central South Atlantic in depths of 1300 – 3000 m from west to east at 20° S and joins the southward current at the African continental margin just north of the Walvis Ridge. The southward transport of deep water reaches as far south as 25 – 27° S where it turns into northwesterly direction and follows the anticyclonic gyre described by *Reid* (1989) across the Atlantic.

2.3 Methods and Processing

Two different echosounding systems were used for the studies presented here. The narrow beam echosounding system Parasound (*Grant and Schreiber*, 1990) provides a high resolution data set which was digitally recorded with the ParaDigMA System (*Spieß*, 1993). The system is operated at a signal frequency of 4 kHz and has an aperture of only 4° (3 dB points) which results in a footprint size of the system on the sea floor of only ~7% of the water depth. Hence Parasound combines the properties of a conventional 3.5 kHz echosounder in signal penetration with an increased lateral resolution. Furthermore the bandwidth of the echosounder signals are broad resulting also in enhanced vertical resolution. To study the local sea floor topography, the swath sonar system Hydrosweep (*Grant and Schreiber*, 1990) was used. Hydrosweep works with a signal frequency of 15.5 kHz and a swath width of 90°. The swath is divided by beam forming into 59 beams of 2.5° aperture each. Both echosounder systems are heave, roll and pitch corrected to ensure a horizontal reference plane and a vertical sound emission.

Parasound data were bandpass filtered from 2 – 6 kHz to suppress low frequency acoustic and high frequency electronic noise. The data were not migrated, which would have been difficult because of non-equidistant shot-spacing and lateral aliasing problems occurring at the larger data gaps. However the extent of diffraction hyperbolae is limited in the profiles analyzed, due to the narrow beam and the small footprint size.

Processing of Hydrosweep data was carried out using the software packages Multibeam (MB) (*Caress and Chayes*, 1996) and GMT (*Wessel and Smith*, 1995). Similar to the processing steps described by *Caress and Chayes* (1996), the data were manually edited to eliminate erroneous values. Subsequently a beam dependent depth correction was applied to remove systematic shifts in depth across the swath, which are known to be system inherent.

Small scaled topographic features could be further enhanced in bathymetric data by consideration of its directional derivative distribution. The directional derivatives of the topography relative to a given azimuth were calculated and displayed using light shades of gray for negative and dark shades of gray for positive gradients, respectively. This is a standard processing option of MB used to 'illuminate' the bathymetry. Plotting only the calculated directional derivatives can reveal very small topographic features.

Where quality and resolution of the swath data was sufficient, it was used to determine the strike direction of the identified linear features directly from bathymetry. At other locations the apparent wavelength observed at cross sections of Parasound profiles was used for this purpose.

For comparison, oceanographic data of a mooring site equipped with a direct current meter were also used, although this current meter was situated at some distance to the study area at 20° 02' S, 09° 09' E in a water depth of 1670 m (see Figure 2.2, WR3U). Processing of this data was limited to a constant shift correction of measured current speed.

2.4 Sedimentary waves

Sedimentary waves, often also referred to as mudwaves, are sinusoidal sedimentary structures, which develop under the influence of bottom current activity on longer time scales. They have been observed in many places of the world oceans, where bottom currents play an important role in the depositional environment. The largest known sediment waves exist at the flanks of the great sediment drifts of the Argentine Basin where heights of up to 150 m and wavelengths of up to 10 kilometers are reached (e.g. *Fox et al.*, 1968, *Flood and Shor*, 1988; *Manley and Flood*, 1993b). Prominent wave fields also occur in regions of contour currents (e.g. *Jacobi et al.*, 1975, *Lonsdale*, 1983). Small and spatially limited waves are often found in the vicinity of channel levee systems (*Damuth*, 1979; *Normark* et al., 1980) and close to current obstacles as seamounts. The

known scale of sediment waves ranges in height from several meters to 150 meters and in wavelength from several hundred to 10000 meters. However, the lower limit of this interval may be determined by the lateral resolution properties of the seismic system used for profiling.

Sedimentary waves are characterized by a distinct internal layering, as for hemipelagic sedimentary sequences. This property distinguishes them from topographically similar bedforms which may be produced by gravitationally induced sediment transport as debris or fluid flows. Different sedimentation rates on both wave flanks may occur, provoking lateral movement of the wave crests with time. Upstream (*Lonsdale*, 1983, *Embley et al.*, 1981) as well as downstream migrating waves (*Roberts and Kidd*, 1979) have been observed.

2.5 Data

The study area is shown in detail in Figure 2.2, where the extent of the observed mudwave field is indicated in gray. The wave field reaches from 19° 30' S to 22° S along the Namibian continental slope. It covers a depth range of 1200 m to 1650 m in the northern part of the study area with a slowly increasing average depth towards the south, reaching a depth range of 1300 to 1800 m. Thick lines indicate the existing Parasound and Hydrosweep profiles in this area. The observed wave field was well covered by the survey data. Two small, detailed echosounder surveys were performed in the northern and in the southern part of the study area.

In the northern part of the study area smooth slopes prevail with several intermittent elevations, whereas in the south the slope gradually steepens. The slope inclination seems to have no influence on the extent and character of the wave field, but apparently bathymetry controls the upper and lower limits of the field. The shallow limit is given by the 1200 m isobath on the Walvis Ridge, descending to 1300 m at 22° S. The deep limit follows the 1650 m isobath on Walvis Ridge down to 1800 m at 22° S. In the north the field is confined by the central elevation of the Walvis Ridge, in the south the wave field ends at 22° S without any topographic peculiarity.

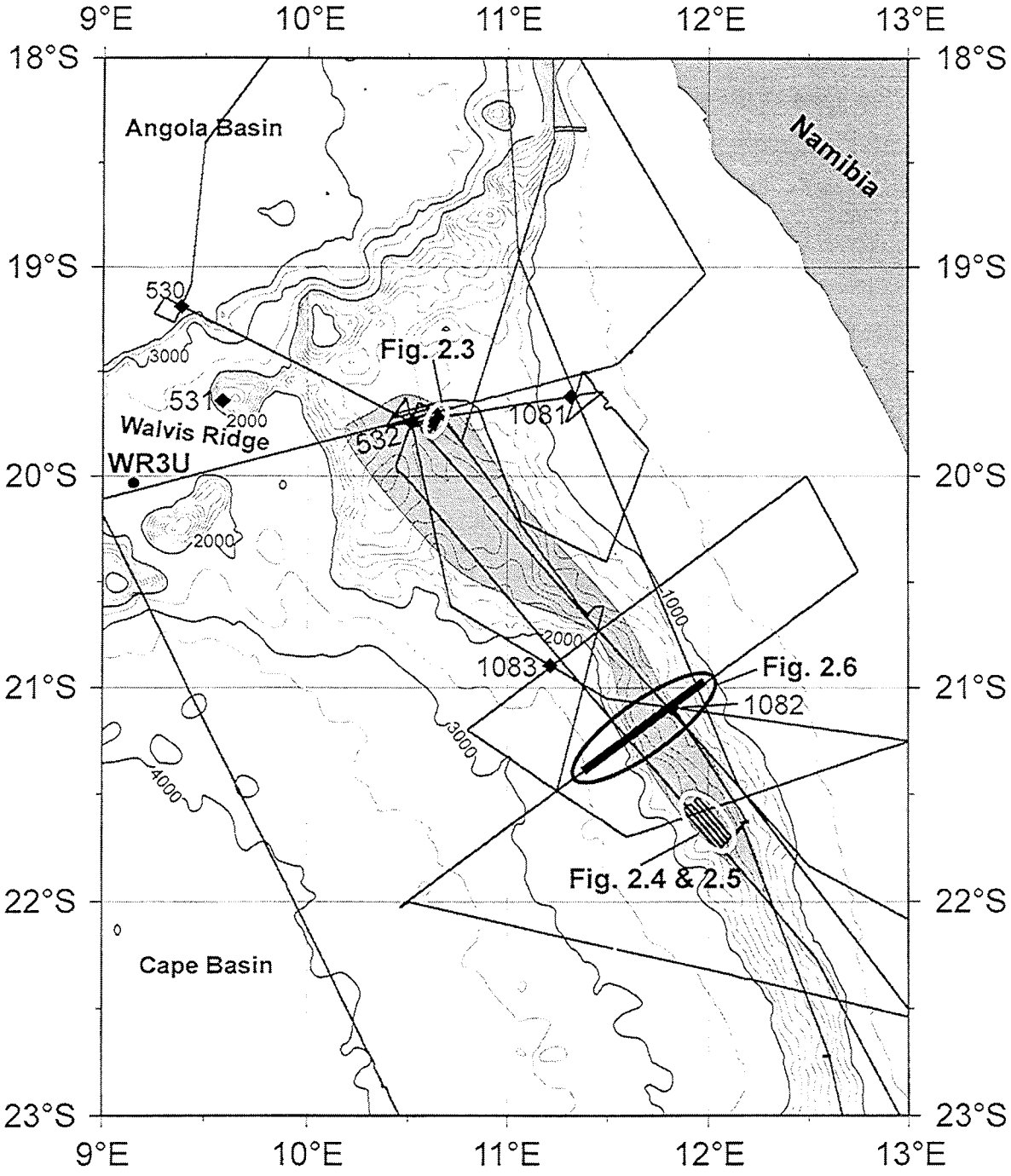

Figure 2.2: Map of the study area. The locations of presented Parasound and Hydrosweep sections are emphasized by small ellipsoids and named accordingly. Existing DSDP and ODP Sites are also given. Isobath spacing is 500 m, but us reduced to 100 m in the depth range from 1000 to 2000 m.

2.5.1 Echosounder data

Figure 2.3 shows a short Parasound profile recorded at 10°38'E, 19°45'S in SW - NE direction on a smoothly ascending slope (0.35°). Regularly spaced sinusoidal structures can be recognized with wavelengths between 250 and 750 meters and wave heights of 5 to 8 meters. Apart from their sinusoidal topography, the sediments show a well stratified internal layering with distinct reflectors. The structures can be traced down to the total signal penetration depth of ~75 meters below sea floor (mbsf). However, changes in wavelength with depth occur at several levels. Two acoustically diffuse zones at ~10 and ~18 mbsf separate the deeper mud waves with wavelengths not exceeding 300 meters from two overlying sedimentary units, where wavelengths of 600 – 750 meters prevail.

The same wave geometry was found all over the study area with conspicuous regularity, but with a predominance of shorter wavelengths (300 to 600 meters) in the south. No dependency of the wave geometry , i.e. wavelength and height, from slope inclination was found. Additionally, comparison of parallel strike lines along the slope in the southern study area show no variation of wave geometry with depth (Fig. 2.4). A difference in the acoustic patterns, however, results from significantly higher sedimentation rates south of the Walvis Ridge (*Giraudeau et al.*,1998). A change of the wave parameters with depth cannot be recognized, but it must be noted that the signal penetration depth is limited to ~30 mbsf.

The Hydrosweep data (Fig. 2.5), corresponding to Profile 4 in Figure 2.4, show linear elongated patterns with a strike direction of 55° azimuth, oriented perpendicular to the slope. As described above the directional derivatives calculated relative to 325° azimuth are displayed in shades of gray. Note, that no bathymetric information is shown in this figure, and the direction of maximum slope angle is therefore given by an arrow. As the calculation simulates illumination from the north-west, light shades of gray represent areas 'facing' to north-west whereas dark shades of gray are oriented to the south-east. Changes from light to dark correspond to wave crests, as indicated.

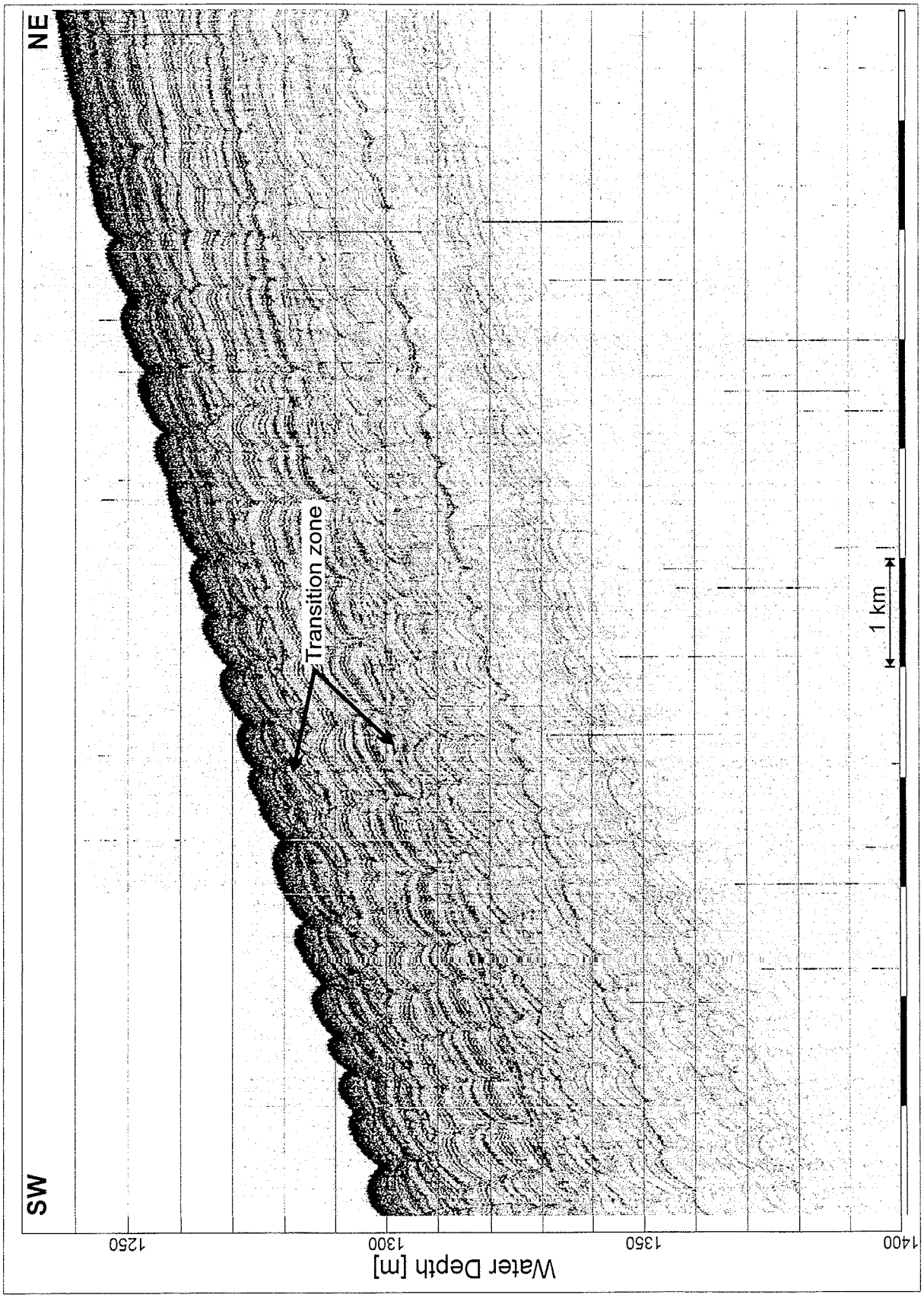

Figure 2.3: Parasound section from the northern part of the study area. Amplitudes are color coded to 256 shades of gray. Water depth is calculated assuming a sound velocity of 1500 m/s. Vertical exaggeration 1:65.

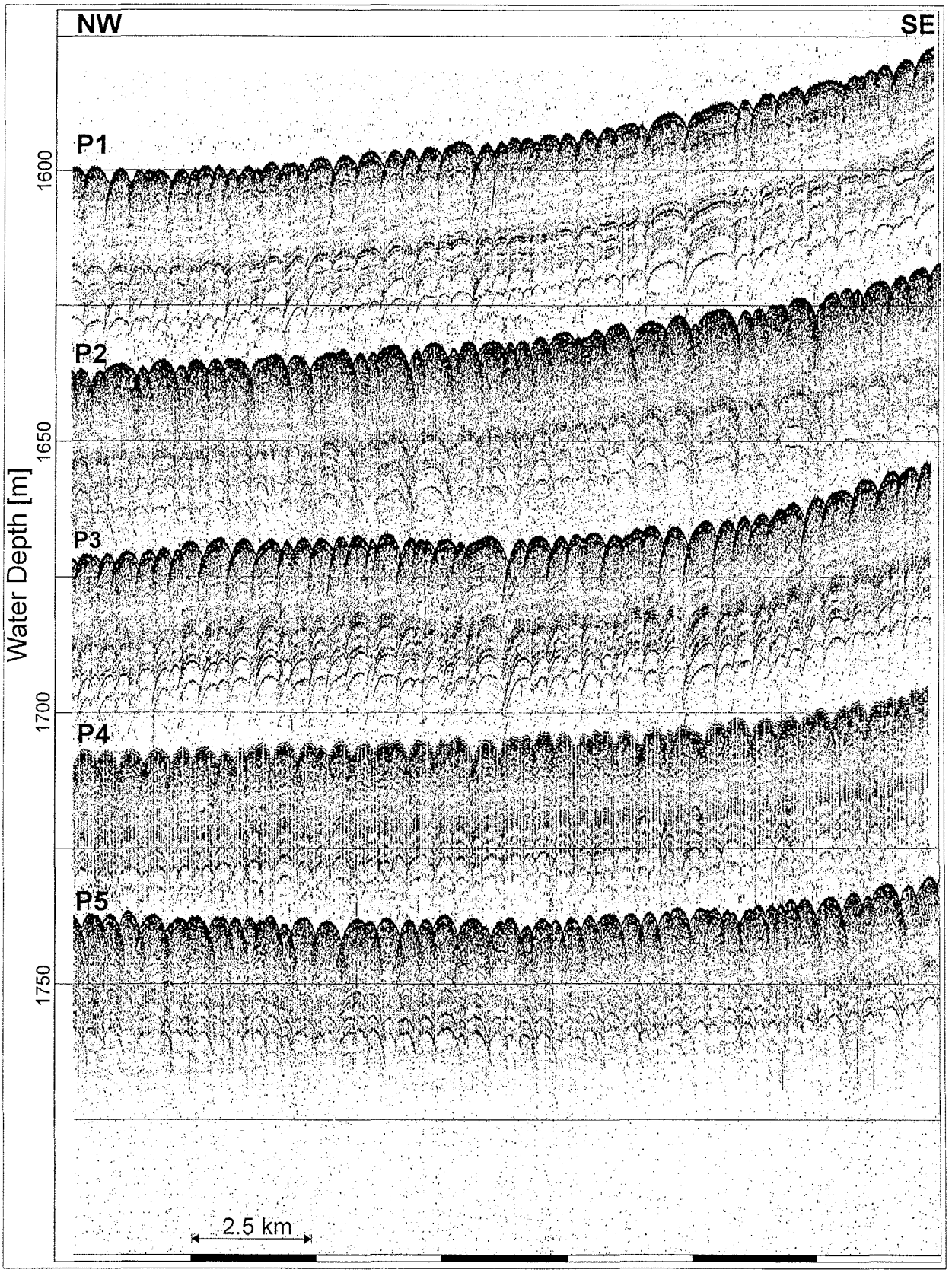

Figure 2.4: Parallel Parasound sections recorded in the southern part of the study area. Lateral distance between individual lines is ~2500 m. Display technique os similiar to that of Figure 2.3, but note the different vertical gridline spacing of 25 m. Vertical exaggeration 1:78.

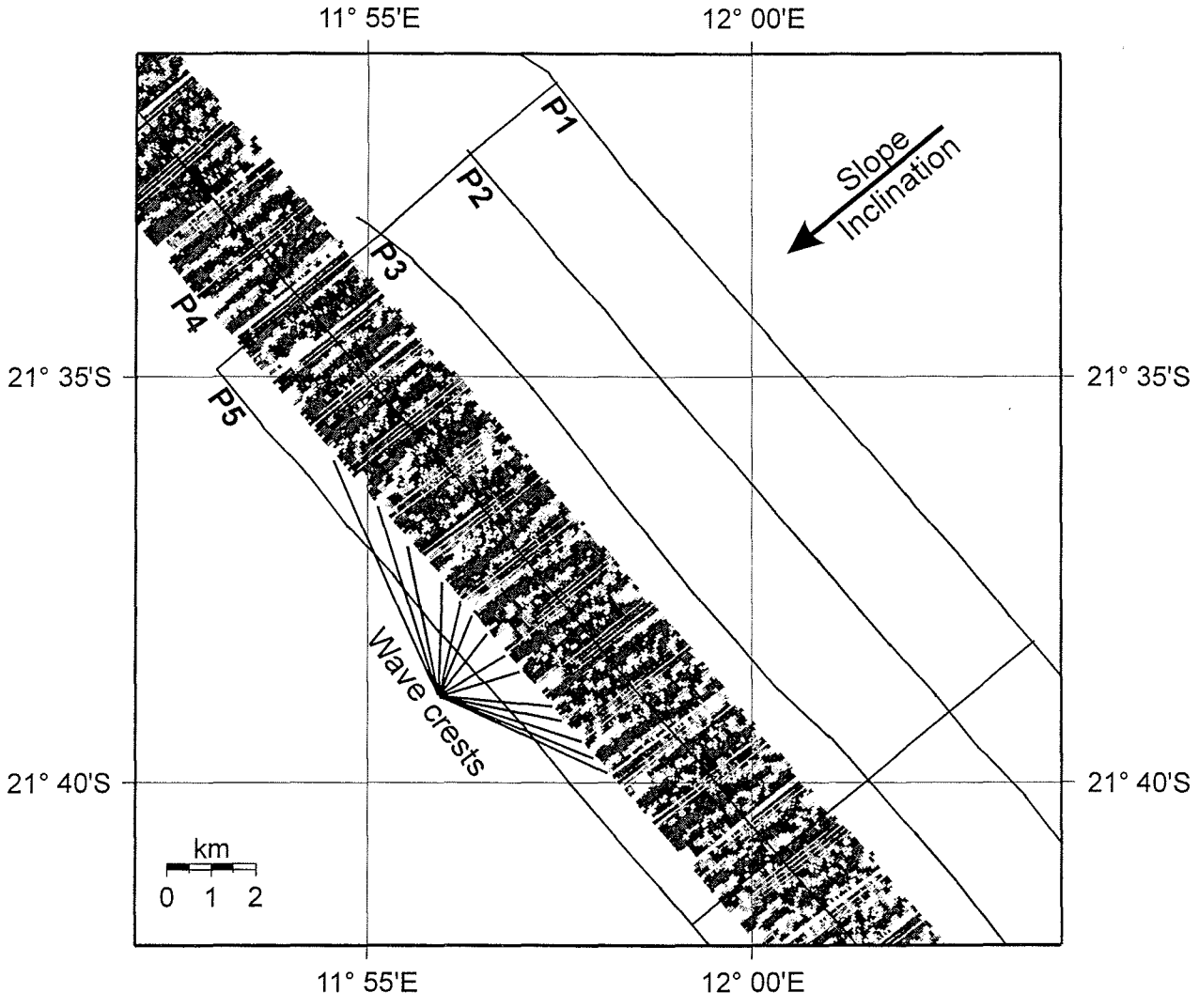

Figure 2.5: Hydrosweep section corresponding Profile 4 (P4) in Figure 2.4. The illumination azimuth is -45°. The location of the parallel Parasound lines is given for reference. The swath sonar data qiality on the other profiles unfortunately suffered from weather conditions. Wave crests and continental slope inclination are indicated.

To investigate variations in sedimentation rate the Parasound data were displayed in an unconventional scheme as shown in Figure 2.6. Seismograms are shifted in time to plot the sea floor as a flat, horizontal reflector. Figure 2.6 shows a Parasound section at 21° 15' S crossing the wave field from west to east in upslope direction (see Figure 2.2 for exact location). A topographic section is shown on top for reference. It can be recognized that the sedimentation rates are reduced within the mudwave field compared to the upslope and downslope deposits. Minimum sedimentation rates are reached at the deepest part of the wave field and rates gradually increase upslope.

2.5.2 Current measurements

Current measurements are available for a period of 12 months from the crest of Walvis Ridge (see location of W3RU in Fig. 2.2). As shown by the trajectory in Figure 2.7a the net water transport at this location follows an easterly direction with a small southward component. This net transport results from times of predominant eastward flow in winter and summer, and from times with high directional variability in fall and autumn (Figs. 2.7a and e). In July and December considerable northern and southern transport can be observed. The mean flow velocity averages to 2 – 4 cm/s (Fig. 2.7d). However, high tidal velocity peaks occur, reaching up to 10 cm/s (Figs. 2.7b and f). The histogram analysis (Fig. 2.7c) shows that velocity peaks up to 6.5 cm/s are very frequent.

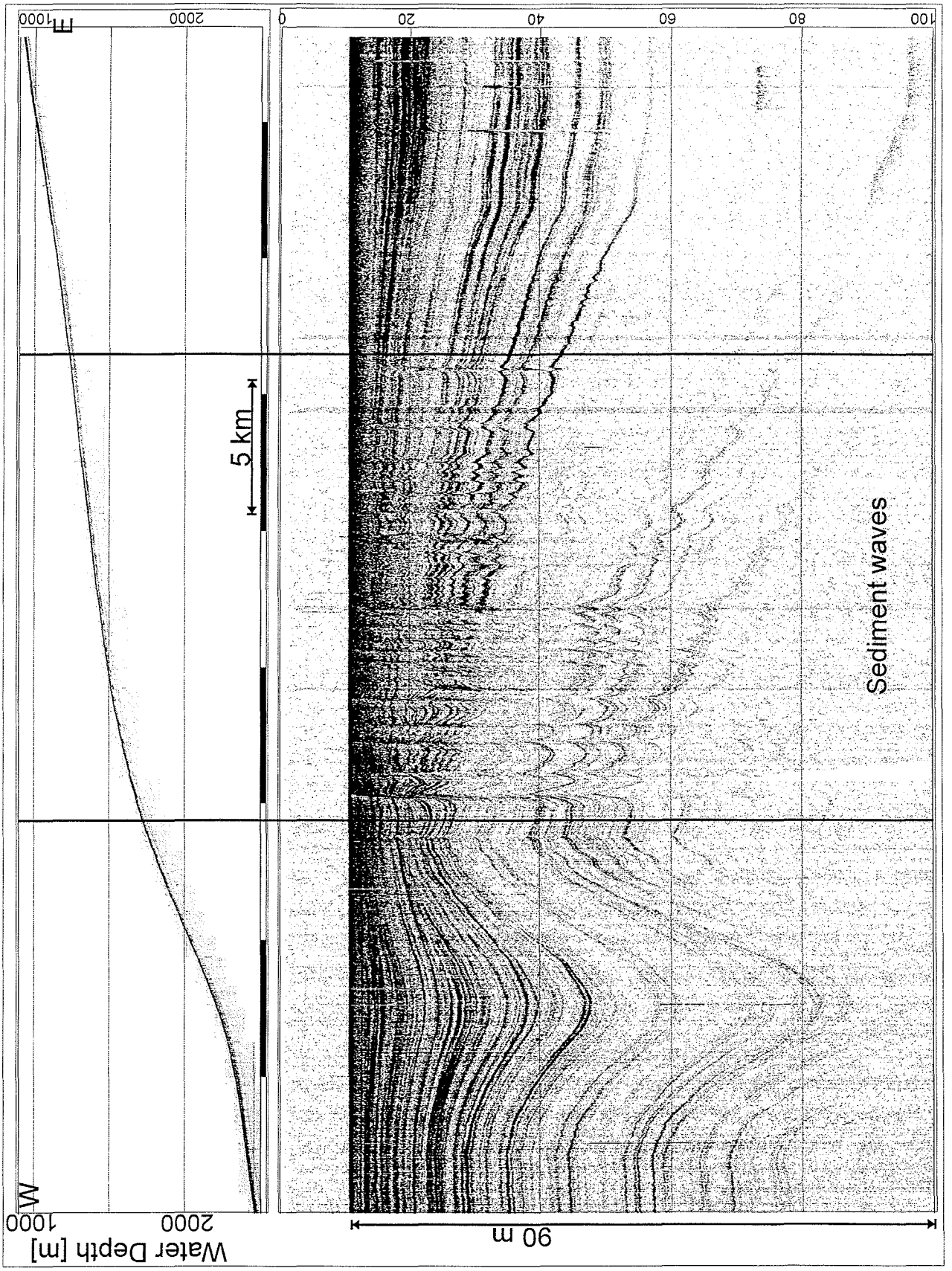

Figure 2.6: Parasound section crossing the southern study area from west to east. Individual seismograms are shifted to yield a flat seafloor. The vertical lines denote the deeper and upper limits of the wave field. The true bathymetry is given on top for reference.

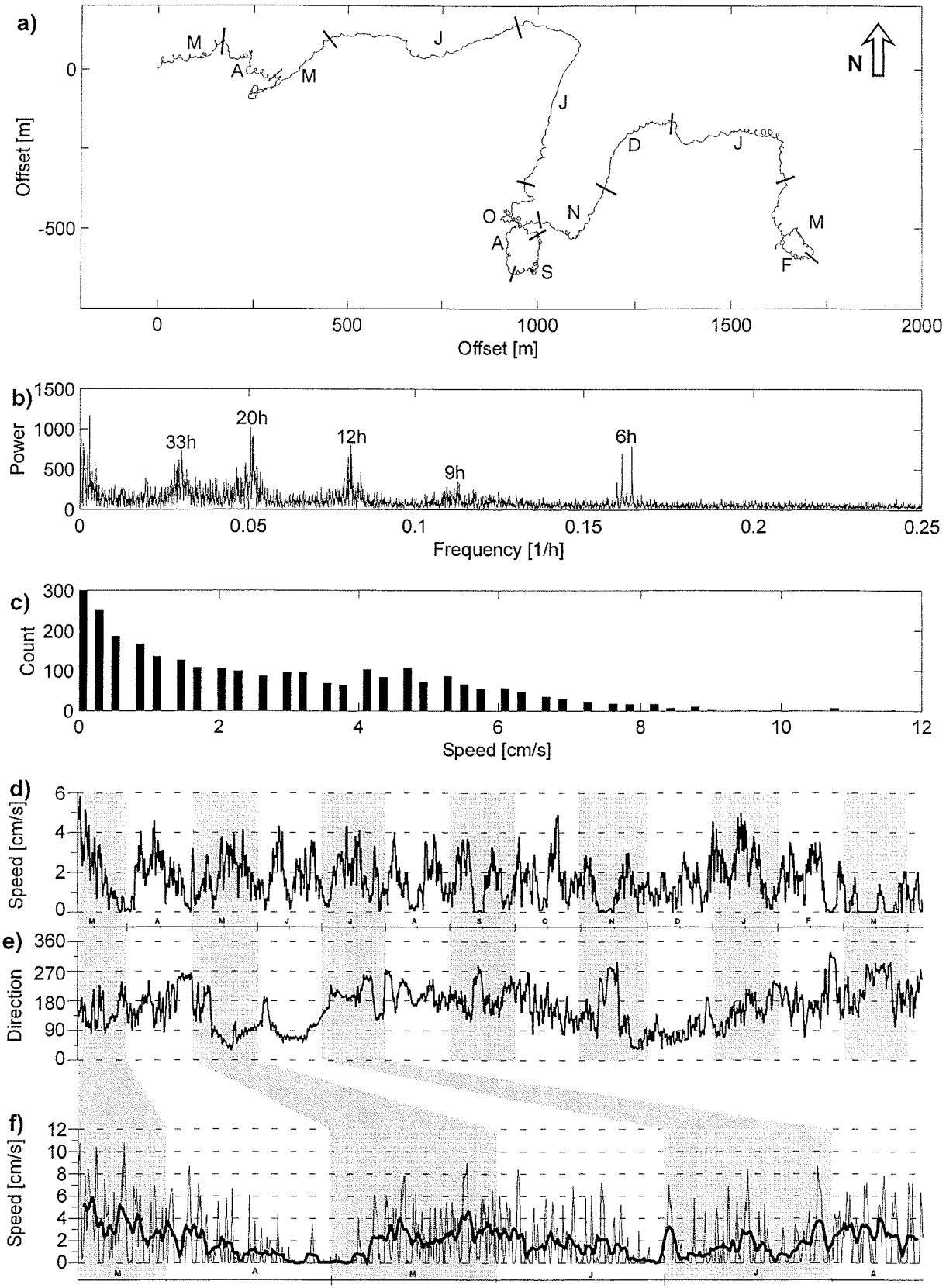

Figure 2.7: Direct current measurements obtained at Site WR3U. a) Flow trajectories, short bars separate individual months; b) Power spectrum of velocities, most significant periods are annotated; c) Histogram of velocities. Count axis (vertical) is clipped to enhance resolution; d) and e) Flow velocity and direction, filtered with a running average of 24 h; g) Flow velocities of the first five months of recording. The thick line corresponds Fig. 2.7d.

2.6 Discussion

Several mechanisms may be considered to be responsible for the formation of the observed structures. They can generally be subdivided into gravity induced and bottom current induced processes.

Gravity driven sediment transport is well known on all continental slopes and includes high energy turbidites as well as low energy sediment mass movements. All turbulent forms of gravity transport (e.g. turbidites, slumps, debris flows, etc.) can be excluded here because the resulting deposits are characterized by a lack of internal structures and a transparent appearance in seismic images. In contrast, the presented examples show a distinct internal layering and smooth transitions to undisturbed sedimentation upslope and downslope of the wave field. Similar bedforms could well be produced by non turbulent forms of gravity transport as a lateral compression of the sediments, which might result in a moderate folding associated with a preservation of the internal structures, or a slight sliding, which causes stepped, faulted structures as proposed by *Bremner* (1981). If gravity is the driving force, however, it is difficult to explain the observed downslope oriented strike direction of the waves. As gravity acts downslope, the related structural features should show in general a strike direction oriented alongslope (slope-parallel). Furthermore, the waves can be expected to change their shape in response to different slope inclinations, because the applied forces change accordingly. This is not observed in the study area.

Bottom currents act on settling sediment particles at the seafloor and may cause erosion, winnowing and preferential deposition / non-deposition as a function of the local current velocity, the particle size and settling properties. High current velocities may form several small erosional channels close to each other, which could result in an undulating topography. However, such channels are carved into the seafloor and would accordingly cut through existing sedimentary layers. In contrast, the observed structures show undisturbed subbottom layers running basically parallel to the seafloor over long distances. Moreover, erosional channels in the observed strike direction would require bottom currents flowing up- or downslope. Also, because the structures are very regular in space and time, the currents need to be extremely space stationary over long time periods. To generate vertical flows, thermohaline density changes or wind driven upwelling processes can be considered. Thermohaline processes are of no importance here, but the

surface oceanography off the west coast of southern Africa is strongly affected by coastal upwelling (e.g. *Hart and Currie*, 1960, *Shannon and Nelson*, 1996), which is implicitly associated with vertical water transport. However, upwelling in the Benguela system is restricted to thermocline waters in the upper 500 m of the water column (*Hart and Currie*, 1960).

The other current induced process influencing the seafloor topography is preferential deposition in a lateral inhomogeneous velocity field. This process may form sedimentary waves if the inhomogenities develop as quasi stationary waves (*Queney*, 1948, *Flood*, 1988, *Blumsack and Weatherly*, 1989, *Hopfauf and Spieß*, 2000). We suggest, that an increase of current velocities of southward flowing water in a depth interval 1300 – 1800 m, caused by narrowing of the cross-section while passing the obstacle Walvis Ridge, may have formed the observed sinusoidal structures, namely sedimentary waves. The waves develop roughly perpendicular to the current and drape the slope without changing their wave length significantly, as their geometry depends primarily on the velocity field and not on the slope inclination. The existence of this current not only becomes apparent by the formation of sedimentary waves, but also through reduced sedimentation rates in the corresponding depth interval (Fig. 2.6). This interpretation also explains the position of the northern and the deeper limits of the wave field. On the central Walvis Ridge the narrowing of the cross-section of the southward flowing current reaches its maximum and therefore the wave field extends to the south. The deeper limit corresponds approximately to the sill depth of the eastern Walvis Ridge and consequentially restricts the passing current. Upslope of the wave field we assume a decrease in current velocity probably associated with a lack of long time stationarity. This also leads to higher sedimentation rates (Fig. 2.6). Deeper and upper wave field limits slowly deepen towards the south following the general trend of water mass boundaries in the South Atlantic (*Reid*, 1989).

This interpretation is also in agreement with the current knowledge of the South Atlantic oceanography, which derives a generally southward oriented deep water transport across the eastern Walvis Ridge (*Reid*, 1989, *Reid*, 1996, *Speer et al.*, 1995, *Roether and Putzka*, 1996). The direct current measurements at site WR3U (Fig. 7) show a great variability and moderate mean current velocities. Nevertheless the current velocities reach with significant frequency velocities exceeding 6 cm/s (Fig. 7c) and net water transport is in southeastward direction. But as the location of site WR3U is more than 100 km off the mudwave field and records only data for one year, whereas sedimentary waves develop over 10'000 of years, its meaningfulness for this discussion is limited.

We therefore conclude that the mudwave field may be viewed as the track of a long-standing high velocity contour current passing the Walvis Ridge in southward direction.

2.7 Modeling

A major goal of a study of sedimentary waves is the quantitative link between the observed geologic features and oceanographic processes, i.e. the determination of bottom flow patterns which are responsible for the development of the waves. If this connection can be established, sedimentary waves could be used to derive properties of palaeocurrents in space and time.

Physical models dealing with this problem were proposed by *Flood* (1988) and *Blumsack and Weatherly* (1989), based on the early work of *Queney* (1948). *Flood* (1988) developed a lee-wave model to calculate the disturbances, which an existing sinusoidal seafloor topography induces on a quasi stationary bottom current crossing the waves normal to their crests, and explained a resulting upstream migration direction. *Blumsack and Weatherly* (1989) introduced a variable flow component parallel to the wave crests to handle the growth of sedimentary waves at arbitrary angles between flow direction and wave strike direction. Both models have in common, that they use the Coriolis parameter as a scalar and hence do not consider the absolute azimuth of the wave strike direction.

In this study we use a model developed by *Hopfauf and Spieß* (2000) as a generalization of existing theory. It takes into account the full three dimensional Coriolis vector and therefore considers the azimuth of the wave crest orientation and an arbitrarily oriented, horizontal current vector. Based on a phase analysis of the stationary waves which develop in the velocity field over the wave topography, the model estimates velocity intervals for the normal to crest components of the flow for which existing sedimentary waves may grow or be destructed (see *Hopfauf and Spieß*, 2000, for details).

Geographic latitude, water depth and strike direction of the observed waves represent the fixed boundary conditions of the model. For the four possible quadrants of flow vectors of a mean bottom current relative to the strike direction, the growth intervals of flow velocities are calculated for a given range of sedimentary wave lengths (see Figure 2.8 for clarification). Plausibility considerations and comparison with the observations are then used to exclude non-meaningful model results and to estimate current parameters.

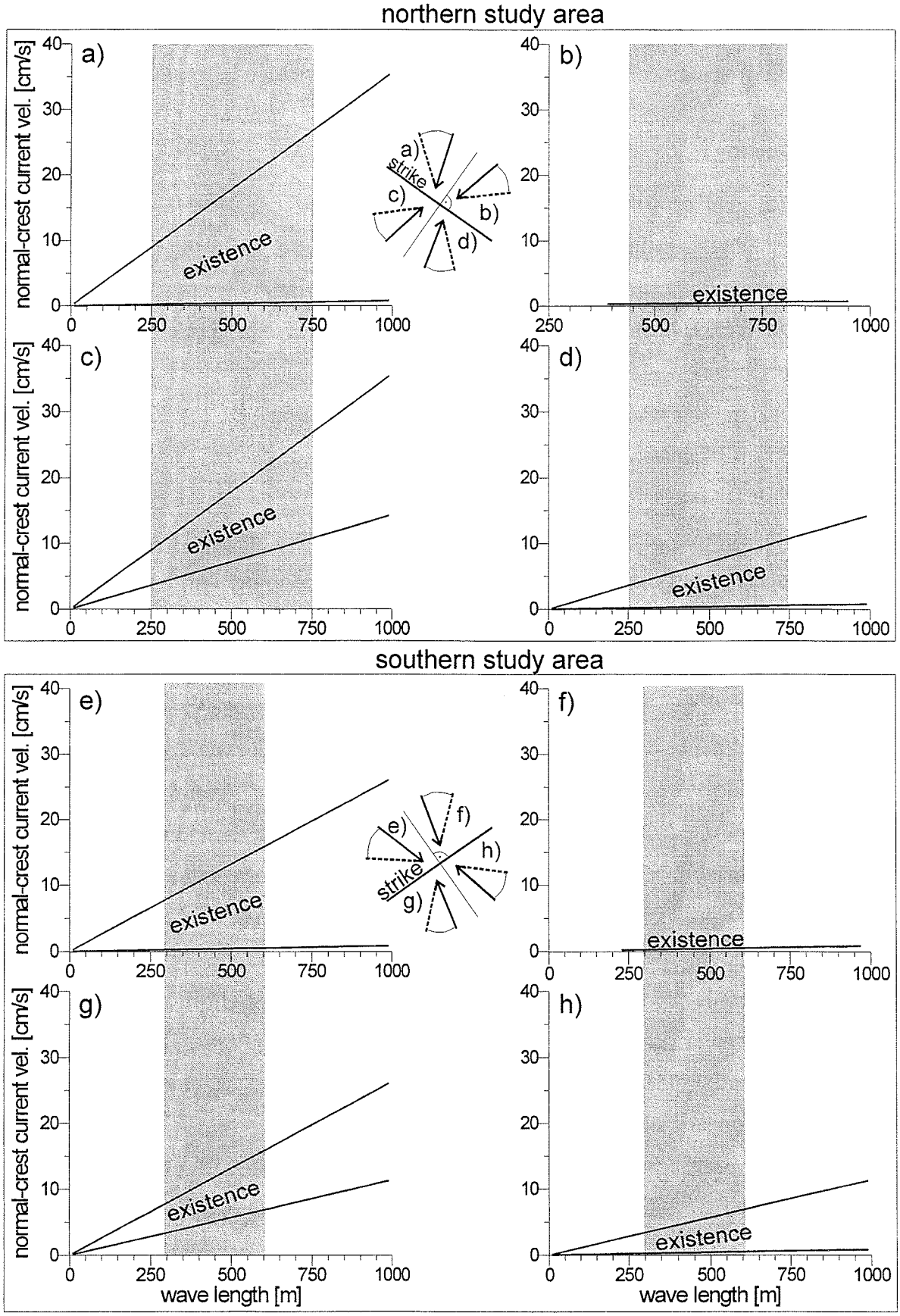

Figure 2.8: Model results for the northern and southern part of the study area. Small sketches describe the geometrical relation between the strike direction of the waves and the assumed flow. The dotted lines in the sketches intimate the ambiguity of flow directions within each quadrant.

2.8 Model results and interpretation

Model results were calculated the for the northern and southern part of the study area using the following parameters:

- North (Walvis Ridge): Latitude 19° 45' S, water depth 1300 m, strike direction 125°.
- South: Latitude 21° 35' S, water depth 1700 m, strike direction 55°.

The results are presented in Figure 2.8. Solid lines mark the velocity interval for which the model predicts growth or preservation of existing sedimentary waves.

As *Hopfauf and Spieß* (2000) point out, the strike direction of the waves becomes increasingly important for the model results with increasing water depth and increasing latitude. For shallower water depths as in this study area, the main controlling parameter for the predicted flow velocities is the Brunt-Vaisala frequency, which depends on the density gradient in the water column. Therefore the general patterns of the model results for the northern and for the southern study area are quite similar, although the strike direction differs by 70°. The Brunt-Vaisala frequency below the thermocline, which is used in the model calculations, is based on the estimation of *Garrett and Munk* (1972) for the free water column. As sedimentary waves are bathed in the bottom-near water layers a contribution of resuspended material in the water column is likely, which may change the local density gradient. The magnitude of this change is not known but it has to be stated that a decreased density gradient would cause a decreased Brunt-Vaisala frequency and vice versa. Accordingly the model velocities may be slightly over- or underestimated, respectively.

In general, higher flow velocities are predicted for the northern study area (Fig. 2.8). Also, greater wave lengths may generally be attributed to higher bottom current velocities. As described above, the results for the four quadrants of current vectors will now be analyzed in their applicability to the local situation.

Cases 2.8b and 2.8f, respectively, which are calculated for a southward flow with a westward component, can be excluded because the predicted interval of growth and preservation is extremely narrow and velocities are very low. This constellation is highly unstable, as slight changes of the mean current velocity will start to destroy existing waves. In contrast, for a southward oriented current with an eastward component (Figs. 2.8a and e) the model predicts a wide and therefore stable interval for growth and preservation of sedimentary waves. Existing sedimentary waves will stay intact over a

wide range of flow velocities and quite high velocities, exceeding 20 to 25 cm/s will be required to destroy them. This result also agrees with the assumption of an eastern contour current which would contain eastward components due to Coriolis deflection on the southern hemisphere.

Assuming a northward flow with an eastward component (Figures 2.8c and g) the model predicts a more narrow velocity interval than for the southward flow with comparably high current velocities. This would imply, that the waves would be leveled at times of low current velocities. Hence the flow velocity is required to remain at a very high level over long periods of time to build up the observed waves. The results for a northward flow with a westward component is shown in Figures 2.8d and 2.8h, respectively. As in Figure 2.8c and 2.8g the model yields a rather narrow velocity interval, but now centered around moderate flow velocities. Moderate flow velocities would therefore support the growth and preservation of waves, whereas high current velocities persisting over longer time scales would cause wave destruction. This constellation is more stable than that of Figure 2.8c and 2.g. Moreover, as mentioned for the southward flow, the westward component may be explained with the Coriolis deflection to the left.

To summarize, both a southward and a northward oriented bottom current yield plausible model results, differing at most in the predicted model velocities. While the results for a southward flow allow velocities of up to 25 cm/s for the greatest wavelengths observed, the estimated velocities for a northward flow are restricted to 10 cm/s. As stated in the discussion above the observed characteristics of the mudwave field suggest a predominantly southward flow. However, an occasional inversion in current direction would not result in a destruction of the wave field.

The model of *Hopfauf and Spieß* (2000) as well as those of *Blumsack and Weatherly* (1989) and Flood (1988) show clearly that changes in wave geometry can be related to changes in bottom current environment. Therefore sedimentary waves provide a high resolution record of palaeocurrent activities and changes. Accordingly, future work in the study area will concentrate on detailed analysis of different sedimentary units, considering also wave migration direction and growth rates, to obtain further insight in the palaeocurrent history in this area.

2.9 Acknowledgements

We would like to thank the participants of the R/V METEOR Cruises M20/2, M34/1, M34/2 and R/V SONNE Cruise So86, which supported us in supervising the echosounding systems. With their help it was possible to collect high quality data on a 24 hour schedule. We also thank W. Zenk and J. Holfort for their suggestions concerning the local oceanographic situation. This study was funded by the Deutsche Forschungsgemeinschaft (Sonderforschungsbereich 261 at Bremen University). This is contribution no. Xxx of SFB 261.

3 Palaeoflow history at the south west African continental margin determined by analysis of a sedimentary wave field

H. v. Lom, V. Spieß and V. Hopfauf

3.1 Abstract

A sedimentary wave field, which developed on the Namibian continental margin and on the eastern Walvis Ridge during the last 5 my under the local current regime, was investigated to reconstruct palaeoceanographic changes through time. High resolution echosounder data reveal changes of the internal wave geometry, indicating that the history of water transport across the eastern Walvis Ridge may be subdivided into 5 major phases since the development of sedimentary waves. A combined approach of modeling the wave growth and analyzing bottom flow induced deposition patterns all over the study area, allows a qualitative and quantitative estimate of palaeoflow history. The onset of sedimentary wave growth started at about 5 Ma and marked the development of a stable contour current in water depths of 1200 – 1800 m with moderate to low current velocities. The current intensity slowly increased until probably pulsed high speed events near 1.9 Ma caused a partial destruction and erosion of the waves. In the following 900 ky current intensity gradually weakened and the wave field regenerated, but at a higher level of mean flow velocity, now reaching ~ 4 cm/s. A comparably quiet phase persisted from ~1 to 0.6 Ma. Afterwards current activity increased again, probably also starting with pulsed events. The mean current velocity in the last 400 ky presumably varies in a range of ~ 3 to 8 cm/s.

3.2 Introduction

Small scaled sedimentary waves drape the Namibian continental margin from 19° 30' S, where the eastern Walvis Ridge abuts the continental margin, to 22° S at water depths ranging from 1200 to 1800 m (*v. Lom et al.*, 2001) (Fig. 3.1). The wave lengths at the seafloor reach 250 to 700 m, the wave heights vary from 5 to 8 m. Extent and location of the wave field suggest a coupling to an eastern boundary current, passing the Walvis Ridge in southward direction (*v. Lom et al.*, 2001).

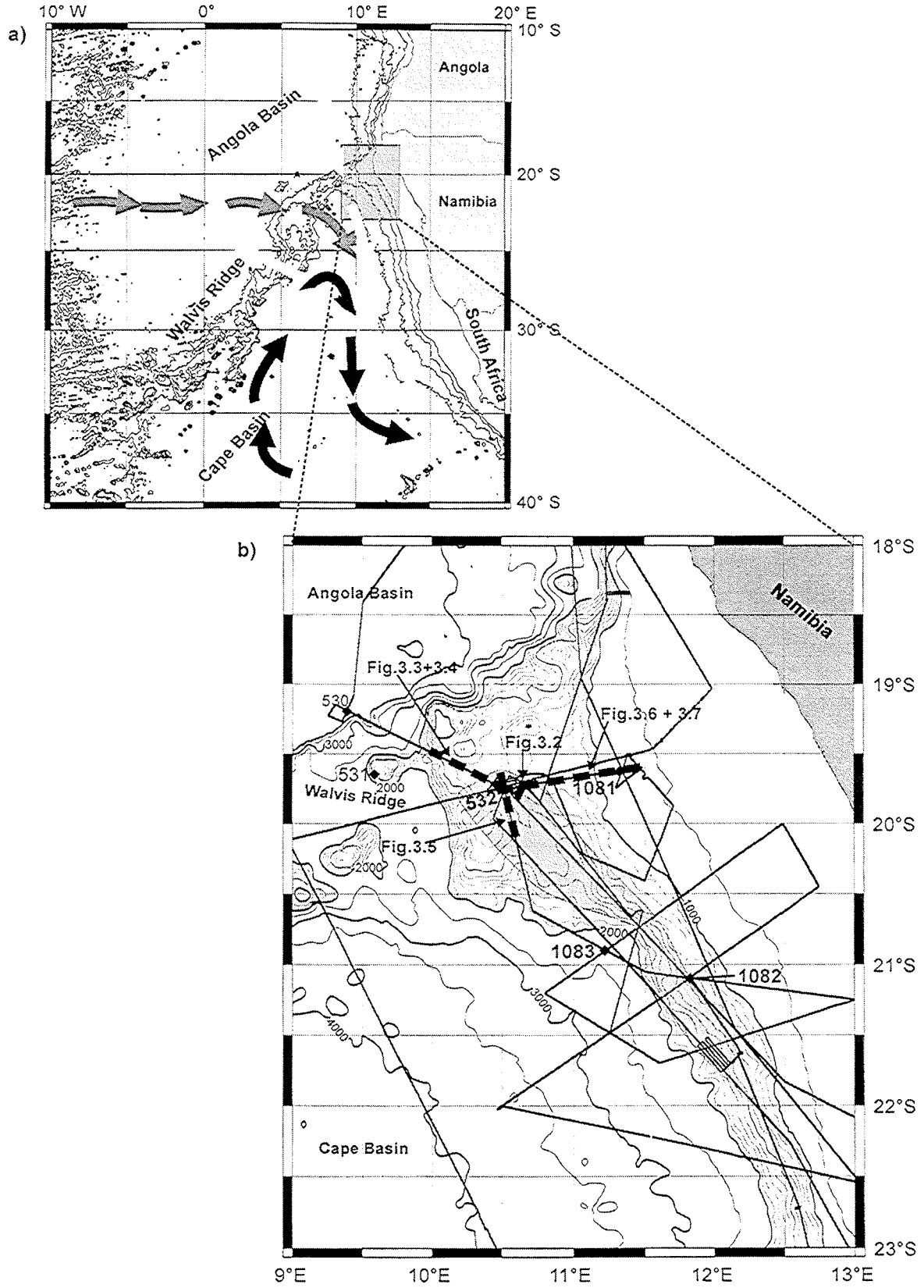

Figure 3.1: Location of the study area on the Namibian continental margin. a) Modern deep water transport paths: AAIW, UCDW, and UNADW (⇧) after *Reid* (1989), Namib Col Current (↑) after *Speer et al.* (1995) and deep basin circulation (↑) after *Nelson* (1989). b) Extension of mudwave field (shaded) and coverage by echosounder lines. Positions of DSDP and ODP Sites are also marked. Isobaths are given in 500 m spacing, but increased to 100 m spacing in the range from 1000 to 2000 m water depth, to emphasize overall topography. Bathymetry is after *Smith and Sandwell* (1997). Presented profiles are pronounced by thick dashed lines and named accordingly.

The availability of a dense grid of high resolution echosounder data in this region (Fig. 3.1b) (*Schulz et al.* 1992, *Bleil et al.*, 1993, *Bleil et al.*, 1996, *Schulz et al.*, 1992, *Schulz et al.*, 1996) and additional seismic lines (*Bleil et al.*, 1993, *Bleil et al.*, 1996) allows a detailed analysis of the development of the waves. As the geometry of sedimentary waves, i.e. strike direction and wave length, and especially the associated changes in these properties, can be attributed to changes in bottom current parameters (*Flood*, 1988, *Blumsack and Weatherly*, 1989, *Hopfauf and Spieß*, 2000), sedimentary waves may be seen as witnesses of palaeocurrent activities. A study of the internal structures of the waves hence yields clues on past bottom flow intensity and stability.

As a second approach to derive palaeoflow information, spatial variations in sedimentation rates are examined in the study area, which are most probably caused by topographically induced fluctuations in bottom current velocity.

The coupling of these two analyses provides insight into the long term palaeoceanographic environment on the Namibian continental margin.

3.2.1 Setting

The Walvis Ridge forms a more than 2000 meter high barrier between the Angola Basin, bordering on the north, and the Cape Basin, bordering on the south respectively (Fig. 3.1a). The topography of the continental margin and also of the ridge slope is quite different on both sides of Walvis Ridge. To the north slopes are steep and rough while to the south smooth slopes prevail with well stratified sediments. The deposited material consists mainly of pelagic biogenic particles with an increasing amount of upwelling related material towards the Namibian coast. Upwelling of cool nutrient rich water, caused by the trade wind activity, is an important process all along the western coast of Africa, which greatly increases biogenic production. However, this process is dominant in a 180 – 200 km wide zone along the coast and is therefore restricted to the inner shelf and the shelf edge (*Summerhayes*, 1983). Small amounts of terrigenous material, mainly clay and silt particles, are contributed by the Orange River, and Namib Desert dust (e.g. *Bornhold*, 1973, *Bremner*, 1975, *Diester-Haass et al.*, 1992).

According to *Reid* (1989) the modern South Atlantic deep waters can be vertically distinguished in five specific water masses. Antarctic Bottom Water (AABW), cold and salty, fills the deep basins to up to 3800 – 4300 m depth and spreads northwards. The Circumpolar Deep Water (CDW) is cold, but lower in salinity. On its way north, it is split into the Lower Circumpolar Deep Water (LCDW), ranging from 3000 – 4000 m, and the

Upper Circumpolar Deep Water (UCDW), varying from 1000 – 1500 m. The huge water mass which is responsible for this splitting, is the southward spreading North Atlantic Deep Water (NADW). NADW is warmer than CDW but higher in salinity and therefore occupies the same range of water densities. The UCDW is superimposed by the Antarctic Intermediate Water (AAIW) in depths of 700 to 1100 m and by the uppermost deep water mass, the South Atlantic Central Water (SACW), which fills the gap to the thermocline.

The surface waters in the eastern South Atlantic Ocean are represented by the cold Benguela current, flowing northward along the south-west African coast until 20° S (e.g. *Hart and Currie* ,1960, *Stramma and Peterson*, 1989), where it meets the southward flowing tropical Angola current (*Moroshkin et al.*, 1970).

The results of SAVE (South Atlantic Ventilation Experiment, 1987 – 1989) and WOCE (World Ocean Circulation Experiment, 1991 – 1997) suggest that deep waters below 400 m pass the eastern Walvis Ridge in southward direction (*Reid*, 1989, *Reid*, 1996, *Speer et al.*, 1995, *Roether and Putzka*, 1996). At 25° S – 27° S this flow turns to north-west and joins the South Atlantic anticyclonic gyre (*Reid*, 1989). The involved water masses are the Upper NADW (UNADW) and the eastern return flows of the UCDW and AAIW (*Reid*, 1989, *Reid*, 1996). The passing of deeper waters is prohibited by the Walvis Ridge.

3.2.2 Palaeoceanography

The oceanography of the modern Atlantic Ocean is thought to be the result of several climatic cooling steps in the last 50 million years and the parallel closing and opening of important interoceanic passages (e.g. *Berger and Wefer*, 1996). The opening of the Drake Passage probably initiated the circum-Antarctic circulation and the closing of the Panama isthmus (e.g *Maier-Reimer* et al., 1990, *Mikolajewicz*, 1993, *Berger and Wefer*, 1996) and the Persian Gulf connection of the Thetys Ocean to the Indian *Ocean (Woodruff and Savin*, 1989) may have supported the development of the modern heat conveyor.

Corresponding to the Miocene deep water circulation reconstruction of *Woodruff and Savin* (1989), early Miocene waters in the South Atlantic mainly consisted of an AABW equivalent water mass. This water was formed by the high latitude cooling of warm saline water from the tropical Indian Ocean, probably supported by the outflow of warm salty Tethys water, pouring over the Persian Gulf sill. The resulting mixture, the Tethys Indian Deep Water (TIDW), could have been the early Miocene equivalent of modern NADW in its function as the source for AABW (see *Woodruff and Savin*, 1989, for details). In the middle Miocene (about 15 – 14 Ma) the Persian Gulf gap closed and the southward

transport of warm salty water from the Indian Ocean weakened. In parallel *Woodruff and Savin* (1989) observe the onset of NADW production in the North Atlantic. NADW production intensified at 11 – 10 Ma, additionally supported by Mediterranean Outflow Water (MOW), and in the following time a water mass stratification began to develop, which resembled closely to the modern situation.

With the closing of the Panama Seaway at about 3.5 – 2.5 Ma (*Keigwin*, 1978, *Coates et al.*, 1992) and the parallel onset of boreal glaciation (e.g. *Berggren*, 1972), NADW production constantly increased as climatic cooling proceeded (e.g. *Jansen*, 1988, *Berger and Wefer*, 1996). This also led to pulsed intensification of deep water activity (*Turnau and Ledbetter*, 1989). Opal accumulation in the Southern Ocean, which is presumably closely coupled to NADW production (*Berger and Wefer*, 1991), shows a maximum in NADW production at the Pliocene – Pleistocene boundary at about 1.8 Ma. Then, in the Pleistocene and Quaternary, orbital forcing began to influence and control NADW production, with weakened NADW in cold periods and strengthened NADW in warm periods.

3.3 Methods

3.3.1 Acoustics

To obtain high resolution echosounding data, a narrow beam Parasound echosounder (*Grant and Schreiber*, 1990) was used. This system, which is one of the permanently installed echosounder systems of the German research vessels R/V METEOR and R/V SONNE, provides a beam width of only ~7 % of the water depth at a main signal frequency of 4 kHz. This ensures a high resolution in horizontal as well as in vertical direction and minimizes the effect of side echoes. In the range of water depths corresponding the study area, the footprint of the system is only ~80 to ~ 130 m. On the other hand, the narrow beam implies a maximum slope angle of the sea floor of 2° to get echoes reflected back to the receiver. Usual signal penetration depths of the Parasound system vary from 20 to 150 m, depending on the sediment properties. However, due to different technical characteristics of the system installed on R/V METEOR, signal penetration depth is often less than on comparable profiles recorded with R/V SONNE.

The data were digitally recorded for further processing and display with the ParaDigMA System (*Spieß*, 1993). Processing was limited to bandpass filtering from 2 to 6 kHz to reduce low frequency acoustic and high frequency electronic noise. Migration of

the data is hindered by the size of the lateral data gaps in comparison with the high signal frequency. However, the extent of diffraction hyperbola is small due to the narrow beam.

Seismic data were recorded during the pre-site survey for ODP Leg 175 (*Bleil et al.* 1996). The use of a GI-gun as the seismic source with a generator volume of 45 in^3 provided signal frequencies up to 250 Hz. For registration a streamer with a total length of 800 m and 600 m of active sections was used, divided into 24 hydrophone groups with a group spacing and length of 25 m each. The shot spacing was approximately 25 m. Recording was performed with a GEOMETRICS ES-2420 at a sampling rate of 0.5 ms. The data were NMO corrected with an appropriate velocity model, stacked and filtered using a pass band of 20 – 200 Hz.

In figures, which present echosounder data or seismic data, amplitudes are color coded using 256 shades of gray. Time to depth conversion was performed using a mean sound velocity of 1500 m/s. This has proven to be an appropriate mean value for the water column as well as for unconsolidated young sediments.

3.3.2 Stratigraphy

For chronostratigraphy and lithology results of DSDP Leg 75 (*Hay et. al.*, 1984) and ODP Leg 175 (*Wefer et al.*, 1998) were used. DSDP Site 532, located at 1331 m water depth at 10° 31.13' E / 19° 44.61' S (see Fig. 3.1b for reference), lies within the limits of the mudwave field. ODP Site 1081 was drilled at 11° 19.16' E / 19° 37.2' S at a water depth of 805 m and is situated on the crest of the Walvis Ridge (Fig. 3.1b), but well above the mudwave field.

At Site 532 a high resolution stratigraphy of the uppermost 16 core meters was performed by *Oberhänsli* (1991), based on oxygen isotope measurements on two different foraminiferal species (*Uvigerina sp.*, *Globigerina bulloides*) and the occurrence of another one (*Gephyrocapsa lacunosa*). This stratigraphy reaches back until 500 ka and was used for this time interval. For deeper and older reflectors the biostratigraphy of *Giraudeau et al.* (1998) from ODP Site 1081 was used. This stratigraphy is much coarser than that of *Oberhänsli* (1991), but coincides well with DSDP 532 for the first 600 ky and provides sufficient resolution for the questions which will be discussed in this paper.

The stratigraphy of *Oberhänsli* (1991) yields significantly smaller sedimentation rates than the age models of earlier works (e.g. *Hay et al.*, 1984, *Diester-Haas*, 1985). As seismic lines (see fig.6) confirm reduced sedimentation rates within the mudwave area and connect Site 532 to Site 1081, this stratigraphy, however, seems to be plausible.

3.3.3 Modeling

To model the development of the sedimentary waves we use an approach of *Hopfauf and Spiess* (2000) as an extension to the existing models of *Flood* (1988) and *Blumsack and Weatherly* (1989). In difference to these older models it introduces the Coriolis parameter not as a scalar but as a three-dimensional vector. In addition to existing theory, it also takes into account the azimuth of the strike direction of the waves and allows arbitrary orientation of the bottom flow vector.

Based on a phase analysis of the calculated sedimentation rate distribution, the model predicts a growth and a migration rate for existing sedimentary waves. These rates depend on the bottom current velocity and direction, as well as on the water depth, geographic latitude, wave length and strike direction. Furthermore it is possible to derive the onset of sedimentary waves for a specific simplified initial topography.

The model still idealizes the sediment-water-boundary in that it does not consider the viscosity terms in the Navier-Stokes-equations and assumes a stratified flow. Yet this idealization may be neglected when dealing with periods which are necessary for sedimentary wave development (see discussion below for further considerations regarding this topic).

3.4 Data

Parasound profiles in the northern part of the study area, where water masses pass the Walvis Ridge, show significant variations in sedimentary wave geometry. One of the best examples (Fig. 3.2) was recorded near the crest of the ridge and is oriented nearly perpendicular to the mudwave strike direction. This section shows short regular waves with wave lengths ranging from 250 – 700 m. Three subbottom units of different wave characteristics can be recognized, which are set apart by two transition units. Reflectors, which mark the boundaries of these units, were picked and traced along the profile. Some pronounced unit-internal reflectors were also picked to ease interpretation and reflector tracing.

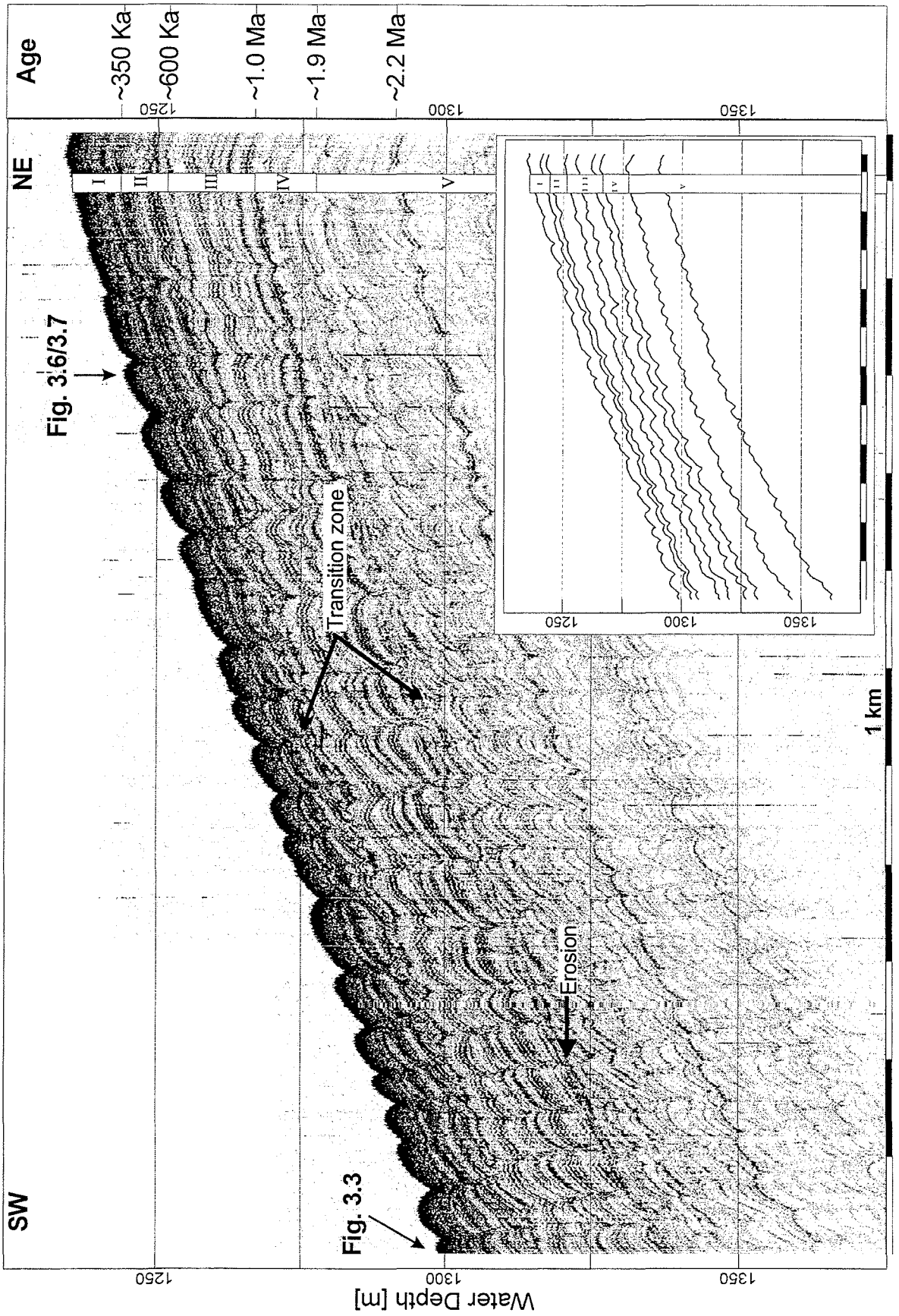

Figure 3.2: Parasound section on the crest of the Walvis Ridge (see Fig. 3.1b). The different acosutic units are indicated to the right. Ages are given conforming to the stratigraphy of *Oberhänsli* (1991) and *Giraudeau et al.* (1998)

The specific characterization of the resulting five acoustic units, named I to V, is as follows:

- **Unit V**: very short and regular waves. The wavelength varies from 250 to 300 meters. A slight northwest migration can be noticed in specific layers.
- **Unit IV**: this unit spans a period of transition from the short regular waves of Unit V to much longer waves. At the upper depth limit of this unit the waves reveal a wave length of 750 meters, which is more than twice the previous wave length. In between the waves are partially destroyed and also areas of erosion can be recognized.
- **Unit III**: comprises the a geometrically stable situation with well developed waves with a wave length of 750 meters. Southwest Migration seems to occur at some wave crests but this property is not pronounced and not laterally consistent.
- **Unit II**: transition situation, where the sedimentation patterns become very complicated and lack lateral consistency. Short waves seem to develop on top of the longer waves and are subsequently destroyed, followed by the growth of longer waves with wavelengths varying from 500 to 600 meters.
- **Unit I**: represents a stable situation with some intermittent phases with southwest migration. Wave lengths range from 500 to 600 meters.

These units can be traced to the northern escarpment of the Walvis Ridge as is demonstrated in a Parasound section (Fig. 3.3a), which connects to the southwestern end of the profile shown in Figure 3.2. This profile also crosses DSDP Site 532, which was used for age assignments of the upper 20 meters of the sediment column. Topography along the profile is characterized by a small elevation in the northwest, which is a foothill of a seamount located to the northeast of the profile (Fig 3.1b), and by a smooth ascent to the crest of the Walvis Ridge. Sedimentary waves of the main wave field are observed at the upper third of the profile. Also, small waves occur in close vicinity to the seamount, most presumably related to the local current regime around the seamount. The area around the seamount is also characterized by erosion / non-deposition, which becomes evident from outcropping deeper reflectors as well as from onlapping reflectors in Unit III.

The accumulation rates, which should be basically spatially constant for pelagic deposition in absence of bottom currents, vary significantly in this region. This can be demonstrated through different presentations of the same profile (Figs. 3.3b & c). The recording delay was shifted to flatten a specific reflector, and to image lateral variations in accumulation for different time periods thereby. The reflector chosen in Figure 3.3b

represents the boundary between Units II and III, and the flattened section shows that sedimentation rates in Unit II are reduced towards the center of the profile as well as towards the ridge crest. In the upper part of Unit III no lateral changes in the sedimentation rate occur. However, with increasing depth again accumulation varies laterally. The flattened reflector in Figure 3.3c represents the boundary between Units IV and V. Strong spatial variability characterizes the sedimentation in Unit IV with distribution patterns, similar to those of Units II and III. In contrast, this effect is very small in Unit V.

The north western part of the profile, where deposition is affected by the presence of the seamount, shows similar variations in sedimentation rate distribution, with strong variability in Units II and IV and modest to weak variability in Units III and V.

A closer look on the erosional zone in the vicinity of the seamount (Fig. 3.4) shows that the location, where non-deposition is changing to deposition, is characterized by truncation and onlap of reflectors. This position, which is further on called critical distance of deposition, is shifting significantly through time (intimated by the dashed line in Figure 3.4). Sediments deposited in Unit V reach close to the seamount and show an undulating topography. In Unit IV sedimentation retreats from the seamount. Deposition starts beyond 10 km distance from the seamount flank compared to 4-5 km in Unit V. In Unit III, sedimentation again occurs closer to the seamount, but not as close as in Unit V. Deposition starts here at 5-5.5 km distance. The critical distance of deposition increases gradually towards the end of Unit III and in Unit II, reaching 9 km at the beginning of Unit I. The critical distance of deposition in Unit I is difficult to trace because of the undulating topography and several incisions, but it seems to be larger than in Unit II.

The presence of sedimentary waves in this region as a response to the local velocity field variations is of limited lateral extent. The width of the wave zone in Unit V is 3 km while in Unit IV waves have nearly vanished. However, in the upper 15 m of Unit V extremely small wavy structures (wave length ~150m, height ~1 m) can be recognized starting at a distance of 11 km and ending at 18 km distance from the seamount. In Unit III, new waves start to develop with increasing wave heights in Units II and I. The width of the wave zone in Units II and I exceeds 10 km.

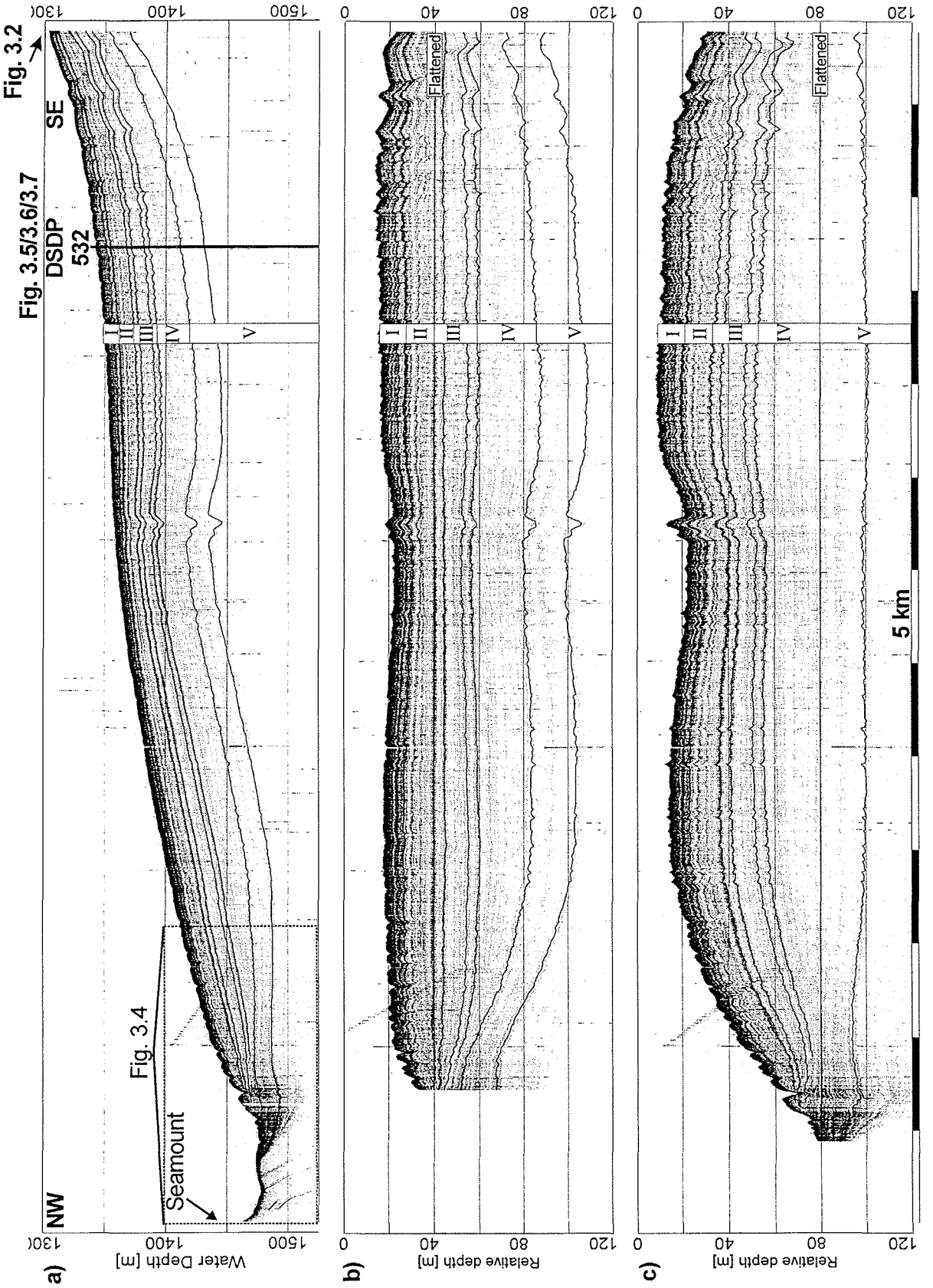

Figure 3.3: Parasound section extending from the crest of the Walvis Ridge in northwest direction. a) profile plotted using correct recording delays. Traced reflectors are indicated by black lines in profile. b) the same profile flattened to the boundary between Unit II and III. c) the same profile flattened to the boundary between Unit IV and V. Note, that a display of echograms in flattened representation is only possible, where the corresponding reflector could be defined. Otherwise the necessary delay shift is unknown. This causes the apparent data gap at the northwestern end of the profile.

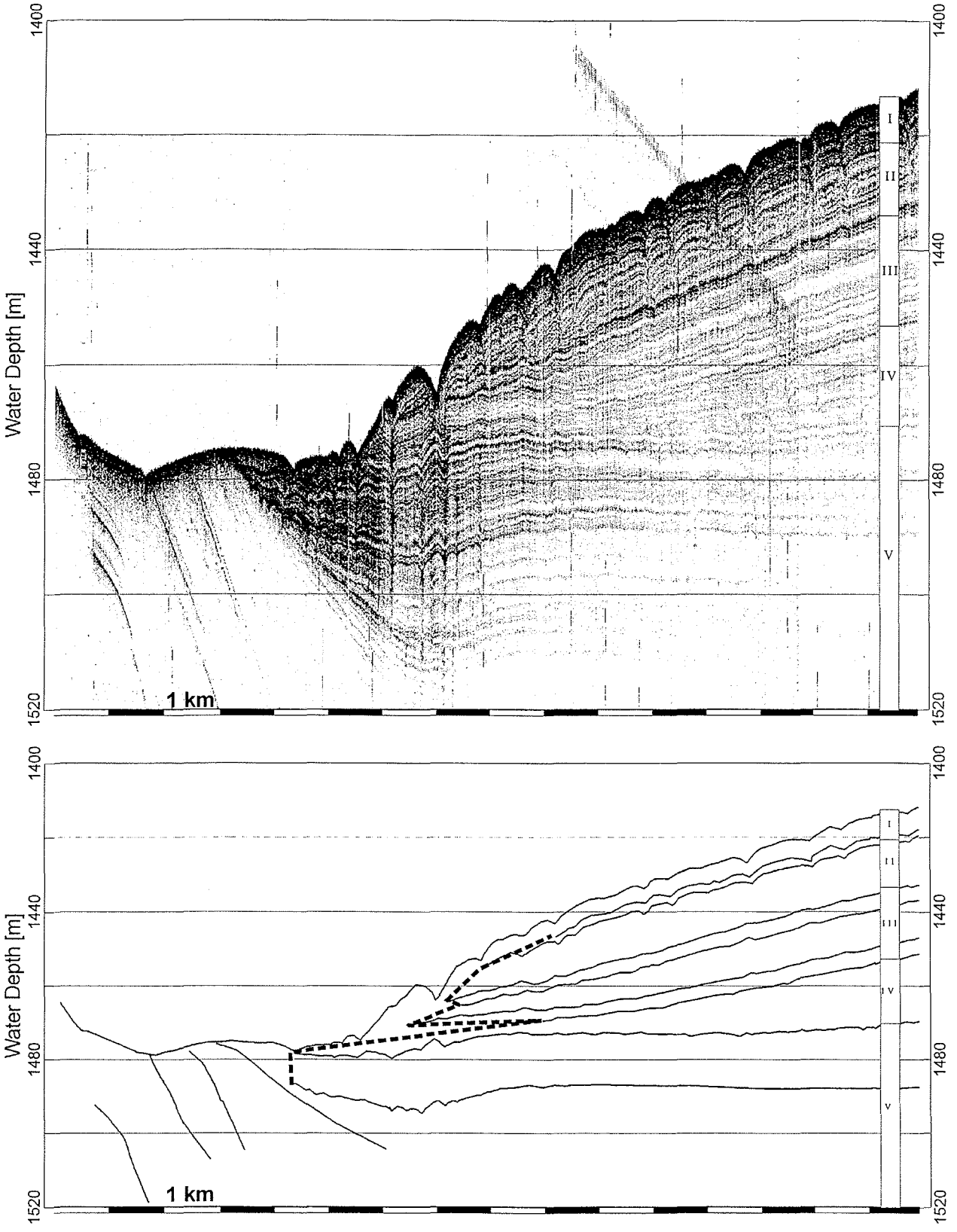

Figure 3.4: Close-up of the northwestern end of the Parasound section shown in Figure 3.3. The lower picture shows a linedraw of the traced reflectors. The dashed line indicates the variations in the critical distance of deposition.

Towards the southern flank of the Walvis Ridge the pattern of sedimentation is quite similar to the northern flank. Figure 3.5 shows a 65 km long Parasound profile from DSDP Site 532 towards the southern flank of the Walvis Ridge (see Fig. 3.1b for exact location). At its northern end it is connected to the profile shown in Figure 3.3. This profile was recorded with R/V Meteor and the signal penetration here is limited to 30 m. Therefore, it is not possible to trace all of the deeper reflectors in this profile and especially the boundary between Unit III and Unit IV can not be determined. Two dotted lines in the unit classification bar show the estimated vertical range of the position of this boundary.

The strong reflector marking the boundary from Unit IV to Unit V can be traced in the study area though. Flattening of this boundary (Fig. 3.5c) and the one between Unit II and Unit III (Fig. 3.5b) shows spatial variations in sedimentation rates, which are even more pronounced than in the northern profile. Note, that the sediment thickness is locally strongly reduced. This occurs not towards the crest of the Walvis Ridge, but at 1370 m water depth 15 km southward from the northern end of the profile. This position is located between the ridge crest to the north-east and a small elevation to the south-west (Fig. 3.1b). Further to the south the profile extends parallel to the flank of the elevation. Sedimentary waves exist only in the northern part of the profile and start again to grow at its southern end.

To better understand the deeper sedimentation structure on the eastern Walvis Ridge a seismic line (Fig. 3.6a) could be used, which was recorded in west to east direction roughly along the crest of the Walvis Ridge (see Figure 3.1b for exact location). This line also crosses the two coring sites DSDP 532 and ODP 1081, which allows chronostratigraphic assignments to the seismic as well as to the Parasound data.

The seismic line also shows a significant reduction in sediment thickness in its central part. The spatial resolution of the seismic data, though containing frequencies of up to 250 Hz, is not sufficient to allow a detailed analysis, but the sedimentary waves of the study area can be recognized on the western flank of this zone. Towards the east, i.e. towards the continental margin, sediment thickness increases significantly, but no sedimentary waves are observed. Wavy structures can also be recognized in the central part, where sediment thickness is at its minimum. These structures were not interpreted to be sedimentary waves due to their strict vertical alignment down to great depths. They may rather be seen as a kind of sedimentary stretching and faulting induced by the underlying basement topography.

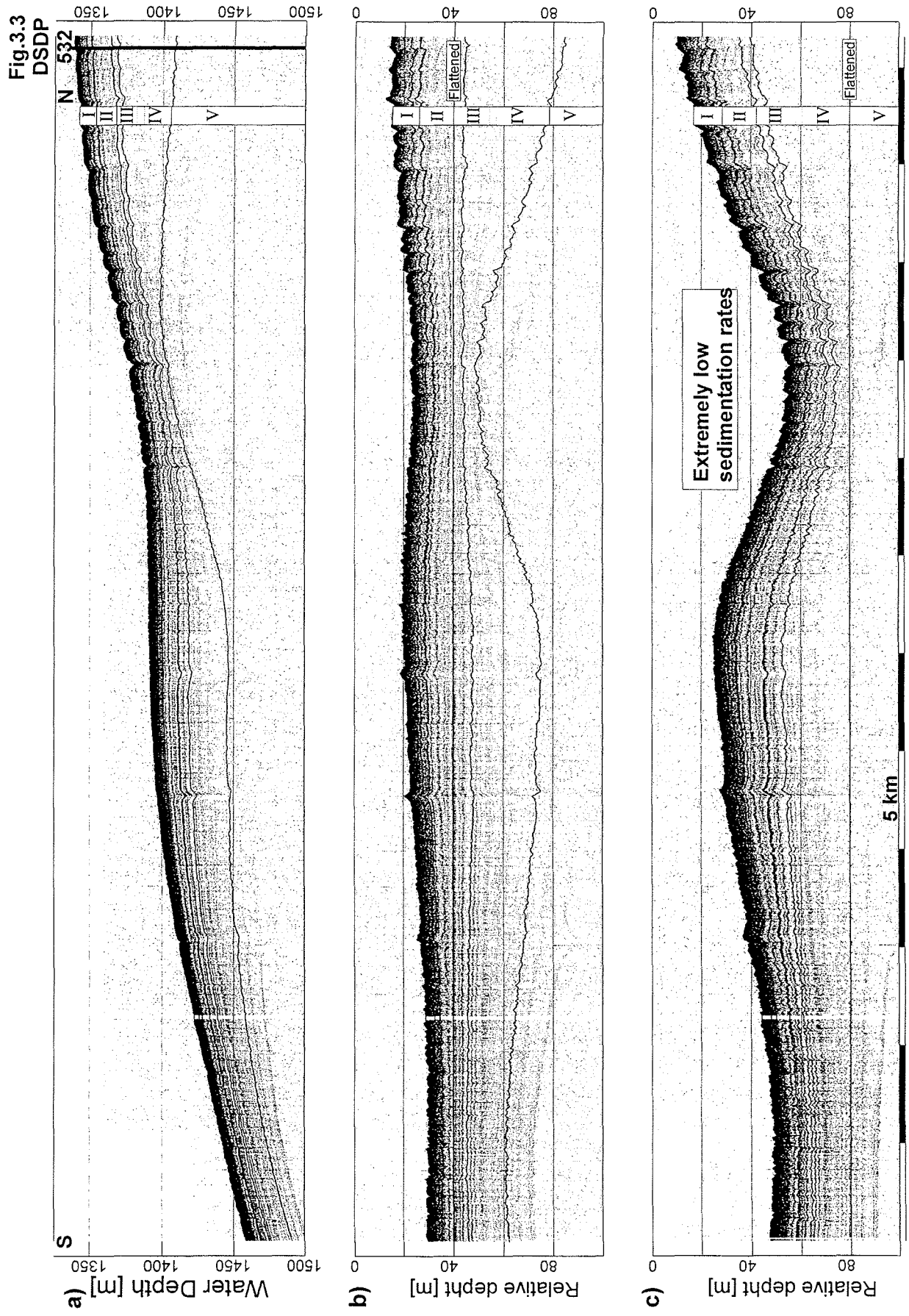

Figure 3.5: Parasound section extending from the crest of the Walvis Ridge in southeast direction. a) profile plotted using correct recording delays. Traced reflectors are indicated by black lines in profile. b) the same profile flattened to the boundary between Unit II and III. c) the same profile flattened to the boundary between Unit IV and V.

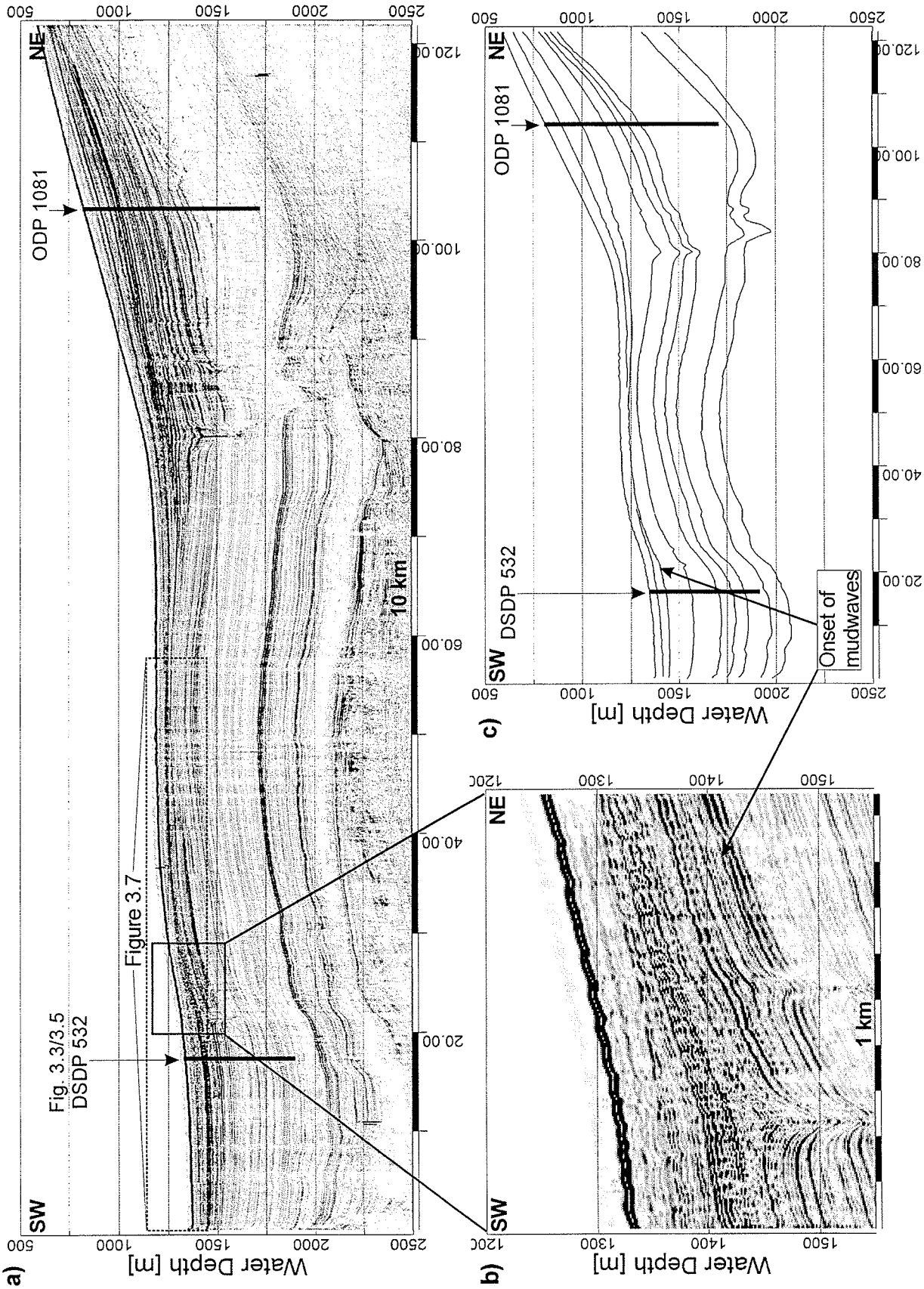

Figure 3.6: Seismic line along the Walvis Ridge crest. a) complete profile in gray scale representation. Position and penetration of DSDP site 532 and ODP Site 1081 is given as vertical black lines in the western and in the eastern part of the profile. b) Close-up of part of the mudwave area. Slight undulations in deeper reflectors mark the beginning of sedimentary wave growth. c) linedraw of the profile. The displayed horizons are chosen to emphasize the change in the sedimentation environment.

Several seismic reflectors were traced along this profile to allow the presentation of a linedrawing of the section (Fig. 3.6c). One of these reflectors, which is denoted by an arrow in Figure 6c as well as in Figure 3.6b, marks a prominent change in the sedimentation environment. Below this reflector, which intersects DSDP 532 at approximately 105 mbsf and ODP 1081 at 270 - 300 mbsf, sediments are well stratified and lateral sedimentation rate variations are neglectable. Above this reflector spatial sedimentation rates vary significantly. This change in depositional environment coincides with the onset of the development of sedimentary waves as can be seen in the enlarged section of Figure 3.6b. Above the marked reflector, sedimentary waves slowly start to grow and in parallel the area covered by waves extends further up- and downslope.

The lateral changes in sedimentation rate in Units I – V can be observed on this line as well, as the Parasound data indicate, which was recorded in parallel to the seismic line (Fig. 3.7, see dashed box in Fig. 3.6a for extension). However, a shift in water depth from 1200 m during Units V and IV to approximately 1250 m in Units II and I for the zone of minimum sedimentation rate can be recognized here. So far this observation is restricted to this along-crest profile and cannot be generalized, because more data from appropriate locations near the upper depth limit of the mudwave field are not available.

3.5 Discussion

3.5.1 Modeling

Mudwave models (*Flood*, 1988, *Blumsack and Weatherly*, 1989, *Hopfauf and Spieß*, 2000) show, that the main decision about the geometry of sedimentary waves is made during their initial creation. To create sedimentary waves, several parameters must match. First, depending on the water depth and geographic latitude only specific bottom current directions may create waves. Second, the bottom current velocity must be stable over time scales which are sufficient to build up sedimentary waves. These two conditions permit the existence of steady waves in the bottom velocity field, which cause the buildup of sedimentary waves. The necessary minimum time period for this process certainly depends on the sedimentary input from the water column which controls the building velocity. The magnitude of the current velocity and current direction as well as the initial topography then control the wave length and strike direction.

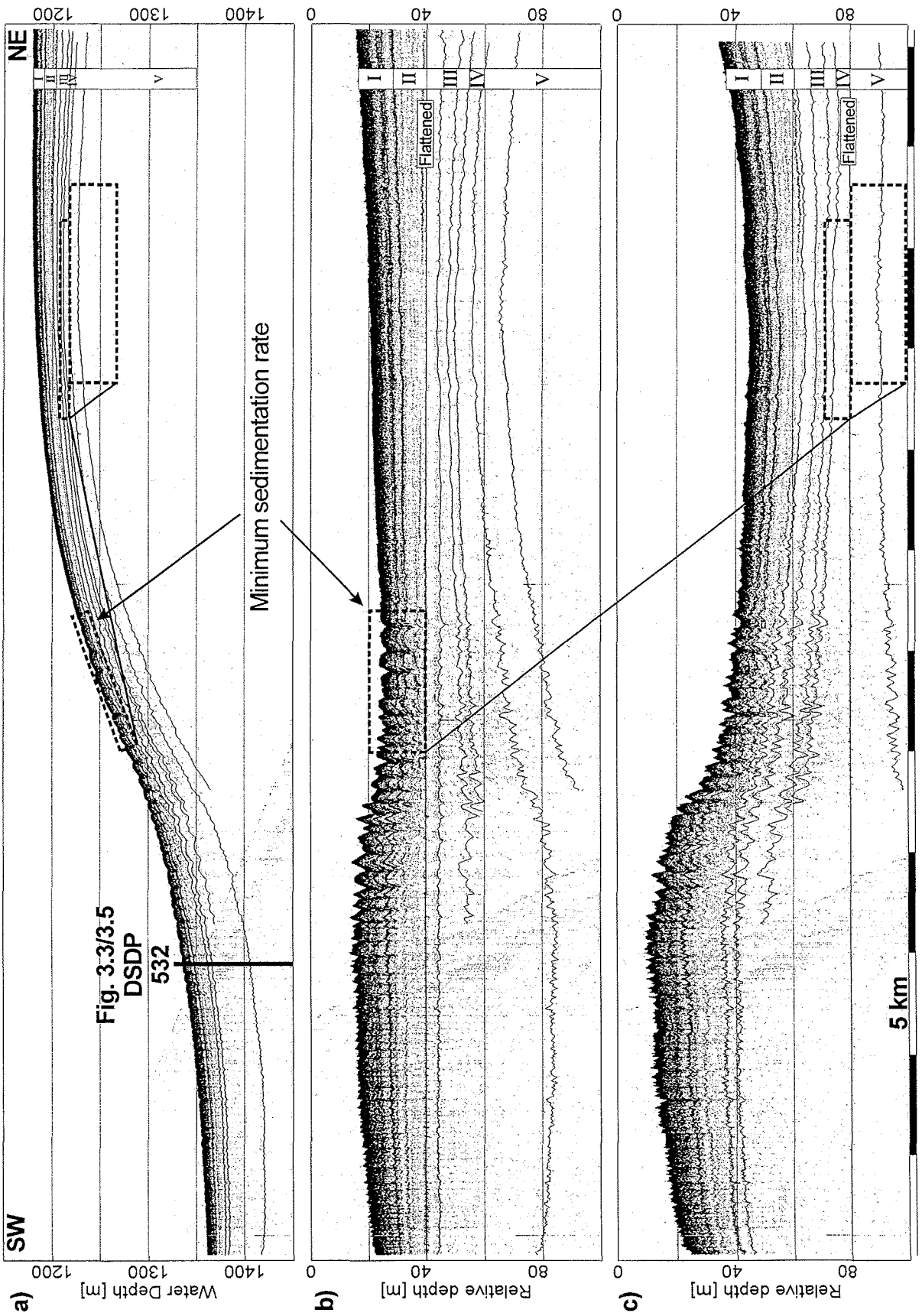

Figure 3.7: Parasound section parallel to the western part of the seismic line of Figure 6. a) profile plotted using correct recording delays. Traced reflectors are indicated by black lines in profile. b) the same profile flattened to the boundary between Unit II and III. c) the same profile flattened to the boundary between Unit IV and V. The dashed boxes mark the zones of minimal sedimentation rate for a specific time period.

The meaning of 'stable current conditions' in respect to the creation and growth of sedimentary waves, however, needs some considerations. As current measurements have shown (e.g.. *Weatherly et al.,* 1993, *v. Lom et al.,* 2001), the bottom flow usually is not stable at all, even in the deep sea. Strong tidal components often may play an important role as well as annual influences and others. These fluctuations also influence the settling of particles on the sea floor. Mudwave development, in contrast, takes place on time scales of several thousand years and therefore the term 'stable' has to be seen from a statistical point of view. As perturbations in the velocity field occur immediately if the outer conditions are appropriate, a 'stable' bottom current means that the majority of the local current situations has the corresponding properties and this over long periods. This will usually, but not necessarily, be close to the mean of the current properties. If we therefore are describing current velocities in the following paragraphs and use the terms 'mean' or 'stable', we always refer to this definition.

Once waves have been created, their topography stabilizes the corresponding bottom current system in respect to velocity perturbations. Changes in growth rate and migration rate of the waves are then the only indicators for long standing changes in bottom current velocity. Thus, a change of the wave length of the waves requires a peak in bottom current velocity to destroy the existing waves and build up new ones with a different wavelength. This process can be observed in Figure 3.2 in vicinity of the interface between the Units V and IV. The short waves of Unit V are eroded and on top of this zone new waves with a longer wavelength grow.

Due to these considerations, the mudwave geometry was used to obtain clues on the palaeocurrent situation on the Namibian continental margin, based on the mudwave model of *Hopfauf and Spieß* (2000). As shown already by *v. Lom et al.* (2001) the model predicts a broad velocity interval (~2 – 25 cm/s), where existing mudwaves persist (further on referred to as existence interval), for a southward flow. This interval becomes less broad (2 - 8 cm/s) for a northward flow but still the predicted situation is comfortable for sedimentary waves (Figs.3.8a, b). The calculated growth and migration rates for a southward flow are given as an example in Figure 3.9 for wave lengths of 300, 500 and 700 meters, respectively (curves are similar for a northward flow, but shifted to slower velocities). The positive part of the growth rate defines the width of the existence interval, but an optimum situation for sedimentary waves growth is reached towards the lower limit of the interval. In contrast, the migration rate increases towards higher velocities. Note that the high peaks in the curves represent a singularity in the model solution, which is a

consequence of the neglectance of viscosity (*Hopfauf and Spieß*, 2000). Positive growth rates are also given as shades of gray in Figure 3.8.

Generally, the growth rate for the study area is low and reaches higher values only in vicinity of the singularity. It can also be noted that the range of current velocities for optimum growth conditions is small, but the existence interval is broad. Hence the model allows a great variability in current velocities, which won't affect the wave geometry. Migration only occurs at high current velocities. Echosounder data, on the other hand, show that the waves do not change their shape significantly over the last 2 my and that they neither grow higher nor migrate. Slight migration trends occur in distinct layers, though, but a clear trend is not established.

It is therefore difficult to propose a quantitative interpretation of the model results in this region. But it may be stated that current velocities were most of the time not in the optimum range for wave growth and also not in optimum range for wave migration, but varying somewhere in between.

For two points in the geologic past we may narrow the broad existence interval. As stated above, the transitions from Unit V to Unit IV and from Unit II to Unit I are characterized by a destruction of existing mudwaves (Fig. 3.2) and a buildup of new ones. We can therefore derive a bottom current velocity at exposed locations, which exceeds 10 cm/s at the beginning of Unit IV and 15 cm/s at the beginning of Unit II. The wave length of the new mudwaves then depends directly on the bottom current situation at the time of creation, but also strongly on the initial topography (*Hopfauf and Spieß*, 2000). As it is difficult in the complex topographic environment of the study area, to consider the topography, we estimated the speed by assuming good growth conditions for waves of the observed wave length. We assume a reduction of current velocities, after the mentioned pulses, to 3 – 4 cm/s in Unit IV and 2 – 3 cm/s in Unit II.

Additional problems in model interpretation arise due to the ambiguity of the current direction within a 90 degree quadrant (*Hopfauf & Spieß*, 2000). The current velocity, predicted by the model and shown in Figures 3.8 and 3.9 is only the velocity component which is oriented perpendicular to the wave crest. Therefore the true current velocity may be considerably higher, depending on the angle of incidence. However, as we are dealing here with a contour current along the continental margin and strike direction of the waves is approximately downslope, the model velocity can be expected to be close to the true velocity.

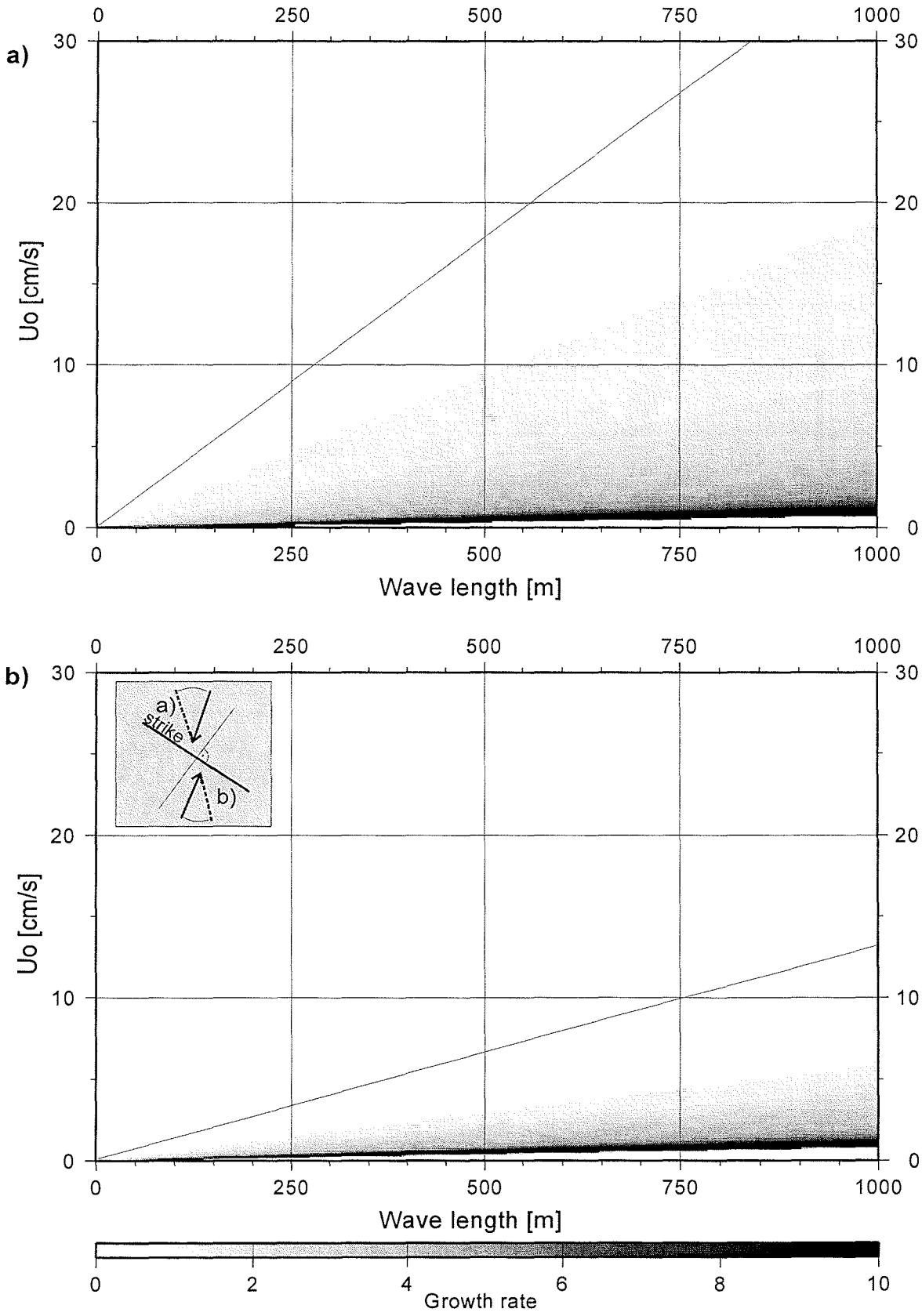

Figure 3.8: Existence interval for sedimentary waves at a water depth of 1300 m and a latitude of 19° 45' S. Strike direction of the wave crests is 125°. Shades of gray represent the calculated positive growth rate using dark shades for high growth rates and light shades for low growth rates respectively. a) southward flow. b) northward flow (see sketch in upper left corner of b for geometric setting).

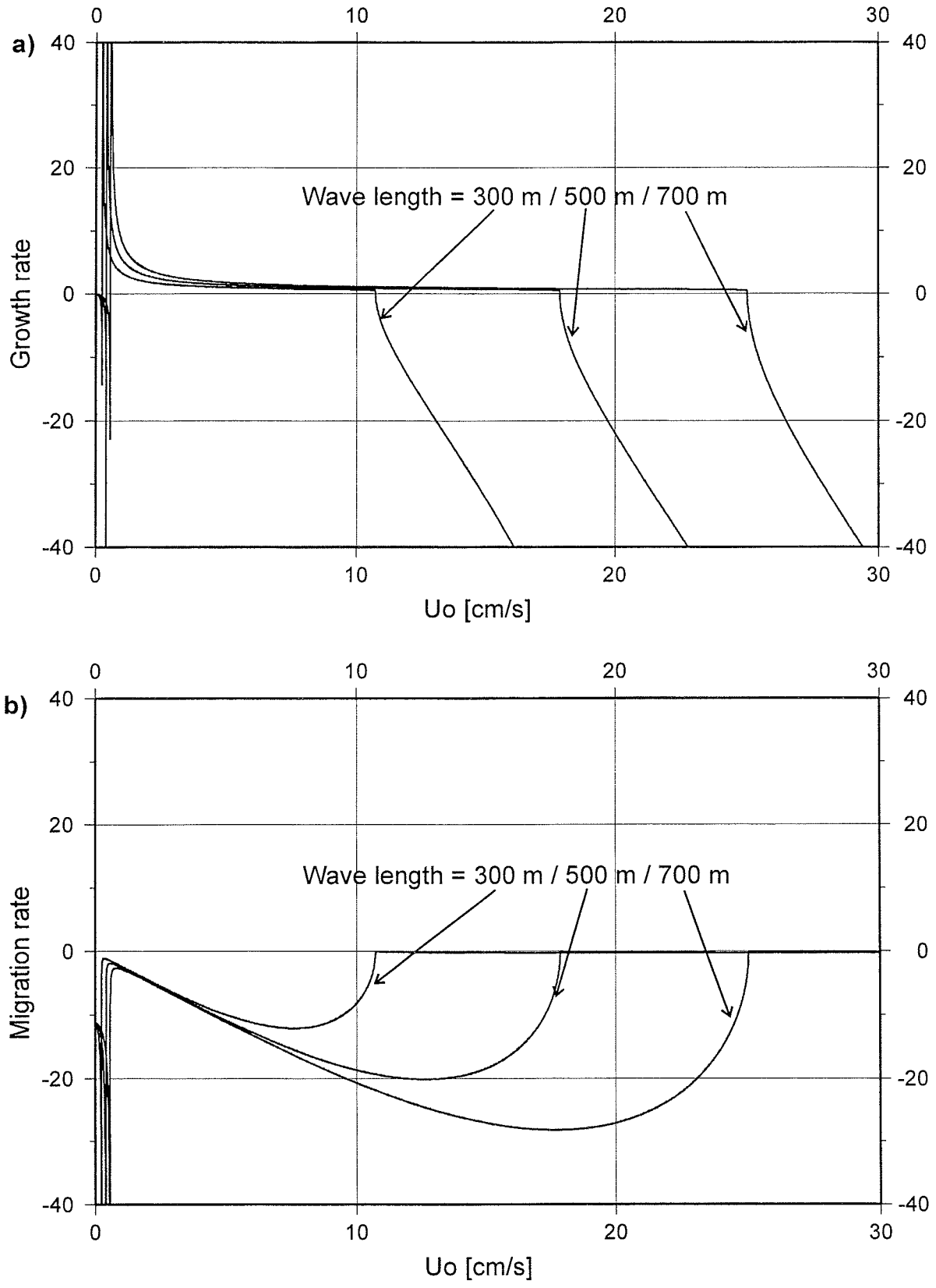

Figure 3.9: Growth (a) and migration rate (b) for a southward flow. Fixed model parameters are as in Figure 3.8. Curves are calculated for 300, 500 and 700 m wave length.

Another problem is our unawareness of the true density gradient in the near bottom layer of the water column. A main controlling factor for sedimentary wave growth is the Brunt-Vaisala-frequency (*Queney*, 1948, *Flood*, 1988, *Blumsack and Weatherly*, 1989, *Hopfauf and Spieß*, 2000) which depends on the density gradient in the water column. The model of *Hopfauf and Spieß* (2000) uses an approximation for the Brunt-Vaisala-frequency published by *Garret and Munk* (1972) for the free water column. However, sedimentary waves generate at the sediment-water interface and the corresponding bottom flow will not only support sedimentary wave growth but also mixing in the lowermost water layers due to small scale turbulences. This in turn may reduce the density gradient and cause a reduced Brunt-Vaisala frequency. As the waves in the study area reach only heights of a few meters and therefore are probably bathed in the mixed layer, this problem may affect the predicted model velocities, shifting them to smaller values.

3.5.2 Sedimentation patterns

In addition to the existence of sedimentary waves, large scale and small scale changes in sedimentation patterns show evidence of a varying influence of bottom currents. The observed effect is a spatial variability of sediment thickness in the different acoustic units. These variations differ depending on the sediment age, as well as on the place of deposition.

Variations in sediment thickness could also be caused by fluctuations in sediment input, especially as the study area is located west of one of the most important upwelling areas of the world, and therefore a drop in biogenic sediment supply outside the upwelling area is likely to occur. A drop in input material could explain the general trend in reduced sediment thickness seen in the seismic data (Fig. 3.6) on profiles leading from upper continental margin to the deep sea. However, as shown already by *v. Lom et al.* (2001), sedimentation rates increase again beyond the deeper depth limit of the wave field. Furthermore, pronounced variations in sedimentation rates occur on small scales of only a few tens of kilometers (Figs. 3.3, 3.4, 3.5, 3.7). These changes cannot be explained by varying sediment input, but only with varying bottom current velocities related to local topographic features.

This interpretation is supported by the coincidence of changes in the lateral sedimentation rate distribution on the one hand and changes in the geometry of the sedimentary waves on the other. The transition from Unit V to Unit IV, where model

results suggest a significant increase in bottom current intensity, is also marked by a noticeable increase in spatial sedimentation rate variability (Fig. 3.3 and 3.5).

The ratio of neighboring maximum and minimum sedimentation rate at a specific location may be taken as a qualitative indicator of bottom current intensity, $v_{bottom} \approx \frac{S_{\max}}{S_{\min}}$. This parameter certainly depends on the sediment composition of the input material, which controls the reaction of settling particles on current velocity. If we assume a mean sediment composition over long time periods, which did not change considerably in the last 2 my, this parameter may nevertheless be used for comparison with the mudwave model results, as is done in Figure 3.10.

Another qualitative parameter indicating the local intensity of bottom currents is the critical distance of deposition to a deep sea current obstacle as a seamount. Such obstacles, located in the path of a bottom current, cause a local increase of current velocity in their close vicinity, which may prevent sediment deposition or even cause erosion, hence yielding onlapping or truncated reflectors. The distance of these onlap points depends on the local topography of the obstacle, the sediment composition and the general current velocity. As topography does not change significantly and if we assume the same for the mean sediment composition (see above), changes in the critical distance of deposition are directly related to changes in general current velocity. We therefore use this parameter derived at the foothill of a small seamount (Figure 3.4) as a second qualitative proof of our model results (Figure 3.10).

3.6 Conclusions

The interpretation of the model results and the qualitative current indicators resulting from sediment distribution as described above show a significant correlation (Fig. 3.10). Therefore we propose the following palaeocurrent history for deep water transport at the eastern Walvis Ridge:

- ~ 5 Ma: Onset and growth of sedimentary waves, accompanied with lateral spreading of the wave field (Fig 3.6b). In parallel a striking reduction in sedimentation rate on the Walvis Ridge occurs (Fig. 3.6a). This was probably caused by the establishment of a stable contour current passing the Walvis Ridge in southward direction. The mean velocity can be expected to reach 2 – 3 cm/s in the corresponding depth range. As the first waves started to grow, they stabilized the

velocity field perturbations and caused a slow lateral extension of the wave field. At the same time the influence of the bottom current lead to reduced sedimentation rates. The development of sedimentary waves and the implied stability of bottom current parameters may probably be seen as an indicator of the evolving stratification of the South Atlantic Ocean (*Woodruff and Savin*, 1989) and the intensification of NADW.

- ~ 5 Ma - ~ 1.9 Ma (Unit V): In the following 3 my the wave field further extends laterally and covers the Namibian continental with small regularly spaced waves. However, at least for the last 500 ky of this period, sedimentation patterns show reduced mean bottom flow velocities, probably only reaching up to 2 cm/s.
- ~ 1.9 Ma: At the transition from unit V to unit IV a notable increase in bottom current velocity leads to an erosional destruction of the waves at exposed locations (Fig. 3.2). The increase in current velocity (probably more than 10 – 15 cm/s) is also quite obvious in the sedimentation patterns (Fig. 3.10). This event coincides with the time of maximum NADW production, derived by Berger and Wefer, 1991) for this period, and suggests a maximum water transport across the Walvis Ridge.
- ~ 1.9 Ma - ~ 1 Ma (Unit IV): Consecutively, NADW production becomes more and more affected by orbital forcing and increases and decreases accordingly with an overall reduction in water transport. As the bottom current wanes, the destroyed waves build up again near the end of this unit, however their wavelength now reaches 750 m, suggesting a mean current velocity of more than 4 cm/s at their time of creation. The corresponding local changes of lateral sedimentation rates show accordingly strong variations at the beginning of Unit IV with a decrease of variations towards Unit III and hence also reflect a relatively intense bottom current, which looses strength with time.
- ~ 1 Ma – 600 ka (Unit III): During the next 400 ky the situation remained stable with slow to moderate current velocities presumably not exceeding 3 – 4 cm/s. The sedimentary waves do not show any significant geometrical changes and lateral sedimentation rate variations still exist, but are not very pronounced.

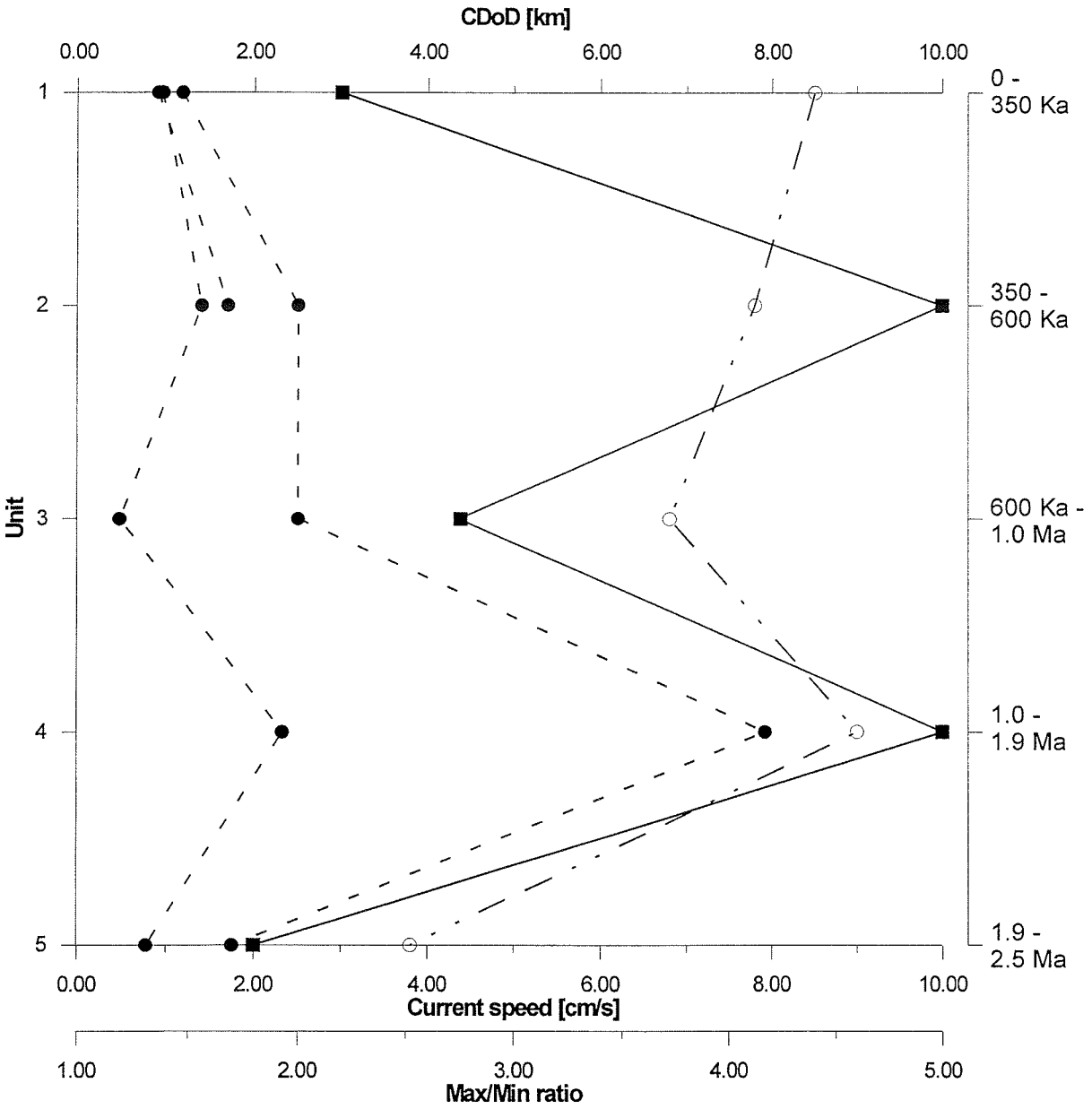

Figure 3.10: Comparison of model results (solid line), max-min-ratio of neighboring zones of maximum and minimum sedimentation rate (dashed lines) at three different positions, and critical distance of deposition in the vicinity of a seamount (named as CDoD, dash-dotted line). The different amplitudes of the max-min-ratio reflect the dependence on local topography of this parameter.

- ~ 600 ka – 350 ka (Unit II): This again is a phase of increased bottom current activity. While it is not possible, to describe exactly what happens to the waves at exposed locations, because the changes of sedimentation patterns here are quite complex (Fig. 3.2), the variations of lateral sedimentation rates suggest another increase in current velocity. This becomes particularly obvious in Figure 3.4, which shows a strong retreat of the reflectors from the seamount. At the end of Unit II the buildup of new waves at several positions with wavelengths of 500 – 600 meters marks the most recent stable situation and suggests slightly lower mean current velocities of ~ 3 – 4 cm/s.
- 350 ka – recent (Unit I): The most recent time of wave existence was a quiet phase regarding the time scales necessary for changes in mudwave parameters. From the model point of view mean current velocities do not exceed 4 cm/s. However, lateral sedimentation rate distributions suggest higher current velocities (Fig. 3.10), as corresponding variations still exist and especially the critical distance of deposition remains high in Figure 3.4. This discrepancy may be explained by the increasing influence of the northern hemisphere glaciation which causes cyclic waxing and waning of NADW production and AABW production, respectively. The fluctuations in deep water production may well result in significant fluctuations in bottom current velocities in the study area with increased activity in glacials and decreased activity in interglacials. This in turn may cause the observed variation in sedimentation rates. In contrast, the temporal resolution of palaeoceanographic changes in the sedimentary wave geometry is not sufficient to resolve glacial cycles, as sedimentation rates are generally low. If changes in bottom current velocities remain inside the existence interval and therefore no wave destruction occurs, they can not be derived with the help of the model here. Hence a current velocity varying between ~ 3 and ~ 8 cm/s is presumed for this period.

3.7 Acknowledgements

We owe thanks to the participants of the R/V METEOR Cruises M20/2, M34/1, M34/2 and R/V SONNE Cruise So86, which supported us in supervising the echosounding systems. With their help it was possible to collect high quality data on a 24 hour schedule. This study was funded by the Deutsche Forschungsgemeinschaft (Sonderforschungs-bereich 261 at Bremen University). This is contribution no. Xxx of SFB 261.

4 Mudwaves on the western flank of the Zapiola Drift, Argentine Basin – Evidence for variations in Late Quaternary bottom flow activity

H. v. Lom, V. Spieß and V. Hopfauf

4.1 Abstract

The extensive fields of deep basin mudwaves, which drape the flanks of the Zapiola Drift in the central Argentine Basin, provide a record of the long term stability of bottom water flow patterns. Combining observations from a dense grid of high resolution narrow beam echosounder data with results of wave growth modeling confirms that a southward oriented current is responsible for the wave geometry at the western flank of the drift. This flow seems to be the western part of a cyclonic gyre, which is centered around the Zapiola Drift. The regional variation of accumulation rates suggests that the flow velocity gradually decreases upslope the drift flank. To the north east of the crest, flow velocities increase again, causing a southwestward migration of the crest itself. Changes in the internal geometry of the mudwaves show evidence for cyclic variations in flow intensity during the last 100 ky. Flow was intensified in the Holocene and from 40 to 25 ka. Periods of weaker current activity occurred from 25 to 10 ka and from 100 to 40 ka. The associated velocities fluctuate between 10 and 20 cm/s, causing erosion, non-deposition and deposition on the less depositional wave flanks.

4.2 Introduction

Sedimentation in the Argentine Basin is mainly influenced by deep water current systems. Especially the Antarctic Bottom Water (AABW), which is spreading below 3800 – 4000 m (*Reid*, 1989), controls the deposition of particles in the central basin. AABW enters the Argentine Basin from the south through the Falkland gaps (*Le Pichon et al.*, 1971a) and around the Falkland Plateau in the east (*Wüst*, 1957, *Le Pichon et al.*, 1971a), turns westward and passes the Falkland Escarpment until it turns to the north at the Argentine continental margin. AABW flow continues as an intensified western boundary current to the north along the continental margin and penetrates to some extent the Brazil Basin through the Vema Channel (*Hogg et al.*, 1982, *Speer and Zenk*, 1993) and

the Hunter Channel (*Speer et al.*, 1992). According to *Reids* (1989, 1996) geostrophic calculations a significant part of AABW turns eastward at the Rio Grande Rise and back southwards at the Mid Atlantic Ridge, forming a basin wide deep water anticyclonic gyre in the Argentine Basin (Fig. 4.1a).

However, the presence of huge drift deposits with sediment thickness exceeding 2 – 3 km in the central basin (*Ewing*, 1971) suggest a more complex pattern of deep water circulation in the Argentine Basin. This circulation is still poorly known. Short term direct current meter measurements were deployed by *Le Pichon et al.* (1971b) and *Reid et al.* (1977) at several locations in the basin. Long term direct current measurements (12 – 18 month) are available for the Vema Channel passage (*Hogg et al.*, 1982) and for some locations on the Argentine continental margin and on the northern flank of the Zapiola drift (*Weatherly*, 1993). Basin wide studies have been performed by *Ledbetter* (1986), who used sediment particle size distributions in core top samples as a proxy for bottom current activity. *Flood and Shor* (1988) analyzed an extensive set of bottom photographs taken throughout the Argentine Basin to derive bottom current directions and intensities. They suggest a secondary cyclonic gyre, centered around the Zapiola Drift complex at 45° S, which implies an eastward oriented counter current along the southern flank of the Zapiola drift (Fig. 4.1a). Recent studies on AABW CFC-distribution (chlorofluorocarbon, CFC) seem to confirm the existence of this cyclonic gyre (*Smythe-Wright and Boswell*, 1998, *Orsi et al.*, 1999).

4.2.1 Argentine Basin mudwaves and the project MUDWAVES

The drift deposits in the Argentine Basin are known to be draped by the largest mudwaves of the world. Mudwaves are nearly sinusoidal, though in the Argentine Basin often asymmetrical, sedimentary structures, which are thought to develop under the influence of bottom current activity. Typical mudwave heights in the deep basin are 25 to 30 m at wave lengths of 5 to 6 km (*Klaus and Ledbetter*, 1988, *Flood and Shor*, 1988), but heights of up to 150 m and wave lengths of up to 10 km have been observed (e.g. *Fox et al.*, 1968, *Flood and Shor*, 1988; *Manley and Flood*, 1993b). According to *Klaus and Ledbetter* (1988), the area covered by mudwaves in the Argentine Basin extends to $1x10^6$ km^2.

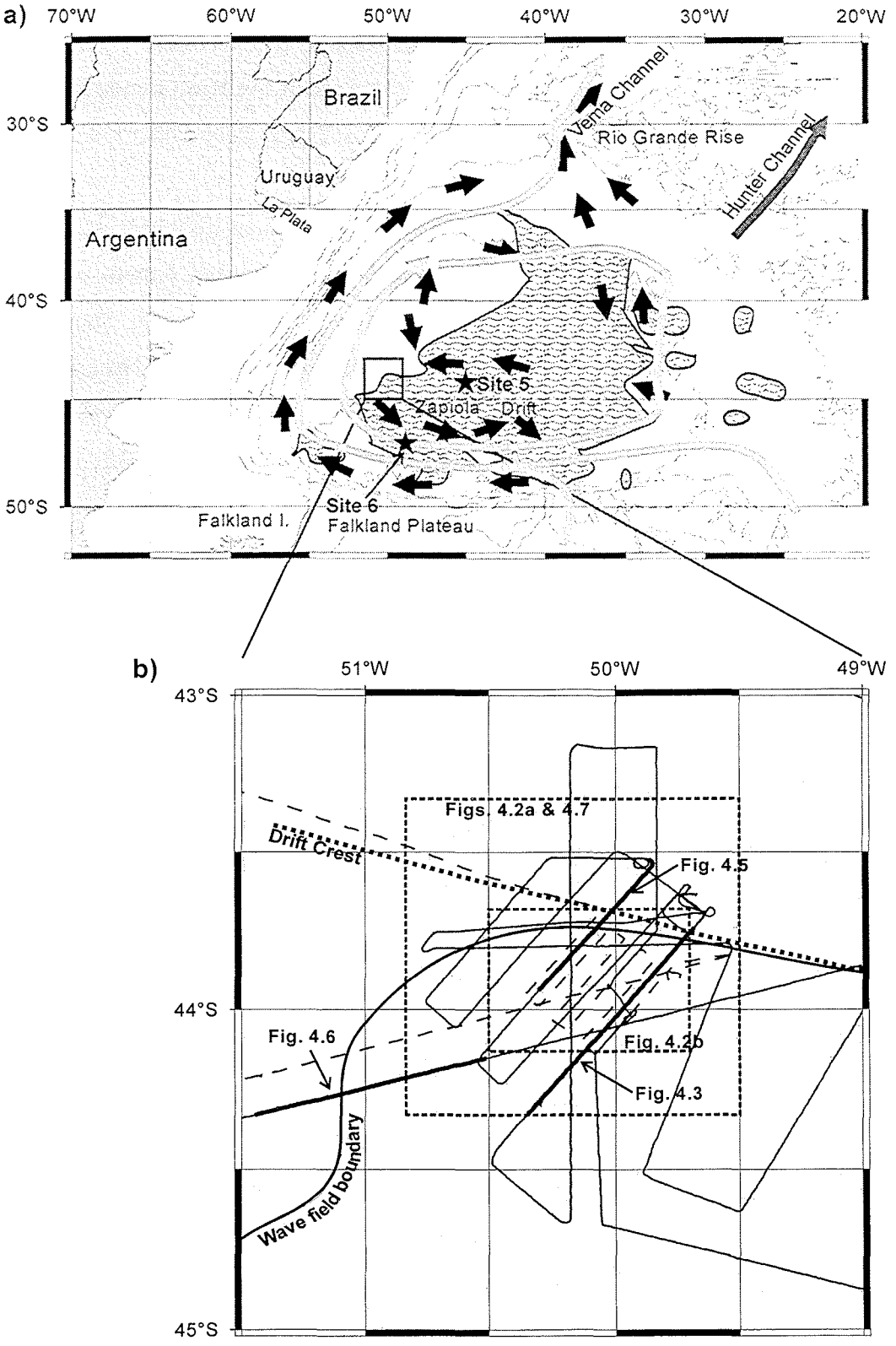

Figure 4.1: a) General AABW flow patterns in the Argentine Basin after *Reid* (1989, 1996) (⇑) and after *Flood and Shor* (1988) (↑). The extent of the mudwave coverage in the deep basin is indicated by the wavy pattern (after *Klaus and Ledbetter*, 1988). The exact location of the study area is denoted by the rectangle on the western Zapiola Drift, locations of project MUDWAVES Sites 5 and 6 are also given. b) Enlarged view of the study area with the cruise tracks of METEOR Cruises M29/1 (*Segl et al.*, 1994) (long dashed line) and M46/3 (*Bleil et al.*, 2000) (solid line). Data sections presented in the following figures are denoted by thicker lines and dashed rectangles. Bathymetry for a and b is from *Smith and Sandwell* (1997).

Mudwaves develop over long time scales. Seismic data from the Zapiola Drift have shown mudwave activity down to 0.4 to 0.5 s TWT below the seafloor (*Flood et al.*, 1993). Mudwaves therefore do not reflect short term variations in bottom flow activity, but provide information about the long term evolution of bottom flow patterns. In an unique effort to better understand the processes, which cause the growth and development of these bedforms, and their relationship to bottom near circulation patterns, a multi-disciplinary study was initiated in 1986 to visit several mudwave sites in the Argentine Basin. During this study, the project MUDWAVES, waves at the northern (Site 5) and southern (Site 6) flank of the Zapiola Drift and from the southern flank of the Ewing Drift (Site 7) were mapped, using multiple acoustic systems (SeaBeam, 3.5 kHz echosounder, watergun seismics), and sampled with piston, gravity and box cores (*Manley and Flood*, 1993a). Bottom photographs, long term current and transmissiometer measurements and CTDs were used to improve insight in the modern oceanographic situation.

The results of project MUDWAVES could confirm the thesis of theoretical models, which attribute the observed migration of the waves to across-wave variations in flow velocity (*Flood*, 1988, *Blumsack and Weatherly*, 1989). Accumulation rates on the steeper wave flanks are much higher than on the more gradual wave flank (*Anderson et al*, 1993, *Jones*, 1994). This is also reflected in water content profiles across the waves (*Flood et al.*, 1993). Grain size analyses of samples from both wave flanks gives also direct evidence of higher flow velocities over the less-depositional, more gradual wave flank (*Ledbetter*, 1993).

The existence of a dense net of high quality narrow beam echosounder data on the westernmost end of the Zapiola Drift (Fig. 4.1b), collected with R/V Meteor in 1994 (*Segl et al.*, 1994) and 2000 (*Bleil et al.*, 2000) now allows a detailed insight into the internal structure of the mudwaves. Past changes in the wave symmetry are attributed to variations in long term bottom flow activity. In combination with a recently developed extended mudwave model (*Hopfauf and Spieß*, 2000), these changes are analyzed to obtain clues on the late Quaternary history of the deep Argentine Basin circulation. The location of the study area also provides the possibility to investigate the processes, which occur at the borders of the mudwave field, in particular at the drift crest.

4.3 Methods

4.3.1 Acoustics

Echosounder data were recorded using a Parasound echosounder system (*Grant and Schreiber*, 1990). The system was operated at a signal frequency of 4 kHz. Henceforth it reaches a penetration depth, which is comparable to a conventional 3.5 kHz echosounder, but vertical resolution is enhanced because of a broader signal bandwidth. Compared to conventional systems horizontal resolution is also improved due to the beam width of only 4° , i. e. ~7 % of the water depth. This results in a footprint of only ~ 350 – 420 m in the study area. Consequently the effect of side echoes is minimized, which is especially important at a rough or undulating seafloor topography.

To obtain along-track bathymetry information, a Hydrosweep swath sonar (*Grant and Schreiber*, 1990) was used with a swath width of 90°. The system is operated at a signal frequency of 15.5 kHz. Through active beam forming the swath is divided into 59 beams with an aperture of 2.5° each. Hence the Hydrosweep system provides bathymetry information on a stripe, which is twice the water depth in width, corresponding to up to 12000 m in the study area.

Both acoustic systems are roll, heave and pitch corrected to ensure a fixed reference plane and a vertical sound emission. However, it has to be noted, that in particular the quality of the Hydrosweep data suffered in rough sea from its mount position in the ships hull of R/V Meteor and good quality swath sonar data are only available on a limited number of profiles.

The Parasound data were digitally recorded using the ParaDigMA system (*Spieß*, 1993) and stored for further processing in a compressed SEGY format. After applying a bandpass filter with a pass band of 2.0 to 6.0 kHz to reduce high frequency electronic and low frequency acoustic noise, the data were displayed using a grayscale presentation. For interpretation, distinct reflectors were picked and manually traced along the profiles.

Hydrosweep data were processed using the public domain software packages Multibeam (MB) (*Caress and Chayes*, 1996) and GMT (*Wessel and Smith*, 1995). The data were carefully edited to remove erroneous soundings (*mbedit*, MB). A spline gridding algorithm (*mbgrid*, MB) was used to grid the data onto a regular mesh. Gridded data were further filtered using a Gaussian weighted mean filter (*grdfilter*, GMT) with a filter width of 4 km to reduce high frequency gridding noise and to emphasize the mudwave topography.

A similar processing was carried out on traced reflectors to obtain contour plots of sediment thickness in the study area. The reflector depth values were resampled on a regular mesh using a mean filter of 180 m width (*blockmean*, GMT). The resulting mesh, however, contains data values only at nodes which are close to the profile. Therefore the mesh was gridded with a spline algorithm (*surface*, GMT) to fill the gaps. Finally, the mesh was filtered with a Gaussian weighted mean filter (*grdfilter*, GMT) of 4 km width. Because the gaps between the profiles are partially wider than a mudwave length, display and contouring of the mesh is restricted to a 'stripe of confidence' along the profiles. This means that only mesh nodes, which are not further away than 5 km from profile data, are considered confidential.

4.3.2 Stratigraphy

Stratigraphic information on the sediments of Argentine Basin drifts is very sparse. Uranium-series analysis (^{210}Pb and ^{230}Th), performed by *Anderson et al.* (1993) on project MUDWAVES Sites 5 and 6, revealed high differences between sediment ages on both wave flanks. These differences could be confirmed by ^{14}C-datings (*Jones*, 1994) on the same locations. However, these measurements were carried out on box core samples and therefore are restricted to the upper 50 cm of the sediment column. *Jones* (1994) also performed AMS-^{14}C-datings on four piston cores from opposite wave flanks at project MUDWAVES Sites 5 and 6, respectively. His results suggested accumulation rates of 30 to 100 cm/ky for the depositional wave flank. At the opposite wave flank, accumulation rates varied from 2 – 10 cm/ky. *Flood et al.* (1993) and *Ledbetter* (1993) used an estimated linear accumulation rate of ~30 - 40 cm/ky on the depositional flank. This estimation was based on the box core measurements mentioned above. Diatom assemblages, complemented by magnetic data, were used by *Manley and Flood* (1993b) to date sediments, retrieved by piston cores on a mudwave site on the southern Ewing drift. Sedimentation rates here could be estimated to reach 100 cm/ky on the depositional flank.

The dating of drift deposits is complicated by the composition of the sediments. They are thought to be a mixture of reworked material from the continental margin, river load, imported material from the Southern Ocean and pelagic biogenic material, originating more or less in place at the sea surface. Eddies and the associated benthic storms are known to be frequent phenomena along the Argentine continental margin and especially in the region of the Brazil / Malvinas confluence (*Cheney et al.*, 1983, *Provost and Le Traon*, 1993, *Fu*, 1996). Benthic storms may stir up deposited material (*Gardner and Sullivan*,

1981, *Hollister and McCave*, 1984), which in turn is transported by bottom currents and deposited in the quieter regions of the central basin (*Flood and Shor*, 1988). Additionally, gravity transport down the steep Argentine continental slope will put already deposited material back to suspension and redistribute it (e.g. *Balsam and Wolhart*, 1993). Material from the Southern Ocean is known to be imported by the AABW and transported over long distances (e.g. *Jones and Johnson*, 1984). Surface plankton blooms, observable by satellites, may considerably contribute organic matter to the drift sediments (*Richardson et al.*, 1993). Finally, material in the wave field may be reworked by local erosion and deposited elsewhere in the wave field. Discrepancies in ages estimated by *Anderson et al.* (1993) and *Johnson* (1994) have mostly been contributed to this problem (*Anderson et al.*, 1993).

Due to a lack of age determinations in the vicinity of our study area, we use the estimation of *Flood et al.* (1993), which was derived in the same depositional environment but some 150 km apart, and extrapolate ages linear to greater depths. We are aware, that this approach implies some inaccuracies, particularly because the high variability of accumulation rates in the working area makes the lateral position of the dated samples an important factor for estimated sedimentation rates. However, the general observations made below remain valid on a relative time scale and the discussed implications on palaeoflow history fit well with results derived at other locations in the mudwave area (*Ledbetter*, 1993).

4.3.3 Modelling

To model the growth and migration of the mudwaves, we use the model of *Hopfauf and Spieß* (2000). The model takes into account the water depth at the specific mudwave site, the geographic latitude, the wave length, the wave height and the strike direction of the waves and calculates the disturbed velocity field of a given bottom current, which flows over the sinusoidal seafloor topography. It extends existing models of *Flood* (1988), and *Blumsack and Weatherly* (1989) in using the full three-dimensional coriolis vector. This allows consideration of the absolute wave strike direction and absolute flow direction. The calculated disturbed velocity field can then be used to estimate a sedimentation rate distribution across the waves and in turn to predict wave migration and growth (see *Hopfauf and Spieß*, 2000, for details of model analysis).

The modeling of mudwave evolution has shown, that it is difficult to explain the onset of mudwave growth. The initial topography of the seafloor in combination with a steady

mean bottom flow controls wave length and wave strike direction of initially created waves, but these starting parameters are usually hard to determine and the interaction between seafloor and bottom flow is arbitrarily complex. A possible mechanism for the onset of a mudwave field was proposed by *Hopfauf and Spieß* (2000) based on an initial topography of a linear elongated obstacle.

In contrast, if a mudwave field and hence a regular sinusoidal seafloor topography already exist, the reactions of a stratified bottom flow on the topography can be modeled with a linear model approach. Corresponding calculations show that a sinusoidal topography on the seafloor causes periodic perturbations in the bottom flow velocity field, which in turn influence the depositional behavior of particles in the water column. Particles will tend to deposit at locations where the flow velocity is reduced, compared to locations where flow velocity is increased. This process of preferential deposition (*Flood*, 1988), causes the growth or migration of mudwaves. The term 'deposition', though, is slightly misleading, as it suggests a true deposition of particles. The sign of the 'deposition' may well become negative, hence effectively describing erosion, if boundary conditions as suspension composition, mean flow velocity and associated perturbation amplitudes are appropriate. The location of maxima and minima of flow velocity in the disturbed velocity field is controlled and stabilized by the initial sinusoidal topography. Therefore changes in the mean flow parameters, strength and direction, cannot change the general mudwave geometry, i.e. the wave length and strike direction, but may result in changes in migration rate and growth rate of the waves. However, model results also showed that the disturbances in the velocity field are small compared to the mean flow velocity. Changes in mudwave geometry caused by changes in growth and migration rate will therefore usually be superimposed by the much stronger effects of mean flow increase or decrease.

4.4 Data

The bathymetry in the study area is characterized by a smoothly ascending slope from the main pathway of AABW in the south-west to the drift crest (Fig. 4.2a). Mudwaves here have a wave length of ~ 5 km and a height of 25 to 30 m, which is typical for Argentine Basin mudwaves (*Klaus and Ledbetter*, 1988, *Flood and Shor*, 1988). The general observed strike direction of the waves could is ~ 135°, although towards the north east the direction changes to ~160° (Fig. 4.2b).

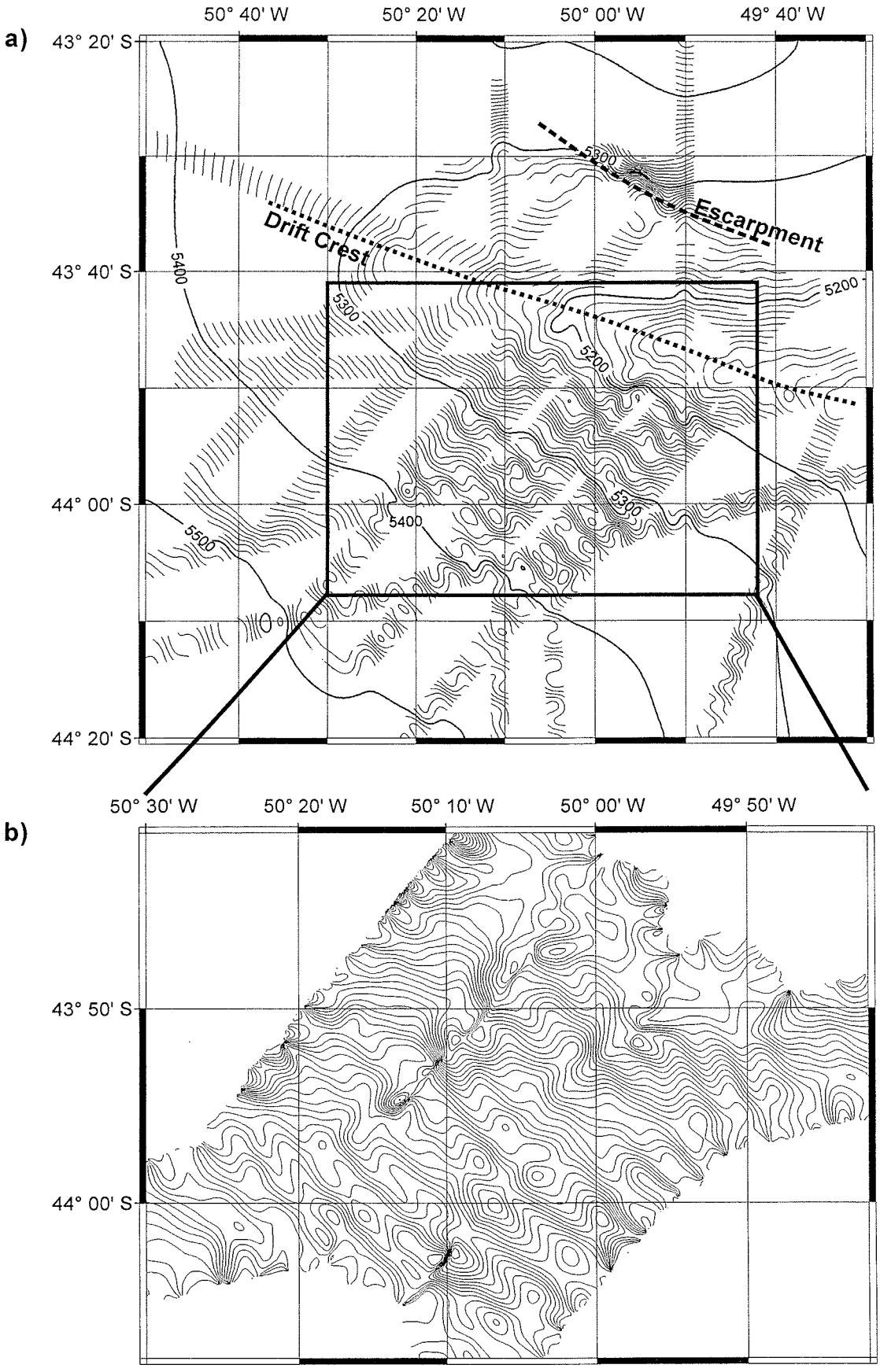

Figure 4.2: High resolution seafloor topography. a) Topography derived from Parasound data. b) Topography derived from Hydrosweep data.

It should be noted, that the bathymetry presented in Figure 4.2a is obtained by interpolation between single echosounder profiles. The line spacing, however, is sufficiently small to identify the mudwaves and to allow a precise determination of their strike direction. The comparison to good quality swath sonar data (Fig. 4.2b) confirms the observations.

The drift crest at the western Zapiola Drift separates two different depositional regimes. To the south, well developed mudwaves exist, whereas in the north waves become increasingly smaller and finally disappear. A distinct step in seafloor topography, caused by erosion or sediment slide, is located ~20 km north-east of the crest. Here older and buried mudwaves are cut off.

The data coverage in the study area therefore allows both an analysis of mudwave evolution, and an investigation of processes, which occur at the upper and lower water depth limit of the mudwave field.

A typical echosounder line from the center of the study area is shown in Figure 4.3a (see Figure 4.1b for reference). This profile is oriented nearly perpendicular to the strike direction of the waves and therefore shows wave length and migration directions not distorted. As described already by *Flood and Shor* (1988), *Klaus and Ledbetter*, (1988), and *Flood et al.* (1993) for other sites on the Zapiola Drift, the waves show an asymmetric morphology with one flank accumulating most of the deposited material (further on referred to as depositional flank), and the other flank accumulating significantly less material or even being eroded (further on referred to as less-depositional flank). The resulting migration direction of the wave crests is oriented upslope towards the crest of the sediment drift.

Examination of the internal structure and acoustic facies of the waves reveals six different acoustic facies types within penetration depth of the echosounder signal. These units differ in reflection strength or in wave asymmetry, i.e. in the sedimentation rate ratio (SRR) on both wave flanks, or both, respectively. The uppermost acoustical Unit I is characterized by a comparably high reflectivity and a high SRR. Beneath this unit, reflectivity in Unit II as well as the SRR is significantly reduced. Unit III resembles Unit I in reflectivity and SRR, while sediments in Unit IV show a lower reflectivity and the SRR is small. The boundary between Units IV and V is marked by a very pronounced reflector, which can easily be recognized all over the study area. Deposition of Unit V occurred nearly symmetrically on both wave flanks and reveal a low reflectivity. The deepest Unit VI shows again an increased SRR. However, the boundary between Unit I and Unit II is

difficult to detect towards the deeper and upper limits of the wave field. Towards the drift crest, reflectivity in Unit II increases, making the position of the boundary indistinct, towards the deeper basin, sediment thickness in Unit I is strongly diminished.

The SRR, as well as the overall sedimentation rate are not equally distributed throughout the wave field. This is demonstrated particularly for Unit IV by shifting the seismogram delay to obtain an approximately flat boundary between Units IV and V (Fig. 4.3b). The thickness of Unit IV, which appears as a transparent band in this laterally condensed presentation, increases by a factor of 2 towards the drift crest. The sinusoidal 'topography' of the flattened section reflects the preferential particle deposition on the upslope wave flanks (maxima) and reduced deposition on the downslope wave flanks (minima).

This presentation is also useful to distinguish between erosion and non-deposition (Fig. 4.4). If the current velocity gradually varies such that it causes a shift from deposition to non-deposition, one would expect bended reflectors, which converge smoothly towards the point of minimum deposition (Fig. 4.4a). In contrast, if the current velocity locally exceeds the critical value, at which erosion occurs, the result would be a steplike break of the reflectors in a flattened section (Fig. 4.4b). According to this assignment, intervals of erosion, non-deposition or deposition in Unit IV vary along the profile. Erosion occurred on downslope wave flanks in the southwestern part of the profile, while in the central part non-deposition prevails. Towards the drift crest, material is also deposited on downslope wave flanks.

Sedimentation rates decrease continuously across and to the north-east of the drift crest. A close-up Parasound section (Fig. 4.5) also reveals decreasing wave heights. At some point on the north-eastern flank of the crest waves vanish completely. 50 m below the crest, a 5 km wide platform with a highly reflective top layer outcrops the drift flank. This platform has a wavy topography and the corresponding subbottom reflectors as well show an undulating mudwave topography. The platform is cut by a 40 m high steep break, which also cuts the underlying reflectors. Further north, signal penetration is limited to only a few meters and the seafloor is characterized by many overlapping hyperbolae. As an effect of the reduced sedimentation rates on the north eastern drift flank, the drift crest itself migrates to the south west, as is indicated by the thick line.

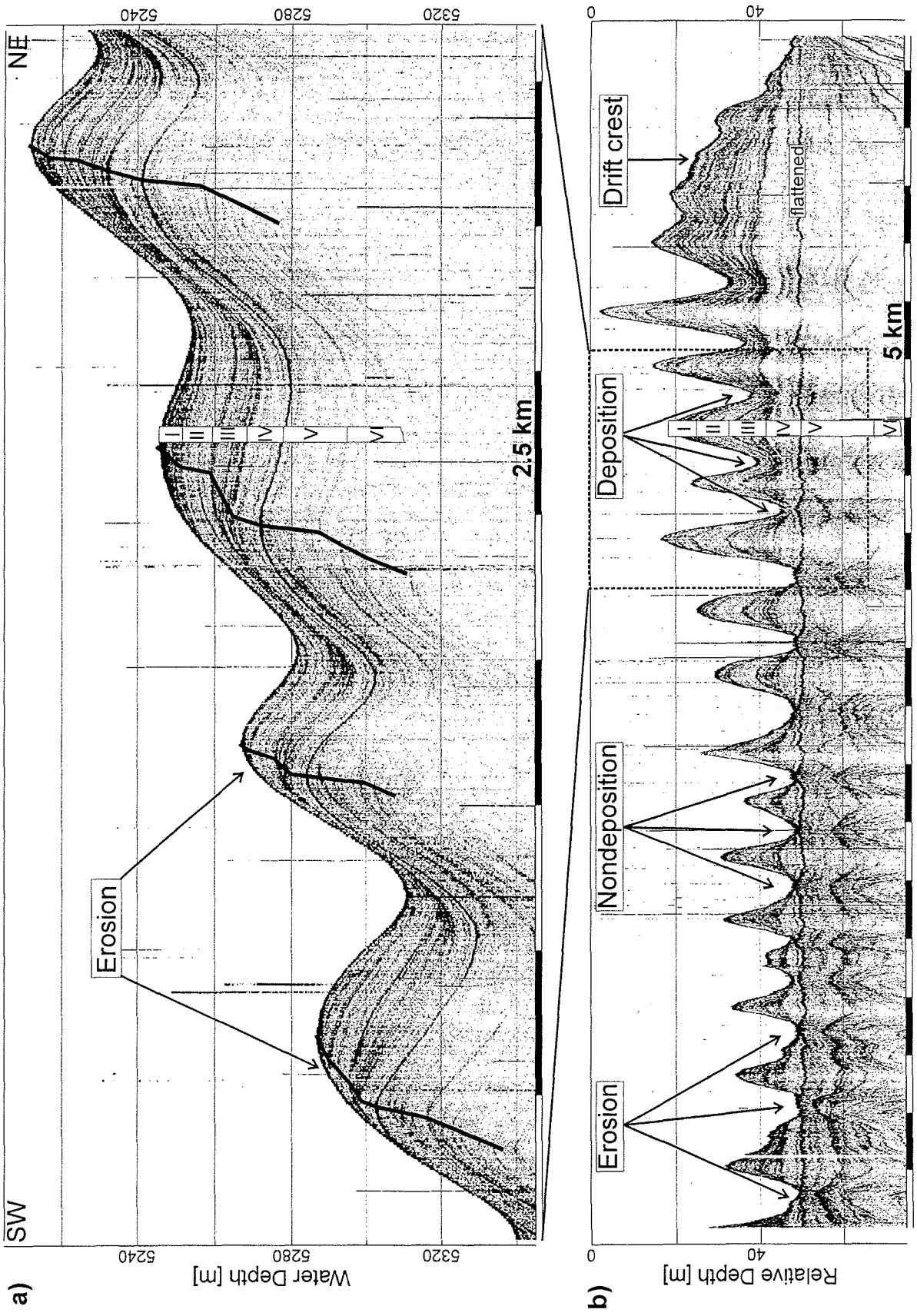

Figure 4.3: Parasound section recorded perpendicular to the wave strike direction in the central part of the wave field. a) short partial section. Thick lines trace the wave crest migration. Distinction in acoustic Units is indicated for one of the waves. b) Lateral condensed section, flattened to the boundary between Unit IV and V. The remaining undulations in the flattened reflector result from inaccuracies in manual reflector tracing.

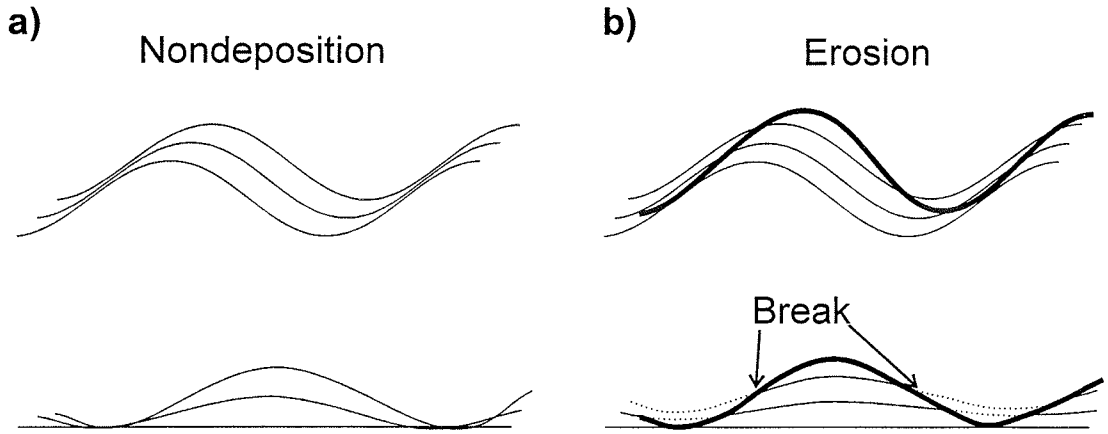

Figure 4.4: Different appearance of non-deposition and erosion in a flattened section. Top sketches show true sedimentation processes, bottom sketches show the resulting flattened reproduction.

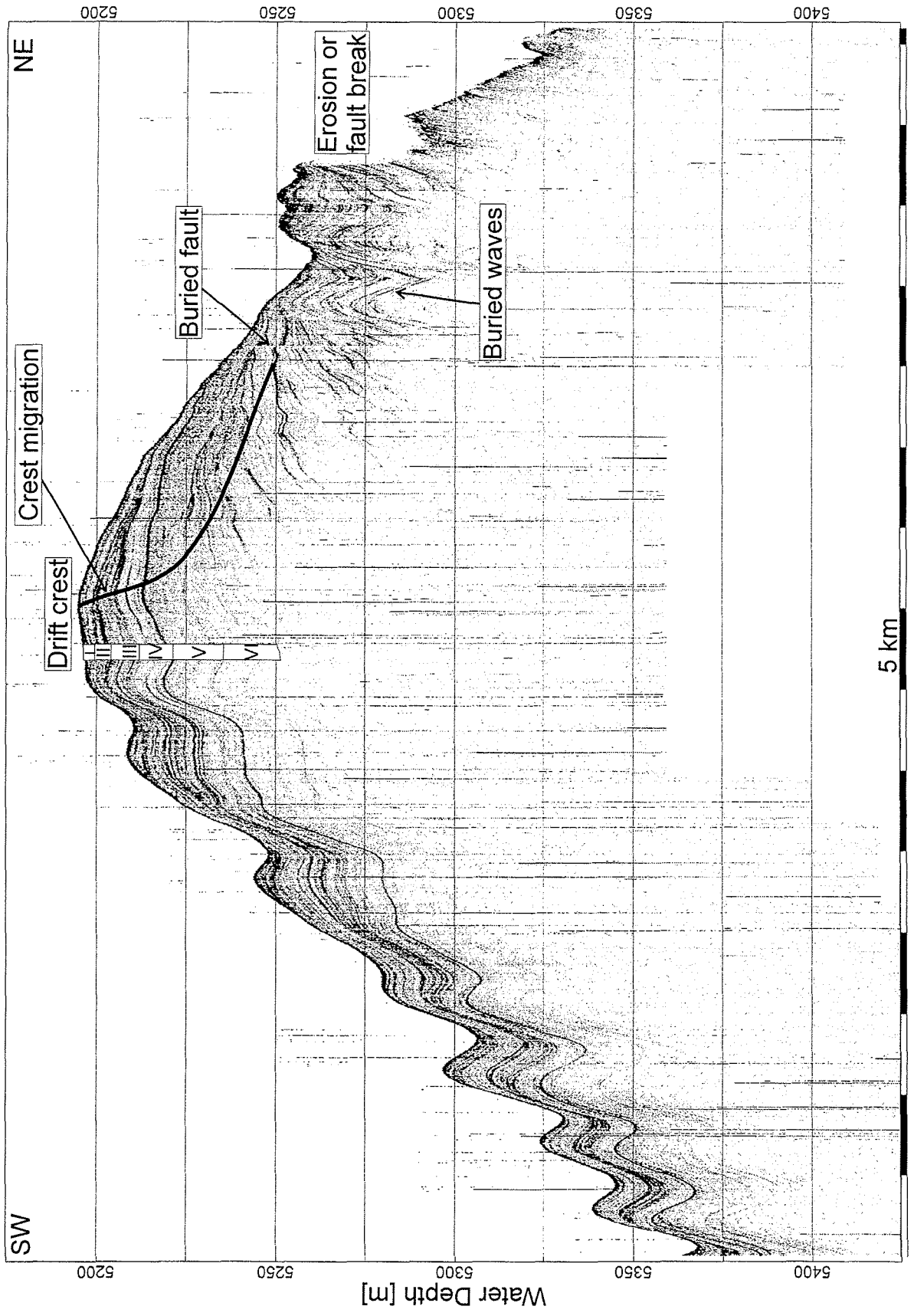

Figure 4.5: Parasound section across the drift crest. Note the older, buried waves, which outcrop on the north eastern drift flank 50 m below the crest. The crest appears to migrate to the south west.

Towards the deeper limit of the wave field (Fig. 4.6), which is here at 5625 m water depth, wave heights also decrease. At greater water depths reflectors appear parallel stratified, but partially show a small-scale roughness. An acoustically transparent layer of 5 to 8 m thickness is found on top on a length of ~35 km, where stratified sediments are present elsewhere. The wave field boundary seems to be stationary in time, at least within the signal penetration depth.

To examine the spatial variation of sedimentation rates throughout the study area, we traced the boundaries between the different sedimentary units (see Figure 4.3) along all available echosounder profiles. The calculated and interpolated thickness of each unit is given as a shaded image in Figure 4.7. The boundary between Units I and II, however, could not be traced all over the study area because sediment coverage in Unit I is often very thin. Therefore sediment distribution in Unit I and II is comprised in a single figure.

Sediment thickness increases towards the drift crest. This trend not only occurs in Unit IV, as shown already in Figure 4.3b, but is a general property of all four units. A similar, but less pronounced trend can be recognized in a direction parallel to the drift crest where the sediment thickness moderately decreases with increasing water depth. Mudwaves still show up as linear elongated features at the south-western drift flank. This is a result of the asymmetric sediment deposition on upslope and downslope wave flanks. Hence the waves appear more prominent in Units I to III, where migration rate and corresponding wave asymmetry are higher than in Units IV and V.

4.5 Model Results

We use in this study the model of *Hopfauf and Spieß* (2000), described above, to obtain clues on the bottom flow pattern in the study area. General model parameters were chosen as follows: a water depth of 5300 m, a latitude of 45° S, a strike direction of 135° and a wave length of 5 km. This is typical for the mudwaves in the study area, because the model is not very sensitive to minor changes to these parameters. The mean bottom current velocity vector was split into its components normal to and along the wave crests, U_0 and V_0, respectively. Both components were varied from –20 to 20 cm/s to simulate all possible bottom current directions and strengths within the given interval.

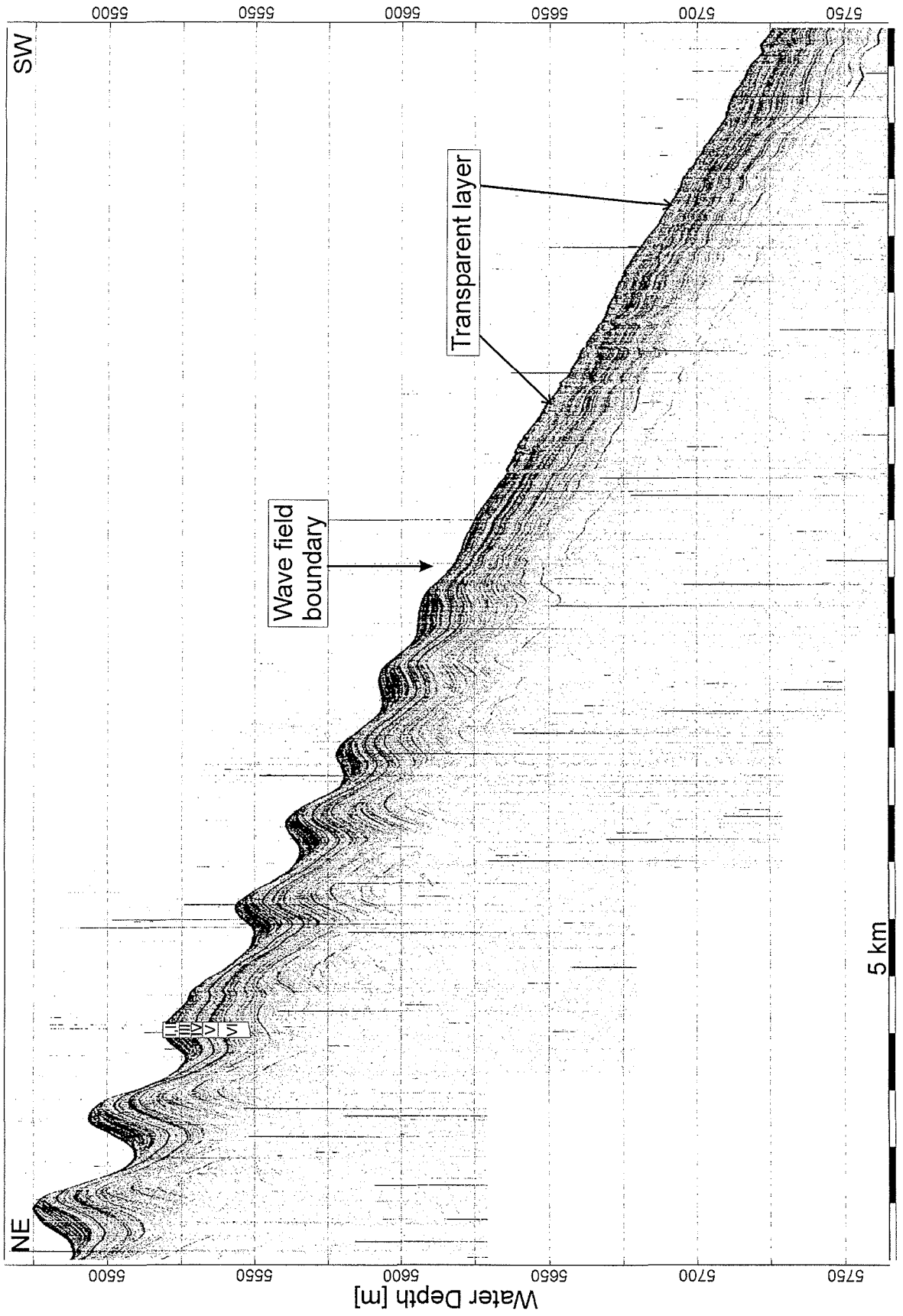

Figure 4.6: Parasound section across the deep border of the mudwave field. Acoustic Unit I could not be traced separately to this depth because sedimentation rates drop below the vertical resolution. Hence Unit I is denoted together with Unit II here. Classification in units is shown in the north east of the profile.

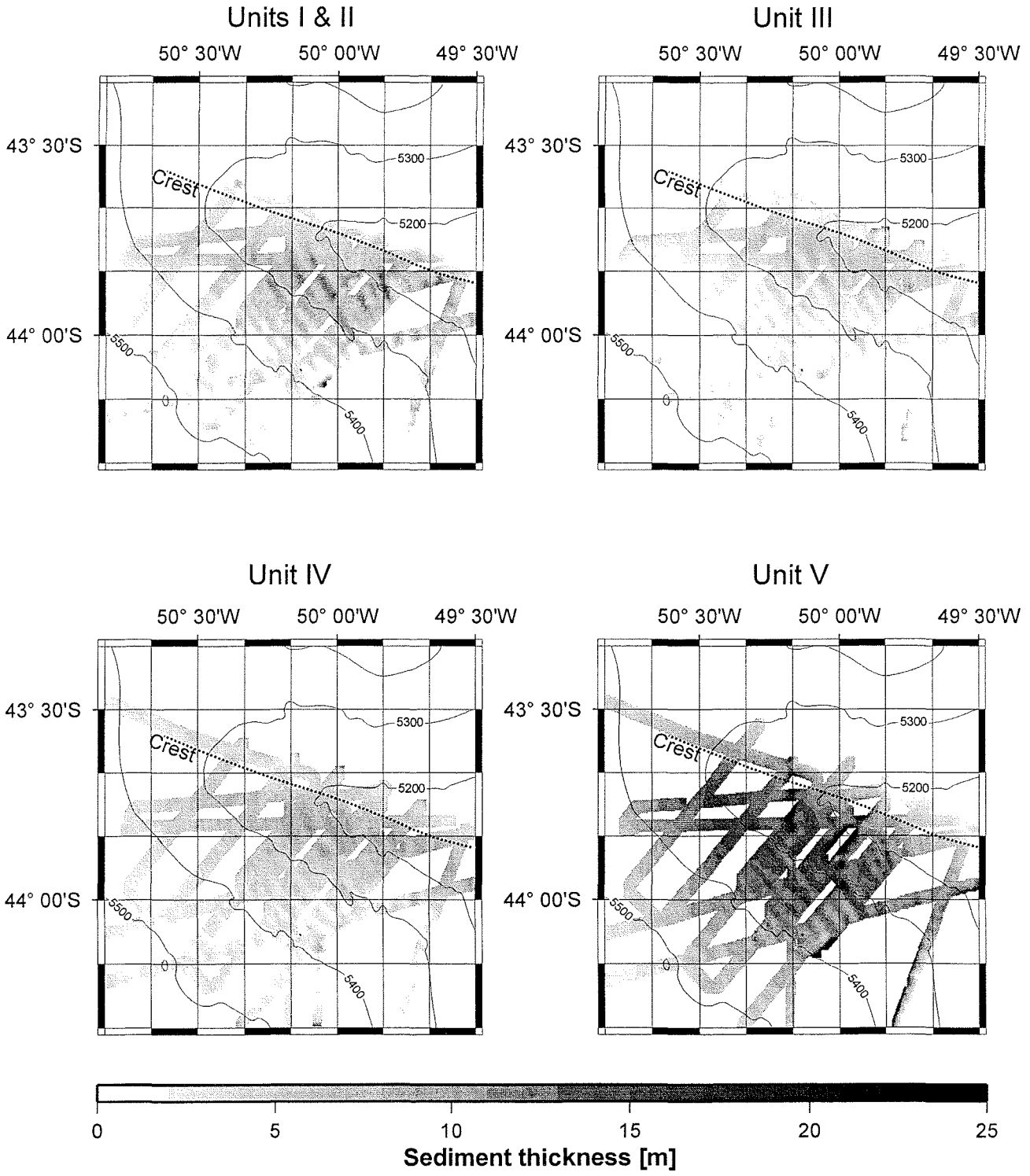

Figure 4.7: Lateral distribution of accumulation rates for the different acoustic units. White zones in the southwestern lines of Unit I, Unit II and Unit III could not be traced, because no sediment is deposited on downslope oriented wave flanks. The bathymetry lines are taken from Figure 4.2a.

The resulting distribution of wave migration rate and growth rate is presented in Figure 4.8. The graphs are oriented parallel to the true strike direction of the waves. Gray shaded regions show combinations of U_0 and V_0, which support a mudwave development as is observed in the study area, i.e. a positive growth rate (Fig. 4.8a) and an upslope migration (Fig. 4.8b). Positive growth rate means, that sedimentation rates are higher on the wave crests, than in the wave troughs, while upslope migration means, that sedimentation rates are higher on the upslope facing wave flanks than on the downslope facing flanks. Note also, that upslope migration implies a negative (upstream) migration rate for U_0 oriented to south west and, vice versa, a positive (downstream) migration rate for U_0 oriented to the north east. At a south-westward oriented U_0 of ~ 8 – 10 cm/s the model has a singularity, which causes growth and migration rates to reach extreme values, but is also associated with an abrupt transition to wave destruction for lower or higher values of U_0, respectively (Fig. 4.8a).

Model results predict a growth of mudwaves only for a very restricted range of flow vectors. In contrast, upslope migration is a wave property, which would occur under very variable flow conditions. To facilitate interpretation, we combined both model results in a single graph (Fig. 4.9). Shades of gray now still are a measure of upslope migration rate, but only displayed, where a positive growth rate prevents destruction of the waves. This further narrows the range of mean velocity vectors, which support the observed wave development. In general, only two different flow constellations are predicted.

- A mainly southward oriented current would require mean velocities varying from 10 to 20 cm/s to maintain the existing wave field. The broad velocity interval and the tolerance against moderate changes of the flow direction make this solution very stable.
- A mainly eastward oriented flow with velocities of about 12 to 16 cm/s would result in a downstream migration of the waves and therefore produce similar sedimentary patterns. However, the velocity interval is much narrower than is predicted for a southward flow and migration rates are small.

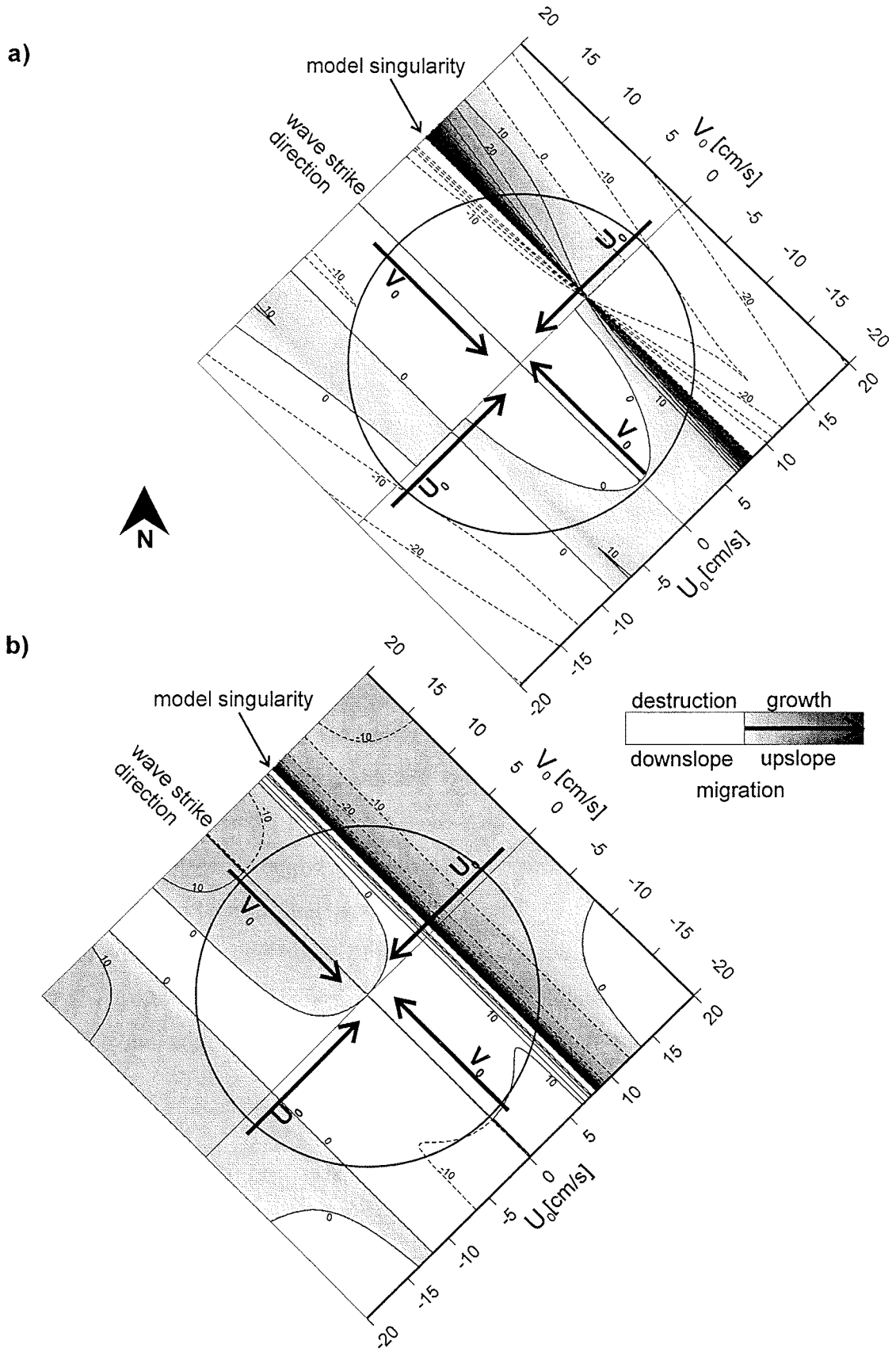

Figure 4.8: Distribution of a) growth rate and b) migration rate as predicted from model analysis. Isolines may be seen as qualitative measure for the rates. Dashed lines are given for negative rates, solid lines for positive rates, respectively. However, the sign of migration rates has to be interpreted relative to the direction of U_0 (see text for details). Shades of gray mark areas, which support the observed mudwave development, non-supporting areas were left blank.

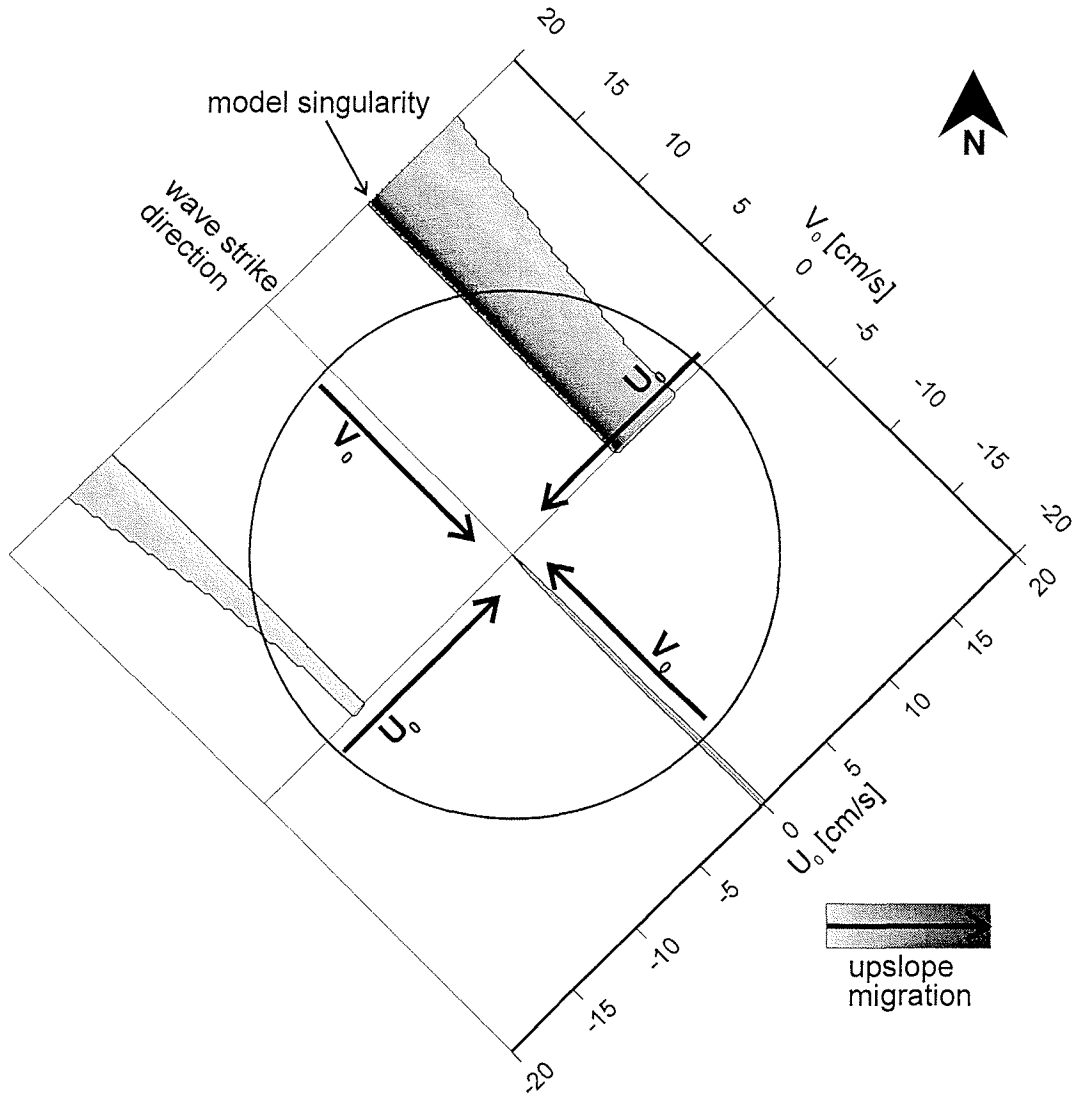

Figure 4.9: Combination of growth rate and migration rate. Shaded are regions, which support wave growth *AND* upslope migration. Shades of gray give the value of the migration rate.

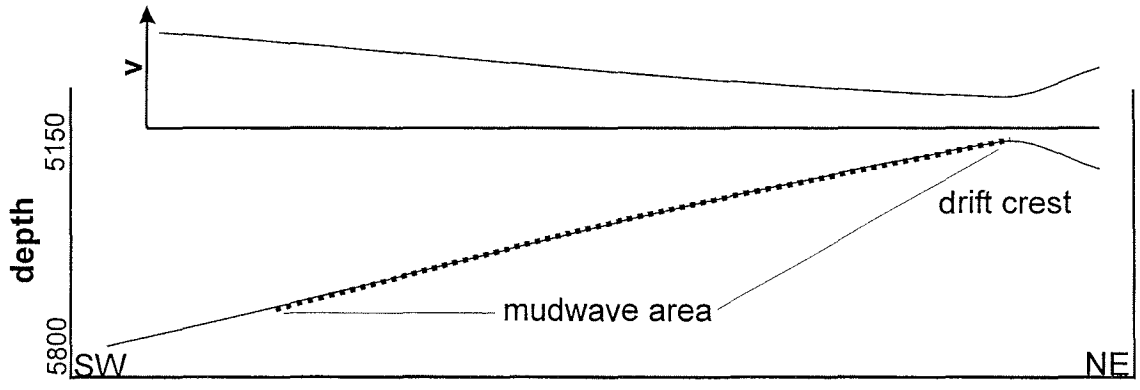

Figure 4.10: General trend of flow speed across the drift flank as estimated from the distribution of accumulation rates.

4.6 Discussion

The concept of preferential deposition is the basis of all interpretations of current related deposition patterns. It assumes that the settling of particles form the water column is controlled by the bottom flow velocity and the composition of the suspension load. Therefore spatial or temporal variations in accumulation rate may be attributed to spatial or temporal fluctuations in bottom flow velocity, if the sediment composition remains homogenous. This concept may be applied on small scales as the development of mudwaves described above, as well as on large scales as the growth of drift deposits. The lateral distribution of accumulation rates on the westernmost flank of the Zapiola Drift (Fig. 4.7) with increasing sediment thickness from the deep basin towards the drift crest therefore suggests a parallel gradual decrease of bottom flow velocities (Fig. 4.10). At and to the north east of the crest sediments show a transition from reduced deposition to non-deposition and finally even to erosion (Fig. 4.5), which may be interpreted with a corresponding increase in flow velocities on a short distance. This general trend may be traced back in time at least for the last 100 ky without significant variations. To quantify these observations and to obtain clues on the bottom flow strengths and directions and their variations in the past we propose a careful investigation of model results and comparison with observed changes in mudwave geometry.

Although model results suggest, that an eastward oriented flow cannot be completely excluded, the broad variability and higher migration and growth rate favor a southward flow to interact with the observed mudwave topography (Fig. 4.9). This is in close agreement with the bottom flow pattern of *Flood and Shor* (1988), who proposed a cyclonic gyre, centered around the Zapiola drift (Fig. 4.1a). This gyre will require a southward oriented branch at its western end, where our study area is located. Model velocities of 10 to 20 cm/s are confirmed by direct current measurements from the northern flank of the Zapiola drift (Site 5 of project MUDWAVES, see Fig. 4.1a), which yielded mean current velocities of 10 – 15 cm/s (*Weatherly*, 1993).

At the drift crest an increase in flow intensity can be inferred from the decreasing accumulation rates. In parallel the mudwaves decrease in height and vanish completely on a short lateral distance (Fig. 4.5). The observed effect agrees with our model results, which predict a decreasing growth rate for increasing flow speeds (Fig. 4.8a). This process may be further promoted by a clockwise turn of the flow direction to the north of the crest.

However, the flow along or over the crest may cause complex flow patterns, probably including turbulence. Based on our knowledge and data we cannot distinguish these conditions.

Similar effects may control the position of the deeper limit of the wave field (Fig. 4.6). An increase in current velocity beyond a critical value may be the cause for the absence of mudwaves in deeper regions. Model results show that also a decrease in current velocity would have this same effect, but a decrease is not likely, as the distribution of accumulation rates shows (Fig. 4.7). The cyclonic gyre, centered around the drift, however, also supports other explanations. It is known that the main flow path of AABW follows the Falkland escarpment westward and then turns northward along the Argentine continental margin. There must therefore exist a transition zone between this flow path and the opposite oriented cyclonic gyre. This transition zone will be highly turbulent, due to the high flow velocities of the involved water masses and this turbulence will most certainly not support the development of mudwaves. The situation is further complicated by the frequent occurrence of benthic storms, which are associated with eddies, travelling along the continental margin. We therefore suggest, that the area upslope of the deeper limit of the mudwave field marks the beginning of a more stable central part of the cyclonic gyre, which is not, or very sparsely, affected by the main flow path turbulence.

The recent history of the waves shows significantly increased SRRs in Units I, III, and VI, while deposition was more symmetrical in Units II, IV and V. The periods with an increased SRR may be explained by higher mean flow velocities, but model results show that an anti-clockwise turn in flow direction may also be a possible cause. Generally, velocity perturbations are small compared to the mean flow, except in vicinity of the model singularity (Fig. 4.8). A turn in current direction might move the current vector close to the singularity and migration and growth rate would increase significantly. However, growth rate and migration rate show a similar trend (Figs. 4.8a and 4.8b). As they represent phase components of the same sedimentation rate distribution across a mudwave, the net effect of growth and migration results from superposition of both. Therefore it is difficult to directly derive true migration rates from the model results. Furthermore, the region of increased growth and migration rate near the singularity is quite narrow and would require an extremely stable flow situation to influence the wave geometry. We therefore assume increased flow velocities as the cause for the observed higher SRRs. This interpretation is also in agreement with the assumption of a decrease in flow velocity from the deep basin towards the drift crest, proposed above, because in

parallel to the increase in overall accumulation rate a shift from erosion through non-deposition to deposition on the downslope oriented wave flanks is observed on the drift flank (Fig. 4.3b).

Based on an estimated linear accumulation rate of 30 – 40 cm/ky we porpose a moderate to fast flow velocity of ~ 15 cm/s for the time before 100 ka, followed by a more quiet period with flow velocities of 10 – 15 cm/s. During this period, mudwaves grew nearly symmetrical and wave crest migration was diminished. At an interpolated age of 40 to 45 ka the bottom flow intensified to mean flow velocities of 15 – 20 cm/s, causing high wave crest migration rates and partial erosion on downslope facing wave flanks of deeper located waves. A period of weaker bottom flow, probably also with speeds of 10 – 15 cm/s occurred from 25 to 10 ka. In the Holocene, bottom currents increased again to up to 15 – 20 cm/s. Evidence for similar flow variations was also given by *Ledbetter* (1993) at project MUDWAVES Sites 5 and 6 for the last 40 ky based on grain size analyses. He predicted a period of higher flow velocity for the time periods from 37 to 22 ka and from 4 to 2.5 ka. Given the uncertainties in both age estimates, the results show a considerable agreement.

Finally we conclude that model results and internal wave geometry show that the cyclonic gyre, which was proposed by *Flood and Shor* (1988), is an exceptionally steady feature of the deep Argentine Basin circulation and lasted with flow speeds of 10 to 20 cm/s at least for the last 100'000 years.

4.7 Conclusions

A dense grid of high resolution narrow beam echosounder data was collected in a mudwave field on the western flank of the Zapiola drift in the Argentine Basin. The combination of an analysis of observed mudwave properties and general depositional patterns on the one hand and mudwave modeling on the other, yielded the following results:

- mudwave evolution of the last 100 ky is controlled by a southward flow with velocities ranging from 10 – 20 cm/s, in agreement with known oceanography.
- the flow intensity varies across the drift flank, decreasing in upslope direction.
- to the north-east of the crest, flow velocities increase, causing non-deposition and erosion and thereby shifting the drift crest to the south-west.

- the deeper depth limit of the wave field probably marks the boundary between the southward flow on the drift flank and the northward flow of AABW along the continental margin.
- geometric variations in the internal mudwave structure suggest variations in late Quaternary bottom flow activity, which agree with results obtained with grain size analyses (*Ledbetter*, 1993).

4.8 Acknowledgements

We would like to thank the participants of the cruises M29/1 and M46/3 with R/V METEOR, who supported us in supervising the echosounding systems. With their help it was possible to collect high quality data on a 24 hour schedule. This study was funded by the Deutsche Forschungsgemeinschaft (Sonderforschungsbereich 261 at Bremen University). This is contribution no. 338 of SFB 261.

5 Summary and perspectives

During several cruises of the German Special Research Project 261 – The South Atlantic in the late Quaternary - to the South Atlantic Ocean, high resolution narrow beam echosounder data revealed sinusoidal structures in deep sea sediments, which showed a conspicuous spatial regularity over large areas in conjunction with pronounced internal layering. They were observed both in the Southeastern and in the Southwestern Atlantic Ocean, and specifically investigated in this study on the Namibian continental margin as well as in the central Argentine Basin

On the Namibian continental margin they are restricted to a sharply defined depth interval of 1200 to 1800 m and extend from the eastern Walvis Ridge at 19° 30' S to 22° S along the continental slope. With heights of 5 to 8 m and wave lengths of 300 to 700 m the waves are close to the resolution properties of surface based echosounder systems and a careful analysis of all geometrical properties is required to determine their origin. By means of a specialized data processing of available swath sonar data it can be demonstrated, that the observed structures are linear elongated and strike in downslope direction. This suggests, that any kind of gravitational sediment transport mechanisms or deformation mechanisms can be excluded for having created the waves.

The sinusoidal structures are therefore interpreted as sedimentary waves, which originated under the influence of a contour current, passing the Walvis Ridge in the depth interval of the wave field. This interpretation is confirmed by an echosounder profile, which crosses the wave field in downslope direction and reveals significantly reduced accumulation rates in the area covered by waves. The known oceanography of this region, complemented by a long term direct current measurement, suggest that the contour current is formed by southward spreading Upper North Atlantic Deep Water (UNADW) and Upper Circumpolar Deep Water (UCDW).

The internal structure of the waves shows evidence for fluctuations in bottom flow intensity through geologic time. Two transition zones can be recognized, where the waves at exposed locations change their wave length, starting with values of 300 m, then switching to longer waves of 700 m and finally ending at a wave length of 500 m. The change in wave length seems to occur quite abrupt. Older waves are completely destroyed and waves with a different wave length are build upon them. To obtain qualitative and

quantitative information about the history of the contour current, two separate approaches were pursued.

An extended model of mudwave growth (*Hopfauf and Spieß*, 2000) was applied to the data to quantify palaeoflow intensities. As this model (and other models as well, see *Flood*, 1988, *Blumsack and Weatherly*, 1989) predicts that an existing wave topography stabilizes the bottom flow velocity field, such that waves may change migration or growth rate, but not wave length and strike direction, the observed change in wave length suggests a pulsed intensification of the bottom flow, causing complete wave destruction. In contrast, periods of continuous wave growth are interpreted as phases of moderate to low, though very steady, flow velocities.

Spatial variations in accumulation rates can also be used as qualitative measures for bottom flow activity. Such variations occur on short distances of only a few tens of kilometers in the study area. They are assumed to be caused by variations in flow velocity related to the local topography (e.g. small seamounts). The ratio of maximum to minimum accumulation rate at two neighboring sites of varying accumulation rate was found to increase at the same time as mudwaves are destroyed at other locations. Another qualitative indicator for palaeoflow variations is derived in the vicinity of a seamount, where a transition from deposition through erosion is observed. The critical distance of deposition, i.e. the point, where non-deposition or erosion changes to deposition on the approach to the seamount, also reflects the intensity of the bottom flow.

Comparison of both the two qualitative flow indicators and the quantitative model results show close agreement in the derived palaeoflow history on the Walvis Ridge. Temporal resolution, however, is reduced due to low sedimentation rates in the wave field. Mudwave onset started at approximately 5 Ma with moderate flow velocities of only 2 to 3 cm/s, probably accompanying the evolving stratification of the Atlantic Ocean (e.g. *Woodruff & Savin*, 1989). Flow intensity is suggested to slowly increase until at ~1.9 Ma existing mudwaves are destroyed. This event probably requires current velocities exceeding 10 to 15 cm/s. Afterwards, flow activity decreases gradually until at ~ 600 ka another peak in current velocity is reached. For the most recent history of the last 350 ky, however, a discrepancy in the model results, which predict reduced flow activity and the qualitative indicators, which suggest a significant increase in flow activity, shows the different resolution properties of the two approaches. As long as the mean flow velocity varies in a specific range and sedimentary waves do not reflect these variations, they

cannot be resolved with modeling. In contrast, these variations may be sufficient to show up in local fluctuations of accumulation rates.

While sedimentary waves on the Namibian continental margin are hard to detect with surface based echosounder systems, mudwaves on the Zapiola Drift in the Argentine Basin, represent the upper end of known sedimentary wave sizes. The waves, which were studied here, are located on the western flank of the Zapiola Drift and reach heights of 25 to 30 m at wave lengths of ~5 km. Echosounder data reveal that the waves migrate upslope towards the drift crest by accumulating significantly more material on the upslope than on the downslope oriented wave flank.

The overall lateral distribution of sedimentation rates suggests a gradual decrease of flow velocities from the deeper parts of the basin towards the drift crest. However to the north-east of the crest, flow velocity increases again over a short distance, causing a transition from deposition to non-deposition and eventually erosion. The reduced accumulation rates to the north-east of the crest combined with a maximum in accumulation rate to the south-west of the crest causes a drift crest migration to the south-west.

The gradual trend in flow velocity, determined by observations of the accumulation rate distribution, is confirmed by model results. The mudwaves, which cover the drift flank, show a decreasing asymmetry from deep shallow, which can be attributed to a parallel decrease in flow velocity. The well resolved internal structure of the waves allows a detailed analysis of the model results for this location. A predicted southward oriented flow across the wave field confirms the observations of a cyclonic deep-water gyre, which is centered around the Zapiola Drift (e.g. *Flood and Shor*, 1988). Also in agreement with measurements (*Weatherly*, 1993) are the predicted flow velocities in the range of 10 – 20 cm/s. Estimates of past time variations in bottom flow velocity for the last 100 ky, based on changes in the wave crest migration rates and a linear estimate of accumulation rate of 30 to 40 cm/ky, suggest that bottom flow activity was increased during the Holocene as well as from 40 ka to 25 ka with mean flow speeds of 15 to 20 cm/s.

The presented studies show that a physical approach of modeling in combination with a careful investigation of current induced bedforms may serve as a tool for the reconstruction of bottom current activity. Sedimentary waves with their well defined geometry and their development over long time scales are appropriate candidates for modeling. In combination with additional information as direct current measurements and

bottom photographs or simply plausibility considerations, the ambiguity of the model results may be reduced and quantitative estimates of flow velocities are possible.

In contrast to direct measurements, which always describe the modern short term circulation, sedimentary waves record long term changes in the mean bottom flow pattern. Therefore the presented studies can also be seen as a new approach for the determination of palaeoflow history, which complements existing methods as grain size analysis.

References

Anderson, R. F., Fleisher, M. Q., Manley, P. L. (1993). Uranium-series tracers of mudwave migration in the Argentine Basin. *Deep-Sea Research II*, Vol. 40, 4/5, 889 – 909.

Balsam, W. L., Wolhart, R. J. (1993). Sediment dispersal in the Argentine Basin: evidence from visible light spectra. *Deep-Sea Research II*, Vol. 40, 4/5, 1001 – 1031.

Berger, W.H., Wefer, G., (1991). Productivity of the glacial ocean: Discussion of the iron hypothesis. *Limnol. Oceanogr.*, 36, 1899 – 1918.

Berger, W.H., Wefer, G. (1996). Expeditions into the past: Palaeoceanographic studies in the South Atlantic. In: *The South Atlantic – Present and Past Circulation*, Wefer, G., Berger, W., Siedler, G. Webb, J. (eds). Springer Verlag, 363 - 410.

Berggren, W.A., (1972). Late Pliocene – Pleistocene glaciation. In: Laughton, A.S., Berggren, et al., *Initial Reports Deep Sea Drilling Project*, 12, Washington DC (US Government Printing Office), 953 – 963.

Bleil, U. and Shipboard Scientific Party, (1993). Report and preliminary results of SONNE Cruise SO 86, Buenos Aires – Capetown, 22.4.1993 – 31.5.1993. *Berichte*, Fachbereich Geowissenschaften, Universität Bremen, Nr. 51.

Bleil, U. and Shipboard Scientific Party, (1996). Report and preliminary results of METEOR Cruise M 34/1, Capetown – Walvis Bay, 03.01.1996 – 26.01.1996. *Berichte*, Fachbereich Geowissenschaften, Universität Bremen, Nr. 77.

Bleil, U. and Shipboard Scientific Party, (2000). Report and preliminary results of METEOR Cruise M 46/3, Montevideo – La Plata, 02.1.2000 – 09.02.2000. *Berichte*, Fachbereich Geowissenschaften, Universität Bremen, in press.

Blumsack, S. L., Weatherly, G. L. (1989). Observations and growth mechanisms for mudwaves. *Deep-Sea Research*, Vol. 36, 1327 – 1339.

Bornhold, B. D. (1973). Late Quaternary Sedimentation in the Eastern Angola Basin. *Technical Report*, Woods Hole, WHOI 773-8.

Bremner, J. M. (1975). Mineralogy and Distribution of Clay Minerals on the southwest African Continental Shelf and adjacent Hinterland. *Technical Report* no. 7, Geology Department, University of Cape Town, 46 – 55.

Bremner, J. M. (1981), Shelf morphology and surficial sediment off Central and Northern South West Africa, *Geo-Marine Letters*, 1, 91-96.

Caress, D. W., Chayes, D. N. (1996). Improved Processing of Hydrosweep DS Multibeam Data on the R/V Maurice Ewing. *Mar. Geophys. Res.*, 18, 631 – 650.

Cheney, R. E., Marsh, J. G., Beckley, B. D. (1983). Global mesoscale variability from collinear tracks of SEASAT altimeter data. *J. Geophys. Res.*, 88, 4343 – 4354

Coates, A.G., Jackson, J.C., Collins, L.S., Cronin, T.M., Dowsett, H.J., Bybell, L.M., Jung, P., Obando, J.A., (1992). Closure of the Isthmus of Panama: The near-shore marine record of Costa Rica and western Panama. *Geol. Soc. Am. Bull.*, 104, 814 – 828.

Damuth, J. E. (1979). Migrating Sediment Waves created by turbidity currents in the north South China Basin. *Geology*, 7, 520 – 523.

Diester-Haas, L. (1985). Late Quaternary sedimentation on the eastern Walvis Ridge, SE Atlantic (HPC 532 and four piston cores). *Marine Geology*, 65, 145-189.

Diester-Haass, L., Meyers, P. A., Rothe, P. (1992). The Benguela Current and associated upwelling on the southwest African Margin: a synthesis of the Neogene-Quaternary sedimentary record at DSDP sites 362 and 532. In: *Upwelling systems: Evolution since the early Miocene.* Summerhayes, C. P., Prell, W. L., Emeis, K. C. (eds.). Geological Society Special Publication No. 64, 331 – 342.

Embley, R. W., Hoose, P. J., Lonsdale, P., Mayer, L., Tucholke, B. E. (1981). Furrowed mudwaves on the western Bermuda Rise. *GSA Bulletin*, 91, 731 – 740.

Ewing, M., Lonardi, A. G. (1971). Sediment transport and distributions in the Argentine Basin. 5. Sedimentary structure of the Argentine margin, basin and related provinces. In: *Physics and chemistry of the Earth*, Ahrens, L. H., Press, F., Runcorn, S. K., Urey, H. C. (eds). Vol. 8, Pergamon Press, Oxford, 123 – 251.

Flood, R. D. (1988). A lee-wave model for deep-sea mudwave activity. *Deep-Sea Research*, Vol. 35, 973 – 983.

Flood, R. D., Shor, A. N. (1988). Mudwaves in the Argentine Basin and their relationship to regional circulation patterns. *Deep-Sea Research*, Vol. 35, 973 – 984.

Flood, R. D., Shor, A. N., Manley, P. L. (1993). Morphology of abyssal mudwaves at project MUDWAVES sites in the Argentine Basin. *Deep-Sea Research II*, Vol. 40, 4/5, 859 – 888.

Fox, P. J., Heezen, B. C., Harian, R. (1968). Abyssal Antidunes. *Nature*, 220, 470 – 472.

Fu, L.-L. (1996). The circulation and its variability of the South Atlantic Ocean: First results from the TOPEX/POSEIDON mission. In: *The South Atlantic – Present and Past Circulation*, Wefer, G., Berger, W., Siedler, G. Webb, J. (eds). Springer Verlag, 63 – 82.

Gardner, W. D., Sullivan, L. G. (1981). Benthic storms: temporal variability in a deep-ocean nepheloid layer. *Science*, 213, 329 –331

Garrett, C.J.R., Munk, W.H., (1972). Space-time scales of internal waves. *Geophysical Fluid Dynamics,* 3, 225-264.

Giraudeau, J., Cristensen, B. A., Hermelin, O., Lange, C. B., Motoyama, I. (1998). Biostratigraphic Age Models and Sedimentation Rates along the Southwest African Margin. *Proc. ODP*, Init. Repts., 175, 543 – 546.

Grant, J.A., Schreiber, R. (1990). Modern swath sounding and sub-bottom profiling technology for research applications: The Atlas Hydrosweep and Parasound systems. *Mar. Geophys. Res.*, 12, 9 - 19.

Hart, T. J., Currie, R. T. (1960). The Benguela Current. *Discovery reports*, 31, 123-298.

Hay, W. W., Sibuet, J.C., et. al. (1984). *Initial reports of the Deep Sea Drilling Project.* 75, Washington DC (US Government Printing Office).

Hogg, N., Biscaye, P. E., Gardner, W., Schmitz Jr, W. J. (1982). On the transport and modification of Antarctic Bottom Water in the Vema Channel. *J. Mar. Res.*, 40 (Suppl), 231 – 263.

Hollister, C. D., McCave, N. (1984). Sedimentation under deep-sea storms. *Nature*, 309, 220 – 225.

Hopfauf, V., Spieß, V. (2000). A threedimensional theory for the development and migration of deep sea sedimentary waves. *Deep-Sea Research II*, in press.

Jacobi, R. D., Rabinowitz, P. D., Embley, R. W. (1975). Sediment Waves on the Moroccan Continental Rise. *Marine Geology*, 19, M61 - M67.

Jansen, E., Bleil, U., Henrich, H., Kringstad, L., Slettemark, B. (1988). Palaeoenvironmental changes in the Norwegian Sea and the northeast Atlantic during the last 2.8 m.y: Deep Sea Drilling Project / Ocean Drilling Program Sites 610, 642, 643 and 644. *Palaeoceanography*, Vol. 3, 563 – 581.

Jones, G. A., Johnson, D. A. (1984). Displaced Antarctic diatoms in Vema Channel sediments: Late Pleistocene / Holocene fluctuations in AABW flow. *Marine Geology*, 58, 165 – 186.

Jones, G. A. (1994). Holocene climate and deep ocean circulation changes: Evidence from accelerator mass spectrometer radiocarbon dated Argentine Basin (SW Atlantic) mudwaves. *Paleoceanography*, Vol. 9, 6, 1001 – 1016

Keigwin, L.D. (1978). Pliocene closing of the Isthmus of Panama, based on biostratigraphic evidence from nearby Pacific Ocean and Caribbean Sea cores. *Geology*, 6, 630 – 634.

Kennett, J. P. (1982). *Marine Geology*. Prentice-Hall, Inc., Englewood Cliffs, N. J. 07632.

Klaus, A., Ledbetter, M. T. (1988). Deep-sea sedimentary processes in the Argentine Basin revealed by high-resolution seismic records (3.5 kHz echograms). *Deep-Sea Research*, Vol. 35, 6, 899 – 917.

Ledbetter, M. T. (1986). Bottom-current pathways in the Argentine Basin revealed by mean silt particle size. *Nature*, 321, 423 – 425

Ledbetter, M. T. (1993). Late Pleistocene to Holocene fluctuations in bottom-current speed in the Argentine Basin mudwave field. *Deep-Sea Research II*, Vol. 40, 4/5, 911 – 920.

Ledbetter, M. T., Bork, K. R. (1993). Post-Miocene fluctuations of Antarctic Bottom Water palaeospeed in the southwest Atlantic Ocean. *Deep-Sea Research II*, Vol. 40, No. 4/5, 1057 – 1071.

Le Pichon, X., Eittreim, S. L., Ludwig, W. J. (1971a). Sediment transport and distributions in the Argentine Basin. 1. Antarctic bottom current passage through the Falkland Fracture Zone. In: *Physics and chemistry of the Earth*, Ahrens, L. H., Press, F., Runcorn, S. K., Urey, H. C. (eds). Vol. 8, Pergamon Press, Oxford, 1 – 27.

Le Pichon, X., Ewing, M., Truchan, M. (1971b). Sediment transport and distributions in the Argentine Basin. 2. Antarctic bottom current passage into the Brazil Basin. In: *Physics and chemistry of the Earth*, Ahrens, L. H., Press, F., Runcorn, S. K., Urey, H. C. (eds). Vol. 8, Pergamon Press, Oxford, 29 - 48.

Lonsdale, P. (1983). Sediment drifts of the Northeast Atlantic and their relationship to the observed abyssal circulation. *Bulletin de l'Institut de Geologie du Bassin d'Aquite*, 31, 141-149.

Maier-Reimer, E., Mikolajewicz, U., Crowley, T. (1990). Ocean general circulation model sensitivity experiment with an open Central American isthmus. *Palaeoceanography*, Vol. 5, 349-366.

Manley, P. L., Flood, R. D. (1993a). Project MUDWAVES. *Deep-Sea Research II*, Vol. 40, 4/5, 851 – 857

Manley, P. L., Floor, R. D. (1993b). Paleoflow history determined from mudwave migration: Argentine Basin. *Deep-Sea Research II*, Vol. 40, 1033-1055.

McCave, I. N., Manighetti, B., Robinson, S. G. (1995). Sortable silt and fine sediment size/composition slicing: Parameters for palaeocurrent speed and palaeoceanography. *Palaeoceanography*, Vol. 10, No. 3, 593 – 610.

Mikolajewicz, U., Maier-Reimer, E., Crowley, T. J., Kim, K.Y. (1993). Effect of Drake and Panamanian Gateways on the Circulation of an Ocean Model. *Palaeoceanography,* Vol. 8, 409 – 426.

Moroshkin, K. V., Bubnov, V. A., Bulatov, R. P. (1970). Water circulation in the eastern South Atlantic. *Oceanology*, 10, 27-34.

Normark, W. R., Hess, G. R., Stow, D. A. V., Bowen, A. J. (1980). Sediment Waves on the Monterey Fan levees: a preliminary physical interpretation. *Marine Geology*, 37, 1-18.

Oberhänsli, H. (1991). Upwelling Signals at the northeastern Walvis Ridge during the past 500000 years. *Palaeoceanography*, Vol. 6, 53–71.

Orsi, A. H., Johnson, G. C., Bullister, J. L. (1999). Circulation, mixing, and production of Antarctic Bottom Water. *Prog. Oceanogr.*, 43, 55 – 109.

Provost, C., Le Traon, P. Y. (1993). Spatial and temporal scales in altimetric variability in the Brazil – Malvinas Current confluence region: Dominance of the semiannual period and large spatial scales. *J. Geophys. Res.*, 98, 18037 – 18051

Queney, P., (1948), The problem of air flow over mountains: a summary of theoretical studies. *Bulletin of the American Meteorological Society,* 29, 16-26.

Reid, J. L., Nowlin Jr, W. D., Patzert, W. C. (1977). On the characteristics and circulation of the Southwestern Atlantic Ocean. *J. Phys. Oceanogr.*, 7, 62 – 91.

Reid, J. L. (1989), On the total geostrophic circulation of the South Atlantic Ocean: Flow patterns, tracers, and transports. *Prog. Oceanogr.* 23(3), 149 - 244

Reid, J. L. (1996), On the circulation of the South Atlantic. In: *The South Atlantic – Present and Past Circulation*, Wefer, G., Berger, W., Siedler, G. Webb, J. (eds). Springer Verlag, 13-44.

Richardson, M. J., Weatherly, G. L., Gardner, W. D. (1993). Benthic storms in the Argentine Basin. *Deep-Sea Research II*, Vol. 40, 4/5, 989 – 999.

Roberts, D. G., Kidd, R. B. (1979). Abyssal sediment wave fields on Feni Ridge, Rockall Trough: long range sonar studies. *Marine Geology*, 33, 175 – 191.

Roether, W., Putzka, A. (1996). Transient Tracer Information on Ventilation and Transport of South Atlantic Waters. In: *The South Atlantic – Present and Past Circulation*, Wefer, G., Berger, W., Siedler, G. Webb, J. (eds). Springer Verlag, 45-62.

Schulz, H. D., and Shipboard Scientific Party, (1992). Bericht und erste Ergebnisse über die METEOR-Fahrt M 20/2, Abidjan – Dakar, 27.12.1991 – 3.2.1992. *Berichte*, Fachbereich Geowissenschaften, Universität Bremen, Nr. 25.

Schulz, H. D., and Shipboard Scientific Party, (1996). Report and preliminary results of METEOR Cruise M 34/2, Walvis Bay – Walvis Bay, 29.1.1996 – 18.2.1996. *Berichte*, Fachbereich Geowissenschaften, Universität Bremen, Nr. 78.

Segl, M. and Shipboard Scientific Party, (1994). Report and preliminary results of METEOR Cruise M 29/1, Buenos Aires – Montevideo, 17.6.1994 – 13.7.1994. *Berichte*, Fachbereich Geowissenschaften, Universität Bremen, Nr. 58.

Shannon, L. V., Nelson, G. (1996). The Benguela: Large scale features and processes and system variability. In: *The South Atlantic – Present and Past Circulation*, Wefer, G., Berger, W., Siedler, G. Webb, J. (eds). Springer Verlag, 163-210.

Smith, W. H. F., Sandwell, D. T. (1997). Global seafloor topography from satellite altimetry and ship depth soundings. *Science*, 277, 1956 - 1962.

Smythe-Wrigth, D., Boswell, S. (1998). Abyssal circulation in the Argentine Basin. *J. Geophys. Res.*, 103, C8, 15845 – 15851

Speer, K., Zenk, W., Siedler, G., Pätzold, J., Heidland, K. (1992). First resolution of flow through the Hunter Channel in the South Atlantic. *Earth Planet Sci. Lett.*, 113, 287 – 292.

Speer, K., Zenk, W. (1993). The flow of Antarctic Bottom Water into the Brazil Basin. *J. Phys. Oceanogr.*, 12, 2667 – 2682.

Speer, K. G., G. Siedler, Talley, L. (1995). The Namib Col Current. *Deep-Sea Research I*, Vol. 42, 11/12, 1933-1950.

Spieß, V. (1993). Digitale Sedimentechographie – neue Wege zu einer hochauflösenden Akustostratigraphie, *Berichte*, Fachbereich Geowissenschaften, Universität Bremen, Nr. 35.

Stramma, L., Peterson, R. G. (1989). Geostrophic transport in the Benguela Current region. *J. Phys. Oceanogr.*, 19, 1440-1448.

Summerhayes, C. P. (1983). Sedimentation of organic matter in upwelling regimes. In: Thiede, J. and Suess, E. (eds) Coastal upwelling, its sediment record, *NATO Conf. Ser.*, vol. IV, 10b, Plenum Press, New York, 29-72.

Turnau, R., Ledbetter, M.T. (1989). Deep circulation changes in the South Atlantic Ocean: responses to initiation of northern hemisphere glaciation. *Palaeoceanograpy*, Vol. 4, 565 – 583.

v. Lom, H., Spieß, V., Hopfauf, V. (2001). Small scaled sedimentary waves on the Namibian continental slope – Evidence of stationary contour current activity, *this issue*.

Weatherly, G. L. (1993). On deep-current and hydrographic observations from a mudwave region and elsewhere in the Argentine Basin. *Deep-Sea Research II*, Vol. 40, 4/5, 939 – 961

Wefer, G., Berger, W.H., Richter, C., et al. (1998). *Proc. ODP*, Init. Repts., 175. College Station, TX (Ocean Drilling Program).

Wessel, P., Smith, W. H. F. (1995). New version of the Generic Mapping Tools released. *EOS Trans. AGU*, 76, 329, 1995

Woodruff, F., Savin, S.M. (1989). Miocene deepwater oceanography. *Palaeoceanography*, Vol. 4, 87 – 140.

Wüst, G., Defant, A. (1936). Atlas zur Schichtung und Zirkulation des Atlantischen Ozeans. *Deutsche Atlantische Exped. Meteor 1925 – 1927*, Wiss Erg, Bd 6, Atlas, 103 pp.

Wüst, G. (1957). Stromgeschwindigkeiten und Strommengen in den Tiefen des Atlantischen Ozeans unter besonderer Berücksichtigung des Tiefen- und Bodenwassers. *Wissenschaftliche Ergebnisse der Deutschen Atlantischen Expedition auf dem Forschungs- und Vermessungsschiff "Meteor"*, 1925 – 1927, 6, 261 – 420.

Acknowledgments

I thank Prof. Dr. V. Spieß for providing me the possibility to work on this dissertation. He offered me constant advice and was always open for fruitful discussions. I also thank the reviewer of the final manuscript for providing the secondary expertise.

Parts of this work were greatly improved by many discussions with my colleagues André Janke (who usually acted as the devil's advocate), Monika Breitzke, Tilmann Schwenk, Christian Hübscher and Lars Zühlsdorff. Vladimir Hopfauf developed the mudwave model, which is one of the basic tools of this work, and was always willing to discuss model results.

Lars Zühlsdorff and Vladimir Hopfauf carefully reviewed parts of the manuscripts and their suggestions were very valuable for my understanding of this thesis. I would also like to thank Walter Zenk and Jürgen Holfort, who deepened my knowledge of the South East Atlantic oceanography and provided additional information based on their own data.

The availability of high quality echosounder data is first of all owed to all those colleagues, who operated the shipboard echosounder systems on a 24 hour schedule during cruises METEOR M20/2, METEOR M29/1, METEOR M34/1 and 2, METEOR M46/3 and SONNE So86. Without their help, this work would not have been possible. I also grateful thank the ships crew on these cruising for doing great work and for the pleasant atmosphere aboard. Special thanks apply to the electronic engineers, who kept the echosounder systems operational under all circumstances.

This work was funded by the Deutsche Forschungsgemeinschaft (DFG) through the German Special Research Project SFB261: Der Südatlantik: Rekonstruktion von Stoffhaushalt und Stromsystemen.

Finally, I owe special thanks to Lars Zühlsdorff, who provided me a roof over my head for the last year, Angelika Rinkel for being (nearly) always in a good mood and Wolfgang Böke for letting me realize that nothing is eaten as hot as it is cooked. I thank my parents for constant support, my wife Esther for her patience and from keeping me starving on vitamin deficiency, and my son Florian for showing me in his merciless way that there are other important things do to, than doing research (e.g. looking that picture-book).

Appendix: A threedimensional theory for the development and migration of deep sea sedimentary waves

Vladimir Hopfauf and Volkhard Spieß, Deep-Sea Research II, in press.

Abstract

A perturbation model is presented for a velocity field of a bottom current flowing over a sinusoidal topography or an obstacle. The model extends existing theory by taking into account the three-dimensional Coriolis vector and an initial horizontal velocity vector at any orientation. One possible mechanism of the development of sedimentary waves in vicinity of an obstacle by an arbitrarily oriented initial horizontal current is analyzed in detail. Space-stationary fluid particle oscillations are initiated on the downstream side of an obstacle, which can result in sedimentary waves. The presented model shows that their wavelength depends on latitude, water depth, obstacle width and orientation as well as the initial current direction and intensity.

The model defines intervals for current velocities normal to the wave crest, for which the sedimentary waves grow (or are destroyed) or migrate in a certain direction. Information derived from bathymetric and seismic surveys as wavelength, height, orientation and migration direction of mudwaves can be used to calculate the velocity component across the wave crest as well as to estimate the current direction, as is demonstrated for an example from the Argentine Basin (Project MUDWAVES, Site 5).

Introduction

Quasi-sinusoidal sedimentary waves of different size, characterized by wavelength and height, are commonly observed wherever a transport of fine-grained sediments occurs. We find examples in deserts, rivers and coastal environments. Abyssal mudwaves are large-scale bed forms found in many ocean basins where deep currents play an important role in sediment transport and deposition. These waves form in fine-grained sediments, and often develop on flanks of large sediment drifts [Fox et al. (1968), Hollister et al. (1974), Flood (1988), Flood and Shor (1988)], along continental margins [Jacobi et al. (1975)], and on the flanks of channel-levee systems caused by overflow of turbiditic currents [Damuth (1979), Normark et al. (1980)]. The heights of these waves range from less than 1 m to more than 100 m, whereas the wavelength ranges from about 100 m up to ~10 km. The waves can be identified in seismic profiles over significant

sub-bottom depth ranges, suggesting that the waves have been built up and preserved over very long time periods, on the order of several 10000 to 100000 years.

Mudwave crests are often oriented almost parallel to the regional bottom flow direction and apparently migrate transverse to the bottom current (upstream) in an upslope direction [Hollister et al. (1974), Jacobi et al. (1975)]. Downstream migration direction has also been reported [Roberts and Kidd (1979)].

The behavior of sediment particles in the presence of bottom currents depends on the physics of particle movement in fluids and on processes at the boundary layer between sea-floor and water, and the velocity field as well as boundary layer processes have an influence on the sediment accumulation or the degree of erosion [McCave and Swift (1976), Flood (1988)].

A basic theoretical approach to deal with the evolution of sedimentary waves was developed by Queney (1947, 1948), who relates a fluid flow over an initial topography to the presence of oscillations within the fluid column. The behavior of a stratified fluid medium can be described on the basis of his perturbation model which was used to determine the influence of topography (sinusoidal topography and elongated obstacle) on atmospheric streams. Queney (1948) described different types of stationary „lee waves" caused by an elongated obstacle. According to his model, the wavelengths of lee waves depend either on the vertical-stream stratification (short stationary or gravity waves), or on the Coriolis-parameter (gravity-inertia lee waves), or on the latitudinal variation of the Coriolis-parameter (long geostrophic or Rossby lee waves). The direction of the horizontal current is taken perpendicular to the obstacle crest and the Coriolis-parameter represents the component of the Coriolis vector normal to the earth surface.

Early qualitative studies of the dynamics of deep-sea sedimentary waves [Normark et al. (1980), Kolla et al. (1980)] make use of models developed for shallow water [Brooke (1959), Kennedy (1963, 1969), Reynolds (1965), Fredsoe (1974), Hand (1974)], in which only the gravity is taken into consideration and which therefore cannot be directly used for the explanation of the origin and geometry of deep sea sedimentary waves.

Flood (1988) proposed a lee-wave model for deep-sea sinusoidal sedimentary waves to describe the velocity field and sedimentation rates and to explain the upstream migration direction. Blumsack and Weatherly (1989) derived a mechanism for sedimentary wave growth which occurs at certain angles between the mean flow and the crest orientation due to preferential deposition at sedimentary wave crests. Both Flood (1988) and Blumsack and Weatherly (1989) use the Coriolis parameter as a scalar as defined by Queney (1948). But because the orientation of sedimentary waves relative to North was not considered (especially for greater water depths), these solutions to

determine the velocity field over the sedimentary wave topography in a deep sea environment are incomplete, as will be shown later.

The most extensive study on sedimentary wave dynamics was carried out during the Project MUDWAVES [Manley and Flood (1993), Flood et al. (1993), Weatherly (1993) and others]. This yielded detailed three-dimensional maps of mudwave fields in the Argentine basin. In addition, Flood et al. (1993) have discussed the interaction between bottom topography and weakly stratified flows. All models proposed so far only describe mudwave development, but could not explain the onset of sedimentary waves in deep sea in detail.

In this paper, a perturbation model for the velocity field over a sinusoidal topography and an elongated obstacle is proposed, which includes (1) the orientation of sedimentary waves relative to North (3-D Coriolis vector) and (2) an arbitrarily oriented mean flow velocity vector.

A phase analysis of the sedimentation rate variation over a sedimentary wave topography allows to divide it into two components: the growth rate, which causes a growth or a destruction of the sedimentary waves, and the migration rate, which causes their apparent migration. These are controlled by the sedimentary wave geometry and location and by the horizontal velocity. Its direction as well as its magnitude normal to the wave crest can be estimated from the behavior of the two sedimentation rate components. To illustrate the impact of the growth and migration rates, a simple modeling of deposition leading to a topography change is carried out.

A possible mechanism of sedimentary wave creation on the downstream side of an elongated obstacle, at first studied by Queney for a stratified fluid with strong stability, is developed for the deep sea situation with weak stability. The frequency analysis of the sedimentation rate variation in the vicinity of an elongated obstacle allows to estimate the geometry of sedimentary waves and conditions for their creation. The model predictions are applied to mudwave fields investigated during the Project MUDWAVES (Flood et al., 1993) .

Velocity field perturbation over a sinusoidal topography

Given a laminar flow, the perturbations of the velocity field in the vicinity of a bottom topography depends on:

- the initial horizontal velocity vector of the fluid medium,
- the shape of the initial topography,
- external forces (Coriolis force and gravity) and
- vertical fluid stratification.

The hydrodynamic equations for incompressible, non-viscous fluids on the Earth's surface are given by LeBlond and Mysak (1978):

$$\begin{aligned} &\rho D\mathbf{U}/dt+\rho(\mathbf{f}\times\mathbf{U})+\nabla p-\rho\mathbf{G}=0,\\ &D\rho/dt=0,\\ &\nabla\cdot\mathbf{U}=0, \end{aligned} \qquad (1)$$

where $D/dt=\partial/\partial t+\mathbf{U}\cdot\nabla$ describes the total derivative with respect to time t. Density ρ, pressure p and velocity vector $\mathbf{U}$ are a function of the space vector $\mathbf{r}(x, y, z)$ in a Cartesian coordinate system with z-axis pointing upwards. As external forces, gravity $\mathbf{G}$ = (0, 0, -g) and Coriolis force $(\mathbf{f}\times\mathbf{U})$ must be considered, with $\mathbf{f}=(f_x, f_y, f_z)$, $f_x=2\Omega\cos\beta\cos\alpha$, $f_z=2\Omega\sin\beta$, $f_y=2\Omega\cos\beta\sin\alpha$ and the earth's angular velocity Ω, latitude β and angle between x-axis and North direction α.

Perturbation theory for a stratified fluid medium (e.g. LeBlond and Mysak,1978) provides:

$$\begin{aligned} &D_1\mathbf{U}'/dt+(\mathbf{f}\times\mathbf{U}')+\nabla p'/\rho_0-\mathbf{G}\rho'/\rho_0=0,\\ &D_1\rho'/dt+w'\partial\rho_0/\partial z=0,\\ &\nabla\cdot\mathbf{U}'=0, \end{aligned} \qquad (2)$$

for deviations of velocity $\mathbf{U}'=(u', v', w')$, pressure p' and density ρ' from an initial state $(U_0,V_0,0)$, p_0 and $\rho_0(z)$, where $D_1/dt=\partial/\partial t+U_0\,\partial/\partial x+V_0\,\partial/\partial y$ is a linear approximation of the operator D/dt.

Following Queney (1947) we introduce a sinusoidal topography, which is two-dimensional in space (Fig. 1). The cross section is given by the real part of

$$z=h\exp(ik_x x), \qquad (3)$$

where h is the wave amplitude and k_x is the wave number in x – direction. A general solution of (2) can then be written as:

$$\{\mathbf{U}',p',\rho'\}=\{\mathbf{U}_a,p_a,\rho_a\}\cdot\exp[i(k_x x+k_z z-\sigma t)], \qquad (4)$$

where $\mathbf{k}=(k_x, 0, k_z)$ is the wave vector for the resulting plane wave, σ its frequency and $\mathbf{U}_a=(u_a, v_a, w_a)$, p_a and ρ_a are amplitudes of the perturbed variables.

Accordingly, considering the full Coriolis vector, a substitution of (4) in (2) provides for the amplitudes of the perturbed variables:

$$\begin{aligned}
&i\omega_0 u_a - f_z v_a + f_y w_a + ik_x p_a/\rho_0 = 0,\\
&f_z u_a + i\omega_0 v_a - f_x w_a = 0,\\
&-f_y u_a + f_x v_a + i\omega_0 w_a + ik_z p_a/\rho_0 + g\rho_a/\rho_0 = 0,\\
&i\omega_0 \rho_a + w_a \partial\rho_0/\partial z = 0,\\
&i(k_x u_a + k_z w_a) = 0,
\end{aligned} \tag{5}$$

with $\omega_0 = k_x U_0 - \sigma$.

The dispersion relation of system (5) has the form:

$$(\sigma - k_x U_0)^2 = \left[(\mathbf{k}\cdot\mathbf{f})^2 + k_x^2 N^2\right]/(k_x^2 + k_z^2), \tag{6}$$

where $N = \sqrt{-g/\rho_0 \cdot \partial\rho_0/\partial z}$ is the Brunt-Vaisala frequency, which describes the stratification stability and introduces the depth dependency. Garrett and Munk (1972) suggested that N in deep sea is:

$$N(z_w) = N(200)\exp\left[(200 - z_w)/1300\right], \tag{7}$$

with $N(200)= 5{,}23\cdot 10^{-3}\,\mathrm{rad}\cdot\mathrm{s}^{-1}$ and z_w the water depth in meters.

For stationary plane waves ($\sigma = 0$) and an assumption $k_x > 0$, the expression for the vertical component of the group velocity $U_{g,z}$ can be derived from the dispersion relation (6):

$$U_{g,z} = \partial\sigma/\partial k_z\big|_{\sigma=0} = -\left[k_z(f_z^2 - \omega_0^2) + k_x f_x f_z\right]/\left[\omega_0(k_x^2 + k_z^2)\right], \tag{8}$$

where k_z has the following form:

$$k_z = k_x\left(f_z^2 - \omega_0^2\right)^{-1} \cdot \left[-f_x f_z \pm \sqrt{f_x^2 f_z^2 - (N^2 + f_x^2 - \omega_0^2)(f_z^2 - \omega_0^2)}\right]. \qquad (9)$$

The real values of k_z lie inside the interval $\omega_{01}^2 < \omega_0^2 < \omega_{02}^2$, where

$$\omega_{01,02}^2 = 1/2\left[N^2 + f_z^2 + f_x^2 \mp \sqrt{\left(N^2 + f_z^2 + f_x^2\right)^2 - 4f_z^2 N^2}\right].$$

The sign in (9) is chosen such that the vertical group velocity in (8) is positive, if k_z is real or is associated with an exponential decrease of perturbed amplitudes for increasing z, if k_z is imaginary. These conditions are fulfilled, if

$$k_z = k_x \cdot \begin{cases} k_{z,1} + k_{z,2}\,\mathrm{sgn}\left(f_z^2 - \omega_0^2\right), & \text{if } \omega_0^2 < \omega_{01}^2 \text{ or } \omega_0^2 > \omega_{02}^2, \\ k_{z,1} - \mathrm{sgn}(U_0)\,k_{z,2}, & \text{if } \omega_{01}^2 \le \omega_0^2 \le \omega_{02}^2, \end{cases} \qquad (10)$$

where: $k_{z,1} = -f_x f_z \cdot \left(f_z^2 - \omega_0^2\right)^{-1}$, $k_{z,2} = \omega_r^2 \cdot \left(f_z^2 - \omega_0^2\right)^{-1}$ and

$$\omega_r^2 = \sqrt{f_z^2 f_x^2 - \left(N^2 + f_x^2 - \omega_0^2\right)\left(f_z^2 - \omega_0^2\right)}.$$

Expression (9) has a singularity at $\omega_0^2 = f_z^2$, but only if the sign of $f_x f_z$ is identical to the sign of the square root in (9) or if f_x=0. If U_0 is directed towards the equator, the singularity can be resolved by a Taylor series expansion in $T = f_z^2 - \omega_0^2 = 0$ for real values of k_z:

$$k_z = -k_x\, T^{-1}\,\mathrm{sgn}\left(U_0\right) \cdot \left\{\mathrm{sgn}\left(U_0\right) f_x f_z + \left|f_x f_z\right| - \left(N^2 + f_x^2 - f_z^2\right)\left|2 f_x f_z\right|^{-1} \cdot T + O\left(T^2\right)\right\} \qquad (11)$$

As was discussed by Queney (1947), this singularity ("resonance") results from a lack of viscous forces, which need to be considered for a physical solution.

For a linearized boundary condition (Holton, 1992) at the sea bed, the perturbed velocity components at the sea bottom (z=0) result in:

$$\begin{cases} u' = h\,\omega_0\,k_{z,0}\cos\left(k_x x - \pi/2\right) \\ v' = h\left(k_{z,0} f_z + f_x\right)\cos\left(k_x x\right) \\ w' = h\,\omega_0\cos\left(k_x x + \pi/2\right), \end{cases} \qquad \text{if } k_z \text{ is real,} \qquad (12a)$$

$$\begin{cases} u' = h\,\omega_0 \left[k_{z,1}\cos\left(k_x x - \pi/2\right) + k_{z,2}\,\mathrm{sgn}\left(f_z^2 - \omega_0^2\right)\cos\left(k_x x\right)\right] \\ v' = h\left[\left(k_{z,1} f_z + f_x\right)\cos\left(k_x x\right) + f_z k_{z,2}\,\mathrm{sgn}\left(f_z^2 - \omega_0^2\right)\cos\left(k_x x + \pi/2\right)\right] \\ w' = h\,\omega_0 \cos\left(k_x x + \pi/2\right), \qquad \text{if } k_z \text{ is imaginary,} \end{cases} \tag{12b}$$

where $k_{z,0} = k_z k_x^{-1}$.

From (12) it follows, that the initial velocity component V_0 parallel to the crest does not cause velocity perturbations, if the topography is two-dimensional and viscosity is not considered. The linearization steps of the model in equations (2), (4) and (9) are valid at the standard conditions [see for example Blumsack (1993)]: uniform density stratification, boundary condition imposed at z=0, velocity perturbations small compared to initial velocity and sedimentary wave height small compared to wavelength.

Equation (12) provides a generalized solution for a perturbed velocity field over a sinusoidal topography. It can be used (1) to understand mudwave development, (2) to study the conditions for the sedimentary wave creation and (3) to develop an inverse model for prediction of current parameters from the wave geometry.

Development and migration of sedimentary waves (method of the phase analysis)

To investigate the relationship between a bottom current, an initial topography and its modification by sedimentation, we start with the stationary oscillation of fluid particles in the water column over a sinusoidal topography. If sediment particles are present in the water column, their accumulation directly depends on the ambient current velocity at the sea floor. Depositional processes may vary from deposition through winnowing to erosion, which image a gradual increase in velocity. Regular velocity variations can therefore be the cause for preferential deposition at locations of lower velocity and lateral transport of some particles and/or non-deposition at locations of higher velocity.

We now investigate how sedimentation rates are affected by the ambient current and sinusoidal topography. Flood (1988) and Blumsack and Weatherly (1989) pointed out that the bed shear stress, which is proportional to the square of the total velocity, is the main factor controlling the deposition of particles on the sea bed along with sediment concentration, particle settling velocity and maximum shear stress at which deposition will occur. Following these authors and McCave and Swift (1976), we define the sedimentation rate SR for the sedimentation process in the form:

$$SR = -RU_{total}^2 + B, \tag{13}$$

where $R = \rho_0 C_d B/\tau_c$. C_d is a drag coefficient, τ_c is the maximum shear stress at which deposition will occur, and B is a product of the sediment concentration in the water, settling velocity and the probability that a sediment particle will stick when deposited, which depends on the adhesion of sediment particles.

Linearized variations in velocity for small deviations from the ambient bottom current, which can cause relative changes in accumulation, are approximately proportional to:

$$U^2_{total}(x) \sim 2\left(U_0 u' + V_0 v'\right) \tag{14}$$

ignoring constants independent on x, which don't affect the topography change and higher order terms $\left(u'^2 + v'^2 + w'^2\right)$. Using equation (12), sedimentation rates (SR) across the wave also reveal a sinusoidal variation:

$$SR(x) = -R\, U^2_{total}(x) \sim S_g \cos(k_x x) + S_m \cos(k_x x - \pi/2) \tag{15}$$

with growth rate

$$S_g = -\begin{cases} 2hV_0\left(k_{z,0} f_z + f_x\right), \text{ if } k_z \text{ is real,} \\ 2h\left[U_0 \omega_0 k_{z,2}\, \mathrm{sgn}\left(f_z^2 - \omega_0^2\right) + V_0\left(f_x + f_z k_{z,1}\right)\right], \text{ if } k_z \text{ is imaginary,} \end{cases} \tag{16}$$

and migration rate

$$S_m = -\begin{cases} 2hU_0\omega_0 k_{z,0}, \text{ if } k_z \text{ is real,} \\ 2h\left(U_0 k_{z,1}\omega_0 - V_0 f_z k_{z,2}\, \mathrm{sgn}(f_z^2 - \omega_0^2)\right), \text{ if } k_z \text{ is imaginary.} \end{cases} \tag{17}$$

The splitting of equation (14) in two cosine functions, which are fixed in phase with respect to the wave crests, allows to analyze the phase lag of the sedimentation rate with respect to the existing sinusoidal topography. The in-phase component is either increasing the topography by accumulating on the wave crest ($S_g > 0$) or decreasing it by deposition in the troughs ($S_g < 0$). Sedimentary wave growth occurs for $S_g > 0$, where their height is basically dependent on the time period of deposition at similar conditions.

The second component is shifted by $\pi/2$ with respect to the topography, which causes deposition on the wave flanks. The ratio between S_m and S_g determines the offset

between the existing wave crests and the depositional maximum. Hence, a shift in deposition causes either downstream (+) or upstream (-) migration of the wave crests depending on the sign of S_m.

Both components S_m and S_g depend on six parameters: water depth, latitude, crest orientation, wavelength, current orientation and velocity. As these parameters also depend on each other, it is not possible to visualize their influence on sedimentary wave development in a single graph. Fortunately, in reality, we are studying in presence of a predefined topography and therefore we can deal with only one unknown parameter, the velocity vector. All other parameters can be determined from bathymetric and seismic data for a given location. In Figure 2, growth (Fig.s 2a, c and e) and migration rate (Fig.s 2b, d and f) is shown as a function of U_0 for different crest orientations α (Fig.s 2a, b) and different values of V_0 (Fig.s 2c - f). The model parameters are: latitude β =-45°; water depth D=5000 m; sedimentary wavelength λ=5000 m. For Figures 2a and 2b, V_0 was set to +5 cm/s, and for Figures 2c - 2f, we chose α=180° (U_0 oriented poleward). The horizontal dotted lines divide figures into growth vs. destruction situation, and downstream vs. upstream direction of migration, respectively. The vertical dashed line corresponds to the resonance at $U_0 = k_x^{-1}|f_z|$.

For U_0 oriented poleward ($f_x f_z > 0$ and 90°<α<270°) as well as parallel to equator (α=90° or (α=270°), the resonance behavior of S_g and S_m can cause a rapid change of the initial topography, as will be shown later. Otherwise, the small values of S_g and S_m cause a relatively slow change of the topography.

An influence of the velocity component V_0 parallel to crest is shown in Figures 2c to 2f for a poleward orientation of U_0. Figures 2c and 2d represent an eastern and Figures 2e and 2f a western orientation of V_0. The velocity V_0 is varied between 1 and 10 cm/s. For real values of k_z (5.7 cm/s < U_0< 14.5 cm/s), the linear dependence of S_g from V_0 can be recognized in Figures 2c to 2 f, whereas S_m is independent of V_0 (see eq. 16 and 17). For imaginary values of k_z, S_g and S_m have a linear, but weak dependence on V_0.

To simplify a geological interpretation of the sedimentation rate components, we assume a linear increase in height with time t. Then equation (14) can be rewritten:

$$\Delta h = c\,\Delta t\left\{B - R\left(U_0^2 + V_0^2\right) - R\left[S_g \cos(k_x x) + S_m \cos(k_x x - \pi/2)\right]\right\}, \qquad (18)$$

where Δh is increase in height for a time increment Δt, and c is a constant inversely proportional to sediment density ρ_0.

Sedimentation can be simulated by an iteration process. The topography afteri+1 time increments is simply calculated from the topography $h_i(x)$ at the time $i \cdot \Delta t$:

$$h^{i+1}(x) = h^i(x) + \Delta h(x). \qquad (19)$$

The linearization of height change is sufficiently precise, if the time increment Δt is kept small enough. This simple approach is only valid for depositional processes. Also, it can not be used in a small vicinity of the resonance frequency.

Figures 3 to 5 show examples of wave development for different velocities in the same setting as was used for Figure 2. The vertical dashed lines show the position of the initial wave crest. The topography change is calculated for a total time span of 2 Million years with a time increment of 2000 years. Depicted layers accumulate within 200000 years. Parameters R and B (see eq. 13), which directly control local sedimentation rate, are taken from Flood (1988) for the Argentine Basin and are assumed to be constant throughout the study area.

Figures 3 and 4 differ in the assumed direction of U_0, which is equatorward (α=0°) in Figure 3 and poleward (α=180°) in Figure 4. Both cases are calculated for: (a) U_0= 6 cm/s,
(b) U_0= 7.5 cm/s, (c) U_0= 9 cm/s and (d) U_0= 12cm/s. For a equatorward oriented flow component U_0 (α=0°, Fig. 3), the influence of parameters S_g and S_m on the topography is relatively weak for velocities U_0 up to 15 cm/s. For U_0= 6 cm/s, which corresponds to the maximum of S_g in Figure 2a, a slow growth of waves is observed. For U_0= 12cm/s, S_g is negative (Fig. 2a) and therefore existing waves are slowly flattened (Fig. 3d). In Figures 3b and 3c only minor changes occur in amplitude, since S_g is near zero. The small negative values of S_m (Fig. 2b) for all four values of U_0 cause slight upstream migration of sedimentary waves.

For a poleward orientation of U_0 (Fig.s 2a and b; α=180°), S_g and S_m are large and more variable compared to a equatorward orientation. Wave development differs significantly (Fig.s 3 and 4). The wave height decreases in Figures 4a and 4b due to negative values of S_g , while wave crests migrate downstream due to positive values of

S_m. In contrast, in Figures 4c and 4d, the wave height increases associated with an upstream migration due to positive values of S_g and negative values of S_m. Topography changes are most pronounced in the resonance situation.

Figure 5 shows the influence of V_0 on the topography, corresponding to Figures 2c to 2f. For a poleward oriented flow component U_0=7.5 cm/s, which is close to the resonance value, we show examples for eastward flow components (a) V_0=1cm/s (total velocity $U_T \approx$ 7.5 cm/s), (b) V_0= 5 cm/s ($U_T \approx$ 9 cm/s), (c) V_0=10 cm/s ($U_T \approx$12.5 cm/s), as well as westward flow components V_0 with the same absolute values (Figures 5d to f). Figure 5f displays only the first 1.2 Millions years, because the model becomes invalid in some areas due to negative values of Δh (erosion). Erosion also occurs near the resonance frequency.

Due to the linear relationship between S_g and V_0, growth or destruction occurs more rapidly for larger V_0. However, the sign of V_0 determines the character of the topography change (growth or destruction), but migration is independent of V_0 for real k_z (Figures 2d to 2f).

As it can be derived from Figures 3 to 5, the singularity plays an important role in the development of sedimentary waves. It delivers conditions for the rapid change in amplitude of sedimentary waves as well as for their remarkable migration."

One possible mechanism of sedimentary waves creation (frequency analysis)

Based on the assumption that the stationary oscillations of water column particles are responsible for laterally variable velocities in laminar currents we can predict a characteristic accumulation pattern as a result. If the currents are acting over sufficiently long time intervals and the oscillations of the water column can be fixed in space due to topographical features as sea-mounts, ridges or slumps, sedimentary waves can be generated.

To model the quantitative evolution of sedimentary waves in deep sea, we follow Queney (1948) and presume the existence of an elongated (or stretched) obstacle, which can be described by the following equation:

$$z = h\left[1 + \left(x/a\right)^2\right]^{-1}, \qquad (20)$$

where h is the obstacle height and a the half-width.

For simplification we assume that the coordinate system is rotated such that the y–axis and the current component V_0 are oriented parallel to the obstacle crest, and that the x–axis and U_0 are oriented perpendicular to it.

For a description of the velocity perturbation near the obstacle we use the Fourier integral:

$$F(x) = a\int_0^{\infty} f(x,k)\exp(-ak)\,dk, \tag{21}$$

where $f(x,k)$ is an arbitrary integrable function.

We can obtain (20) by substituting f with (3) for $k_x = k$. The corresponding solutions U' (12) for the sinusoidal topography (3) lead to velocity perturbations caused by the obstacle:

$$U'_{obs} = (u'_{obs}, v'_{obs}, w'_{obs}) = a\int_0^{\infty} U'\exp(-ka)dk\,, \tag{22}$$

based on Queney's (1947) investigations.

Following the same approach as in the last paragraph, we can rewrite (15) for the sedimentation rates in the vicinity of an elongated obstacle as:

$$SR_{obs}(x) = -R\,U^2_{total}(x) \sim R\,a\int_0^{\infty}\left[S_g\cos(k_x x) + S_m\cos(k_x x - \pi/2)\right]\cdot\exp(-k\,a)\,dk\,, \tag{23}$$

with S_g and S_m from (16) and (17), respectively.

The integral (23) includes a singularity at the "resonance" frequency $\omega_0 = |f_z|$, if the velocity component U_0 is oriented from the equator to the pole on both hemispheres (i.e. $f_x f_z \geq 0$), which can not be correctly calculated for these cases.

From a detailed analysis of periodicities in (23) we could infer that the general solution reveals up to four different stationary oscillations. The observed velocity field results from a superposition of these oscillations, which are filtered by the obstacle frequency $\omega_{obs} = U_0 a^{-1}$ (Queney, 1948). The main frequencies of these oscillations $\omega_{c,i}$ (i=1..4) can be determined by differentiation of (23) by the frequency ω_0 and the search for positions

of sign change (furtheron abbreviated as PSC) of S_g and S_m. In general, we have four PSCs – two for S_g and two for S_m. However, under certain circumstances, the number of PSCs can be less. This is a case, for example, for $V_0 = 0$ and $f_x = 0$ (Queney, 1948).

To illustrate the influence of the model parameters on the behavior of S_g and S_m as well as on the resulting sedimentation rate, series of numerical experiments for different parameter sets were carried out. First, we will discuss the effect of the obstaclehalfwidth a for a stratified water column with strong and weak stability (Fig. 6). The model parameters are: obstacle crest orientation α=0°, latitude β=-45°, velocity components U_0=10 cm/s, V_0=5 cm/s (obstacle crest is oriented anticlockwise to current). Figures 6a and 6c show the behavior of the growth rate S_g (full line) and of the migration rate S_m (dashed line) as a function of frequency ω_0 (horizontal axis) for water depths of 2000m (strong stability) and 5000m (weak stability), respectively. The vertical dotted lines represent the oscillation frequencies $\omega_{c,i}$. Figures 6b and 6d illustrate the effect of the obstacle filter on the sedimentation rate in the vicinity of obstacles with halfwidths calculated from the condition $\omega_{c,i} = \omega_{obs}$ for strong (2000m) and weak (5000m) stability, respectively. The two frequencies of stationary oscillations corresponding to PSCs of S_g in 6a differ by an order of magnitude. The PSC of S_g at the lower frequency shows quasi-resonance behavior for equatorward oriented U_0. This can be explained by the dominance of the term $\left(N^2 + f_x^2 - f_z^2\right) \cdot \left|2\, f_x f_z\right|^{-1}$ in (11) for $N >> \Omega$. The high frequency is present, although not dominant, if the obstacle is narrow (curve 2; Fig. 6b), but is subdued for wider obstacles (curve 1; Fig. 6b).

In greater water depths with a weakly stratified water column (Fig. 6d) the obstacle halfwidth is far less important for the lateral variation in sedimentation rates, since the frequencies at the PSCs in Figure 6b are nearly of the same order. Differences occur only above the obstacle and vanish with increasing distance in the lee region. The sedimentation rate curve resulting for a halfwidth corresponding to the fourth PSC (second of S_m) is similar to the dashed line and not explicitly shown.

To define, which frequencies are dominating in the sedimentation rate distribution, numerical experiments for different velocities and obstacle shapes must be carried out. We derived from these experiments that the gradient of S_g and S_m in the vicinity of their PSCs is a characteristic parameter for the weight of each frequency.

Figure 7 shows the influence of the obstacle crest orientation on S_g and S_m as well as on the resulting sedimentation rate. The model parameters are: latitude β = -45°, water depth 5000m, obstacle halfwidth 1000 m, velocity components U_0=10 cm/s, V_0=5 cm/s. Figures 7 a-c show S_g (full line) and S_m (dashed line) as a function of the frequency (horizontal axis) for obstacle crest orientations α= 45°, 65° and 85°, respectively. Figures 7 d-f show the sedimentation rate across the obstacle corresponding to cases in Figures 7 a-c.

With increasing α the difference between the PSCs of S_g and S_m decreases. Note that the first PSC of S_g reveals the steepest gradient of all PSCs, and this frequency is most visible in the sedimentation rate curve. In Figure 7a the gradient of S_m at its first PSC is of the same order as the gradient of S_g at its first PSC. The corresponding frequencies differ by a factor of two. As a result, sedimentation rates (Fig. 7d) are reduced due to destructive superposition. For a smaller difference in PSC frequencies (Fig. 7b), we observe a shift in the sedimentation rate maximum (Fig. 7 e). Near the resonance situation (Fig. 7 c) the frequency of the first PSC of S_g dominates. Sedimentation rates (Fig. 7 d) show regular stationary waves with decreasing amplitudes at greater distance.

Resonance occurs for a poleward orientation of U_0 (90°<α<270° or $f_x f_z > 0$) at $\omega_c = |f_z|$. The frequency of at least one of the PSCs of S_g or S_m become identical to resonance frequency. Although it is not possible to calculate sedimentation rates in the resonance case, we can at least predict the dominance of the resonance frequency in the observations.

To simplify the inversion problem and to determine flow velocity from sedimentary wave observations, we can calculate S_g and S_m as a function of the velocity component U_0 for a given wavelength λ, using the following relation:

$$U_0 = \lambda \omega_0 (2\pi)^{-1}, \qquad (24)$$

($\omega_0 = \omega_{c,i}$ in PSCs of functions S_g and S_m).

In general, all six parameters, which affect the behavior of S_g and S_m, cause changes of sedimentation rates in the vicinity of the obstacle. For example, a change in the

relationship between the two velocity components U_0 and V_0 can cause a change in the PSCs location of S_g and S_m as well as a change of their relative weight in the superposition. As a special case at $V_0 = 0,\ f_x = 0,\ N >> \Omega$, two frequencies $\omega_{c,1} = |f_z|$ and $\omega_{c,2} = N$ can be found (Queney, 1948).

The discussion of Blumsack & Weatherly (1989) about optimum wave growth conditions (anticlockwise orientation of sedimentary waves relative to the current direction) for the special case $f_x = 0$ (U_0 parallel to equator) can also be confirmed with our approach. However, for all real situations with different crest orientations and current directions, case $f_x \neq 0$ (U_0 oriented equatorward or poleward) must be considered. Accordingly, the frequency and velocity analysis of the functions S_g and S_m provides an additional tool for the investigation of sedimentary waves and conditions of their creation, which was previously not available.

Comparison to existing models

The first effort to understand oscillatory behavior in the presence of currents/flows was undertaken by Queney (1947, 1948) with application to atmospheric flow using specific physical parameters of air as stability and compressibility. He provided a perturbation theory for flow over a sinusoidal topography, which, however, was simplified by assuming a flow perpendicular to wave crests and treating the Coriolis force as a scalar.

Flood (1988) applied this approach directly to ocean circulation and its impact on sedimentary deposits and related current parameters to sedimentation rates for an explanation of upstream mudwave migration. Blumsack and Weatherly (1989), henceforth referred to as **BW**, allowed an arbitrary current orientation with respect to the wave crests. They modeled the situation at the Project MUDWAVES Site 5 in the Argentine basin to explain the observed sedimentary waves. They identified the importance of the current component parallel to the crest for the growth of sedimentary waves and studied the optimum angle between crest orientation and current direction.

They were applying the same theoretical platform as in this paper, but decided to simplify the set of equations by using the Coriolis parameter instead of the Coriolis vector, which in turn results in slightly less complex definitions from the dispersion relation through the perturbed velocity components (equations 6 to 12).

The simplification to treat Coriolis force as a scalar, however, is only allowed in the case of "strong stability" ($N >> \Omega$), as was pointed out by Queney (1947). A comparison between Ω and Brunt-Vaisala frequency N as a function of the water depth can be found

in LeBlond & Mysak (1978) and is presented in Table 1. The condition of strong stability assumed by previous authors can only be fulfilled for water depths <3000 m. At greater water depth, the perturbed velocity field is sensitive to the sedimentary wave crest orientation and grows with increasing water depth. For example, for the Argentine Basin (latitude ~-45°, water depth >5000 m) both frequencies are of the same order. If the crest orientation (3-D Coriolis vector) will not be taken into account, the error can become large, as can be seen from the curves of S_g and S_m for different crest orientations α in Figures 2a and 2b, which are directly proportional to perturbed velocity components. In this respect, the solution of **BW** should be_modified for the deep sea examples investigated in their paper.

Starting with equation (12) (or equivalent equation (5) of **BW**), different approaches were used to relate observation and model. **BW** applied differential and integral methods to predict the modification of topography and to derive conditions for sedimentary wave growth. The results can be used only for cases, which are sufficiently distant from the singularity point and for velocities $f_z k_x^{-1} < U_0 \leq N k_x^{-1}$. The solutions of **BW** as well as of Flood (1988) were furthermore limited, since they exclusively used an initial sinusoidal topography in their models.

In contrast, in this paper the oscillatory behavior of the perturbed field on the downstream side of an elongated obstacle, which gives the necessary conditions for sedimentary wave creation, was studied. It could be shown that a creating frequency depends on the water depth, geographic position, obstacle width and orientation, current magnitude and orientation.

The phase analysis of sedimentation rates, based on the calculation of perturbed velocity components, allows detailed studies of growth and migration intervals dependent not only on current parameters, but also on the geographic location, crest orientation and water depth, which makes the model representative for any location, where sedimentary waves exist.

We could also avoid the extensive mathematical development of **BW** for the growth and migration conditions and directly use the analytical solutions (equations 16-17) for appropriate parameters. For example, by replacing $k_{z,0}$, $k_{z,1}$, $k_{z,2}$ in (16) and (17) and for the, however in deep sea incorrect, assumption $f_x = 0$, the growth condition for real k_z would be given by $\mathrm{sgn}(U_0 V_0 f_z) > 0$. Also, for $f_x = 0$ migration could only occur upstream, but both upstream and downstream migration of sedimentary waves is possible from our model. These results are equivalent to the results of **BW**, but they do not need the additional differentiation and integration methods as applied by **BW**.

In summary, the characteristics of the presented model and the implications for geophysical and geologic studies are the following:

- The physical model is based on the oscillations, which occur within the water column when a bottom current interferes with a topographic irregularity in its pathway.
- For a steady flow, stationary waves develop behind the obstacle, which reveal a creating frequency depending on water depth, latitude, obstacle width and orientation and current magnitude and direction.
- The resulting regular variations in velocity can influence local sediment accumulation in a way that a regular pattern of depositional maxima and minima evolves, creating mudwaves with a sinusoidal topography.
- Steady conditions can produce sediment structures of considerable thickness, which image continuous growth of mudwaves.
- Depending on current parameters and location, a phase shift between stationary waves and sinusoidal topography can result in migration of the wave crest upstream or downstream of the current.
- The mathematical model, which extends the models of Flood, Weatherly and Blumsack, overcomes most numerical and conceptual deficiencies of previous attempts and further allows to establish direct numerical relationships between current parameters and sedimentary structures, which was not possible from earlier studies.

Field observations in mudwave fields as the data collected in the project MUDWAVES (Flood et. al., 1993 and Manley et al., 1993) provide descriptive parameters of mudwave geometry as wavelength, height and migration direction from seismic lines and the orientation of mudwave crests from swath bathymetry, which can then be directly compared with model calculations to quantify certain characteristics of the flow regime.

Application to field observations

To relate bathymetric and seismic data to the characteristics of the acting bottom currents, we make use of the relationships presented above to estimate the normal-crest velocity component U_0, to derive the orientation of the current flow, and to determine, whether the mudwave topography will be stationary and the observed migration direction is consistent with the model predictions.

To determine the interval of current velocities for a given wavelength and geographic location, for which mudwaves can exist or grow and for which they migrate in the observed direction, the velocity diagram of S_g (16) and S_m (17) has to be analyzed. The

PSCs of these functions deliver the possible value of U_0, by which the sedimentary waves with the observed wavelength should be created. This can be more precisely determined by the comparison of the gradients of functions S_g and S_m in the vicinity of PSCs and by additional calculation of the resulting sedimentation rates from (23).

It should be noted that it is not possible to determine from this approach the velocity component V_0 along the crest. Only if information about the total velocity or current direction is available from other sources (e.g. sedimentologic grain size studies or oceanographic data), it might be possible to estimate V_0, too.

As an example, the presented approach is applied to a survey area visited during the Project MUDWAVES expedition (Site 5: Flood et al., 1993). Two types of mudwaves were observed, one with amplitudes up to 150 m and wavelengths of 6-7 km and the second type of 25-50 m amplitude and 4-5 km wavelength (Table 2).

For the given wave crest orientation, flow velocity vectors in four different quadrants with different signs of U_0 and V_0 are considered. Figures 8 and 9 show the velocity diagrams of Site 5 for functions S_g and S_m, respectively, for different sedimentary wavelengths, which cover the range of observed values. The cases a-d correspond to all four quadrants of possible current directions. The vertical dashed lines represent for each wavelength the velocity corresponding to the resonance frequency. A value of 5 cm/s is chosen for V_0 in all cases.

From a comparison of the four diagrams in Figure 8 and 9, those cases can be selected, where observation and model are consistent. Whereas case a reveals a discrepancy between the observed migration direction and the direction predicted within the existence or growth interval. Cases b to d fulfil the requirements for migration for different velocity intervals.

The presence of the high amplitude sedimentary waves with wavelengths >6 km suggests that the velocity field is close to resonance behavior, which is true for the case b for a poleward direction of U_0. Under optimum conditions for growth of these giant mudwaves the velocity is estimated between 8 cm/s $<U_0<$10 cm/s.

The existence of the smaller sedimentary waves with wavelengths <5000 m as well as the migration direction are not in agreement with these velocity conditions. Instead, for these parameters, optimum velocities range from 4.5 cm/s to 7.5 cm/s for anequatorward velocity component U_0 (case d). Case c is unlikely due to the narrow overlap of growth and migration intervals.

Since two wave types are coexisting and growth conditions are supportive of case b due to high growth rates, we expect conditions as for case d to be present over significant time periods to explain short wave existence.

If a current direction of 270° can be assumed (**BW**, Project MUDWAVES) the total velocity vector can be determined. For case d, V_0 can be estimated between 7 cm/s and 9 cm/s, and the total velocity will range between 8.5 cm/s and 11.5 cm/s. For case b and an assumed current direction of 160° (Project MUDWAVES: regional contour orientation) we predict total velocities between 9 cm/s and 11 cm/s.

Current velocity measurements carried out over a period of one year at Site 5 yielded an average value of 10 cm/s (**BW**), which is in close agreement with the predicted long term average derived from our analysis.

Conclusions

To date, existing theoretical models for the description of sedimentary wave dynamics in water are not taking into account all factors which turn out to be important for the onset and development of deep sea sedimentary waves. These factors are the three-dimensional Coriolis-vector and an arbitrarily oriented initial horizontal velocity vector. The model for the velocity perturbation field over a sinusoidal topography proposed in this paper provides a new solution, which can also be used to relate structural geophysical and geological observations to parameters of the bottom currents as velocity or direction. The main results are:

(1) A space-stationary velocity field oscillation in the lee-zone behind an elongated obstacle represent one possible mechanism for creation of sedimentary waves. A creation frequency can be determined from the frequency or velocity diagram of growth and migration rate and by the calculation of the resulting sedimentation rate from (23). This frequency depends on water depth, latitude, obstacle orientation and current parameters.

(2) The creating frequency can be used for the inversion problem to predict the creating velocity component normal to a wave crest from equation (24).

(3) The coherency of the sinusoidal topography with the sinusoidal velocity perturbation field can be studied from equation (16) to identify velocity intervals for growth or destruction of sedimentary waves.

(4) A migration direction of sedimentary waves can be predicted from equation (17) and can be compared to observations to constrain the current direction.

(5) An overlap of growth and migration intervals for a given wave location allows to define from the velocity diagram the interval for the velocity component U_0, which would provide optimum conditions for existence and/or growth sedimentary waves.

However, it is not possible to determine the magnitude of the velocity component V_0 along wave crests, because it does not directly affect the fluid perturbations over the sedimentary wave topography.

A comparison with field data from Project MUDWAVES leads to a striking consistency of modeling results and observations, which will be used in future studies to derive information about deep water paleocurrents from structural, namely seismic and sediment echosounder studies in current controlled environments.

Acknowledgements

This research was funded by the Senator für Bildung und Wissenschaft der Hansestadt Bremen and the Deutsche Forschungsgemeinschaft. This publication is contribution no. 318 of the Special Research Project 261: The South Atlantic in the Late Quaternary.

We want to thank L. Zühlsdorff, H. von Lom, A. Macario, Christoph and David Völker for reviewing this manuscript and providing helpful advice.

References:

Blumsack, S.L., Weatherly, G.L., 1989. Observations and growth mechanisms for mudwaves. Deep-sea Research, vol. 36, 1327-1339.

Blumsack, S.L., 1993. A model for the growth of mudwaves in the presence of time varying currents. Deep-sea Research II, vol. 40, N 4/5, 963-974.

Brooke, B.T., 1959. Shearing flow over a wavy boundary. Journal of Fluid Mechanics 6, 161-205.

Damuth, J.E., 1979. Migrating sediment waves created by turbidity current in the northern South China Basin. Geology 7, 520-523.

Flood, R.D., 1988. A lee-wave model for deep-sea mudwave activity. Deep-sea Research 35, 973-983.

Flood, R.D., Shor, A.N., 1988. Mudwaves in the Argentine Basin and their relationship to the regional bottom circulation patterns. Deep-sea Research 35, 943-971.

Flood, R.D., Shor, A.N., Manley, P.L., 1993. Morphology of abyssal mudwaves at Project "MUDWAVES" Sites in the Argentine Basin. Deep-sea Research II, vol. 40, N 4/5, 859-888.

Fox, P.J., Heezen, B.C., Harian, A.M., 1968. Abyssal antidunes. Nature 220, 470-472.

Fredsoe, J., 1964. On the development of dunes in erodible channels. Journal of Fluid Mechanics 64, 1-16.

Garrett C.J.R., Munk, W.H., 1972. Space-time scales of internal waves. Geophysical Fluid Dynamics 3, 225-264.

Hand, B.M., 1974. Supercritical flow in density currents. Journal of Sedimentary Petrology 44, 637-648.

Hollister, C.D., Flood, R.D., Johnson, D.A., Londsale, P.F., Southard, J.B., 1974. Abyssal furrows and hyperbolic echo traces on the Bahama Outer Ridge. Geology 2, 395-400.

Holton, J.R., 1992. An introduction to dynamic meteorology. Third edition. Acad. Press: San Diego, 511pp.

Jacobi, R.D., Rabinowitz, P.D., Embley, R.W., 1975. Sediment waves on the Moroccan Continental Rise. Marine Geology 19, M61-M67.

Kennedy, J.F., 1963. The Mechanics of dunes and antidunes in erodible-bed channels. Journal of Fluid Mechanics 16, 521-544.

Kennedy, J.F., 1969. The formation of sediment ripples, dunes and antidunes. Annual Reviews of Fluid Mechanics, vol.1, 147-168.

Kolla, V., Eittreim, S., Sullivan, L., Kostecki, J.A., Burckle, L.H., 1980. Current-controlled, abyssal microtopography and sedimentation in Mozambique Basin, south-west Indian Ocean. Marine Geology 34, 171-206.

LeBlond, P.H., Mysak, L.A., 1978. Waves in the Ocean. Elsevier oceanography series, Elsevier scientific Publishing Company, New Jork, 602 pp.

Manley, P.L., Flood, R.D., 1993. Project "MUDWAVES". Deep-sea Research II, vol. 40, N 4/5, 1033-1055.

Manley, P.L., Flood, R.D., 1993. Paleoflow history determined from mudwave migration. Argentine Basin. Deep-sea Research II, vol. 40, N 4/5, 1033-1055.

McCave, I.N., Swift, S.A., 1976. A physical model for the rate of deposition of fine grained sediments the deep sea. Bulletin of the Geophysical Society of America 87, 541-546.

Normark, W.R., Hess, G.R., Stow, D.A.V., Bowen, A.J., 1980. Sediment waves on the Monterey Fan levees: a preliminary physical interpretation. Marine Geology 37, 1-18.

Queney, P., 1947. Theory of perturbations in stratified currents with applications to air flow over mountain barriers. Miscellaneous Reports of the Department of Meteorology of Chicago, N. 23, 81 pp.

Queney, P., 1948. The problem of air flow over mountains: a summary of theoretical studies. Bulletin of the American Meteorological Society 29, 16-26.

Reynolds, A.J., 1965. Waves on the erodible bed of an open channel. Journal of Fluid Mechanics 22, p.1, 113-133.

Roberts, D.G., Kidd, R.B., 1979. Abyssal sediment wave fields on Feni Ridge, Rockall Trough: long-range sonar studies. Marine Geology 33, 175-191.

Weatherly, G.L., 1993. On deep-current and hydrographic observations from the high mesoscale variability region and from a mudwave region in the Argentine Basin. Deep-Sea Research II, vol. 40, 939-961.

Table captions

Table 1. Comparison between Earth's angular velocity Ω and Brunt-Vaisala frequency N dependent of the water depth from (7) (all values messed in rad/s).

Table 2. Parameters for mudwave geometry required for modeling from Site 5 investigated during the Project MUDWAVES expedition (Flood et al., 1993).

Tables

Table 1 : Comparison between Earth's angular velocity Ω and Brunt-Vaisala frequency N

Ω	N (2000 m)	N (3000 m)	N (4000 m)	N (5000 m)	N (6000 m)
7.27×10^{-5}	1.31×10^{-3}	6.07×10^{-4}	2.8×10^{-4}	1.3×10^{-4}	6.03×10^{-5}

Table 2: Parameters of mudwave geometry for Site 5 of Project MUDWAVES

Site	Latitud	Longitud	Water Depth	Curren directio	Crest-Direction	Wave-Length	Migrati directio	Height
5	42°30'S	45°05'W	5050m	270°	55°	6-7km	145°	150m
					55°	4-5km	145°	25-50m

Figure captions

Fig. 1. Cartesian coordinate system and vector components of current fixed to the orientation of sedimentary wave crests (x, U_0: perpendicular to wave crest; y, V_0: parallel to wave crest; z: vertical upwards; α: angle between x and geographic North).

Fig. 2. Growth and migration rates S_g and S_m for different crest orientations (a-b) and different signs and magnitudes of V_0 (c-f), as a function of the velocity component U_0 normal to the wave crest. Model parameters: latitude β =–45°; water depth D=5000 m; wavelength λ=5000 m; V_0=+5 cm/s for (a,b) and α=180° for (c – f).

Fig. 3. Synthetic cross sections of isochrones in mudwave deposits illustrating the sedimentation over a period of two millions years on a sinusoidal topography for different magnitudes of U_0 and an equatorward directed current ($\alpha = 0°$): a) U_0= 6 cm/s, slow growth ~8% of amplitude change; b) U_0=7.5 cm/s and c) U_0=9 cm/s, minor change in amplitude;

d) U_0=12 cm/s, slow destruction (~8%). All cases reveal slow upstream migration. Model parameters: latitude β =–45°; water depth D=5000 m; wavelength λ=5000 m; V_0=+5 cm/s; crest orientation $\alpha = 0°$. The dotted lines connect the apices at different times, indicating the apparent migration trend from comparison to the vertical dashed line.

Fig. 4. Synthetic cross sections of isochrones in mudwave deposits illustrating the sedimentation over a period of two millions years on a sinusoidal topography for different magnitudes of U_0 and a poleward directed current ($\alpha = 180°$): a) U_0= 6 cm/s, slow destruction (~15%) and slow downstream migration; b) U_0= 7.5 cm/s, rapid destruction (~200%) and rapid downstream migration; c) U_0= 9 cm/s, rapid growth (~270%) and rapid upstream migration; d) U_0= 12cm/s slow growth (~5%) and slow upstream migration. Model parameters were chosen as in figure 4.

Fig. 5. Synthetic cross sections of isochrones in mudwave deposits illustrating the sedimentation over a period of two millions years on a sinusoidal topography for varying

values of V_0: (a) V_0= 1 cm/s; (b) V_0= 5 cm/s; (c) V_0= 10 cm/s; (d) V_0= -1 cm/s; (e) V_0= -5 cm/s; (f) V_0= -10 cm/s. Model parameters: latitude β =–45°; water depth D=5000 m; wavelength λ=5000 m; poleward directed ($\alpha = 180°$) U_0=7,5 cm/s.

Fig. 6. Frequency diagram of growth rate S_g (full line), migration rate S_m (dashed line) and the resulting sedimentation rate for different obstacle halfwidths corresponding to creating frequencies. a) and b) show the situation for a stratified fluid with strong stability (water depth 2000m), c) and d) for a stratified fluid with weak stability (water depth 5000 m). Model parameters: obstacle crest orientation α=0°, latitude β=-45°, velocity components U_0=10 cm/s, V_0 =5 cm/s. Vertical dashed lines in (a) and (c) correspond to PSCs.

Fig. 7. Frequency diagram of growth rate S_g (full line) and migration rate S_m (dashed line)

(a - c) and the resulting sedimentation rate over an elongated obstacle for different crest orientations: α=45° (a and d), α=65° (b and e) and α=85° (c and f). Model parameters: water depth D=5000 m, latitude β=-45°, velocity components U_0=10 cm/s, V_0 =5 cm/s, halfwidth 1000 m.

Fig. 8. Velocity diagram of growth rate S_g for Site 5 of Project MUDWAVES (Flood et al., 1993) for four different wavelengths coexisting in modeled area. Four different current directions are modeled: (a) U_0: 145°, V_0: 235°; (b) U_0: 145°, V_0: 55°; (c) U_0: 325°, V_0: 55°; (d) U_0: 325°, V_0: 235°. Model parameters: latitude β =–42.5°; water depth D=5050 m; V_0=+5 cm/s. Vertical dashed lines show velocities corresponding to the resonance situation. e) orientation of current vector components (fixed V_0, variable U_0 and U_T) for cases a to d, crest orientation (55°) and observed migration direction (145°).

Fig. 9. Velocity diagram of migration rate S_m for Site 5 of Project MUDWAVES (Flood et al., 1993). Vector component orientation according to Figure 8e. All parameters correspond to Figure 8.

Figure 1

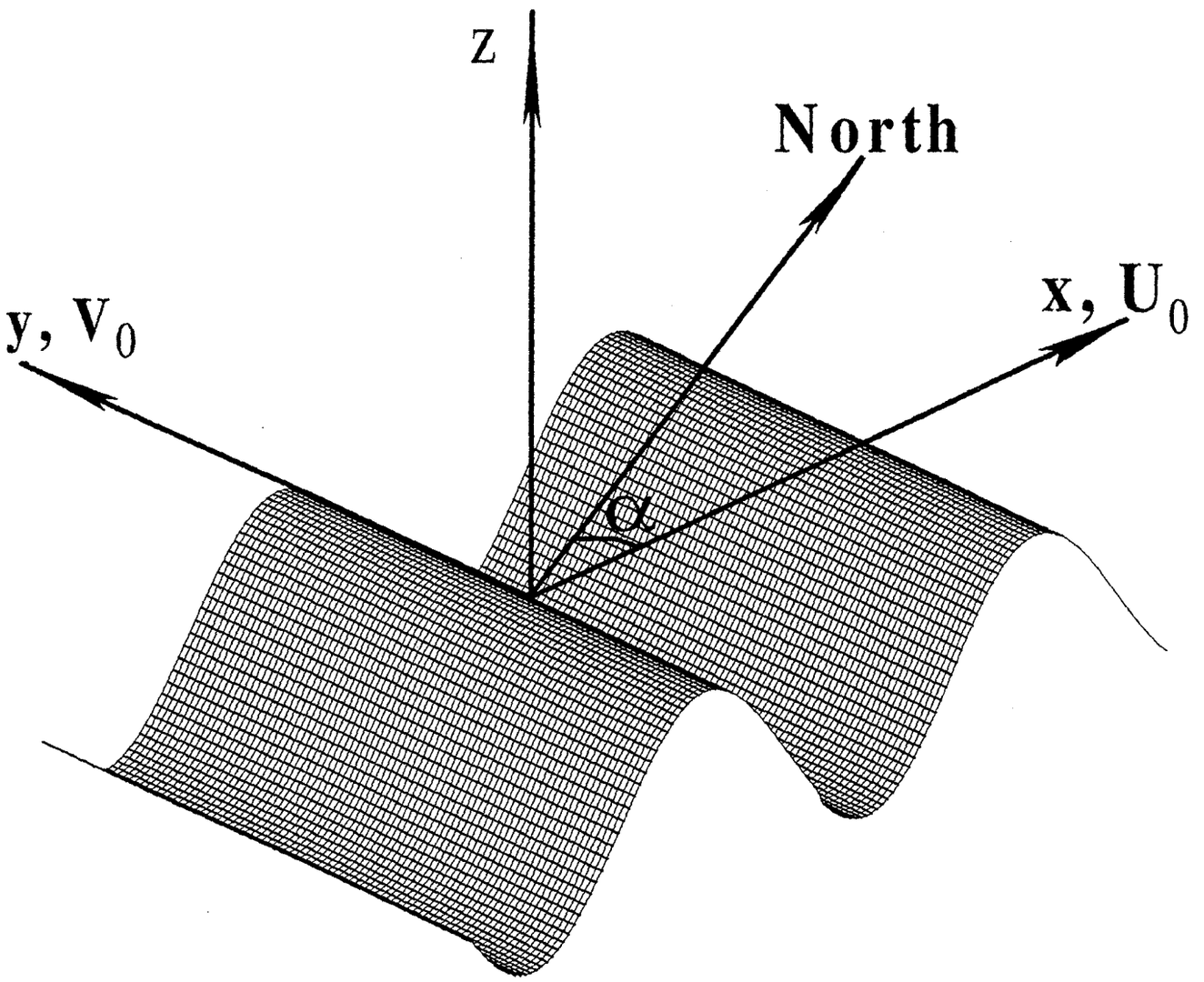

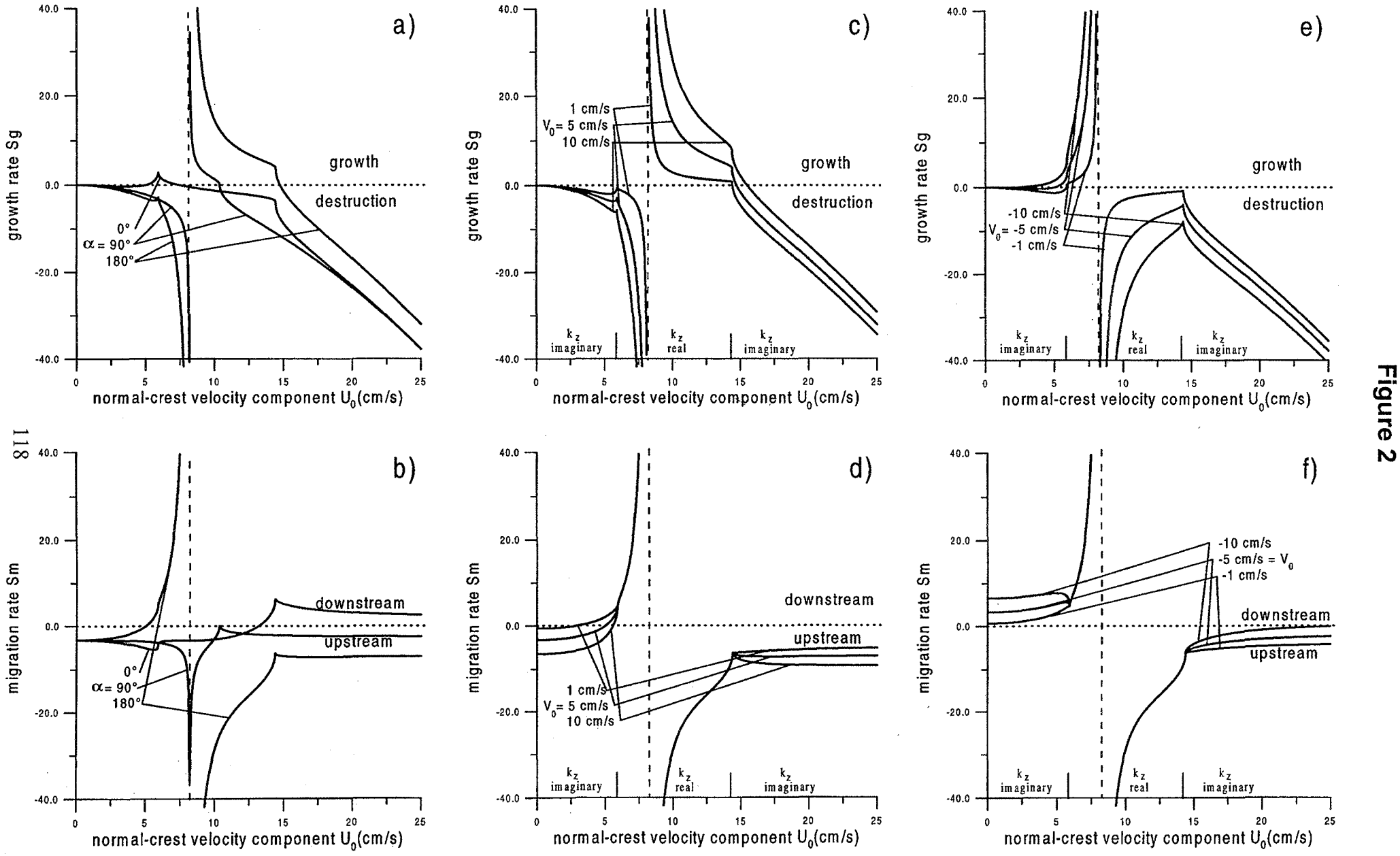
a)
b)
c)
d)
e)
f)
growth rate Sg
migration rate Sm
normal-crest velocity component U_0(cm/s)
growth
destruction
downstream
upstream
0°
α = 90°
180°
1 cm/s
V_0 = 5 cm/s
10 cm/s
-10 cm/s
V_0 = -5 cm/s
-1 cm/s
-5 cm/s = V_0
k_z imaginary
k_z real
k_z imaginary

Figure 2

Figure 3

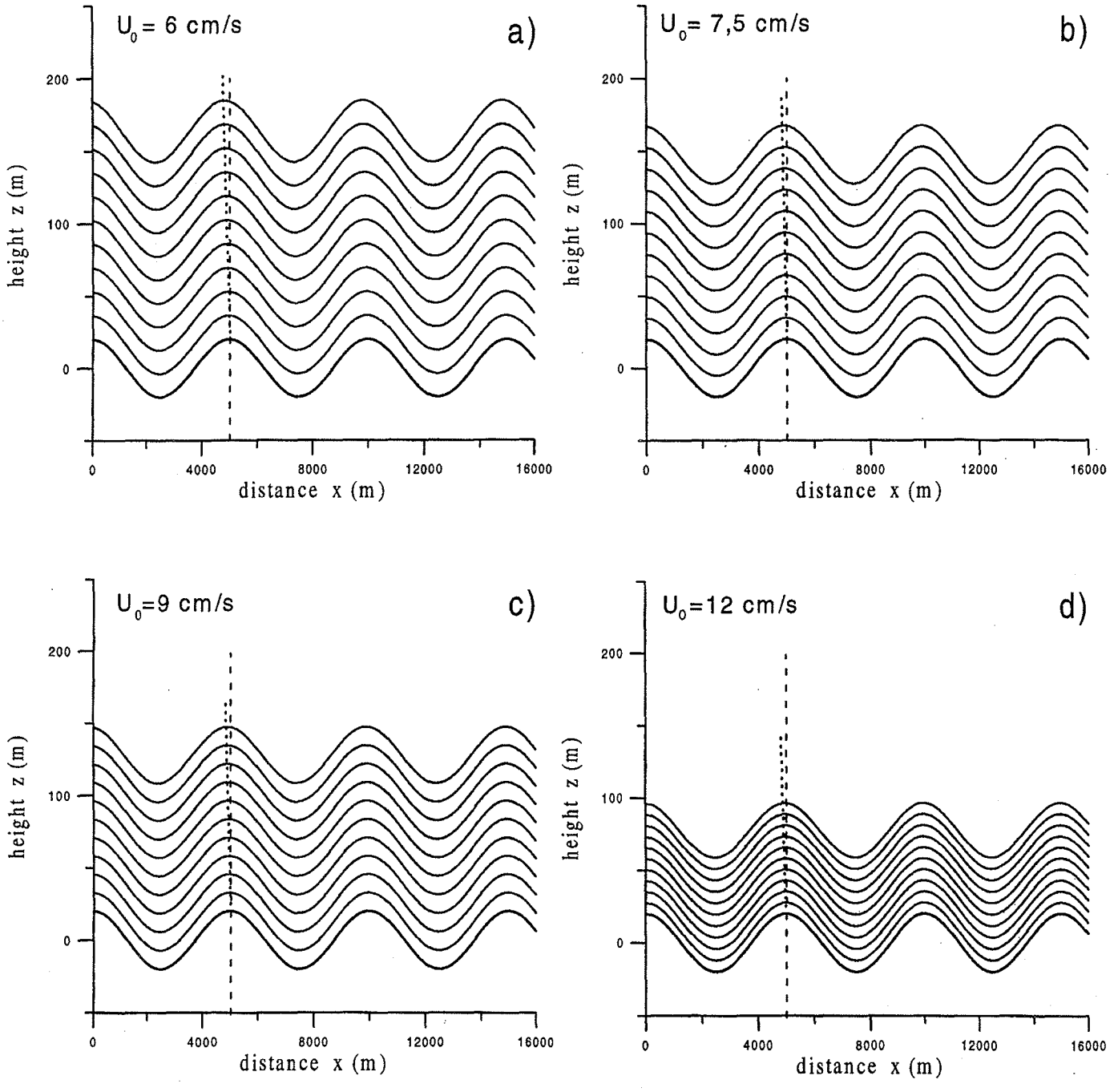
U0 = 6 cm/s
a)
U0= 7,5 cm/s
b)
U0=9 cm/s
c)
U0=12 cm/s
d)
height z (m)
distance x (m)
0
100
200
4000
8000
12000
16000

Figure 4

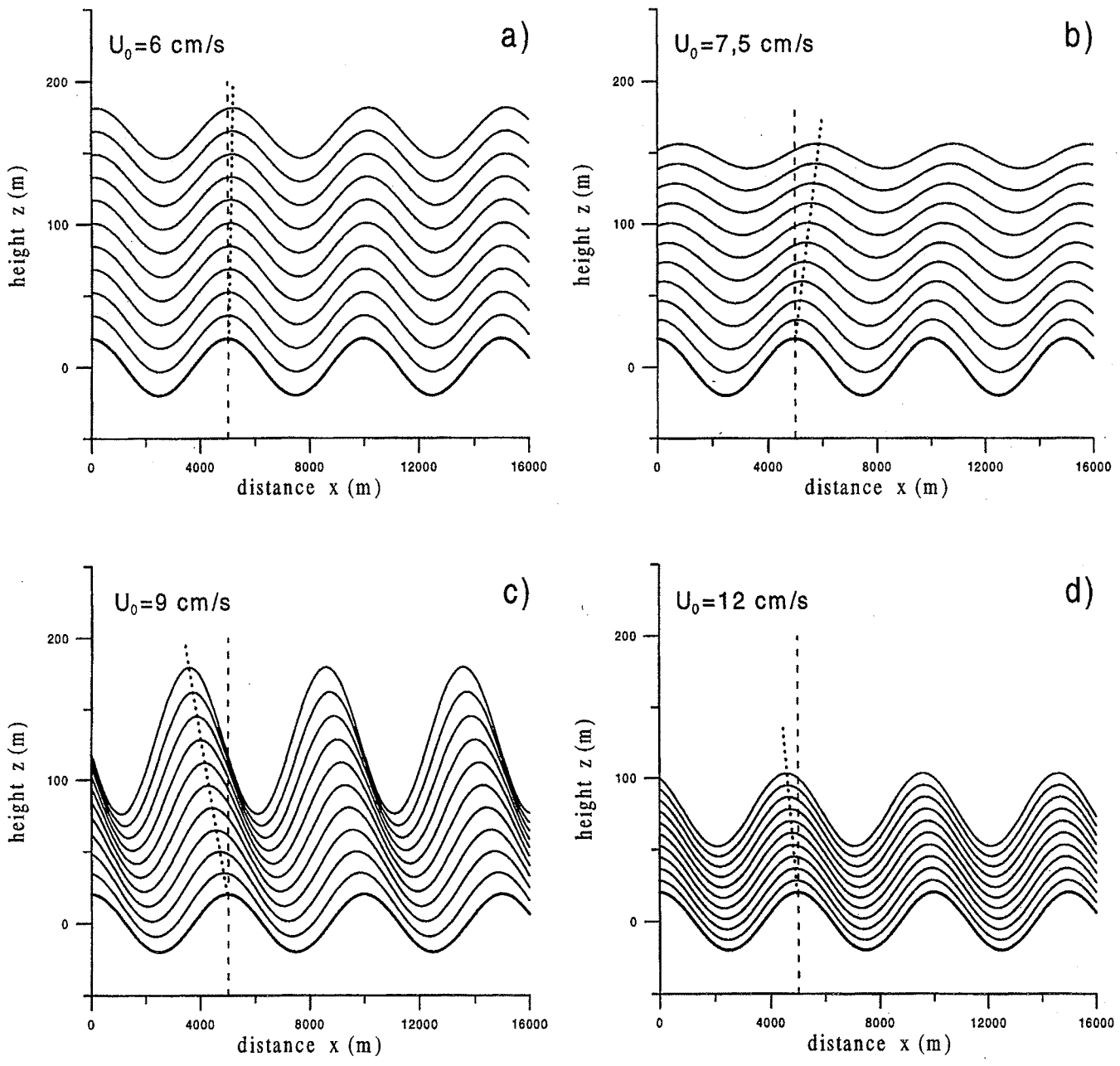
U0=6 cm/s
a)
U0=7,5 cm/s
b)
U0=9 cm/s
c)
U0=12 cm/s
d)
height z (m)
distance x (m)
0
100
200
4000
8000
12000
16000

Figure 5

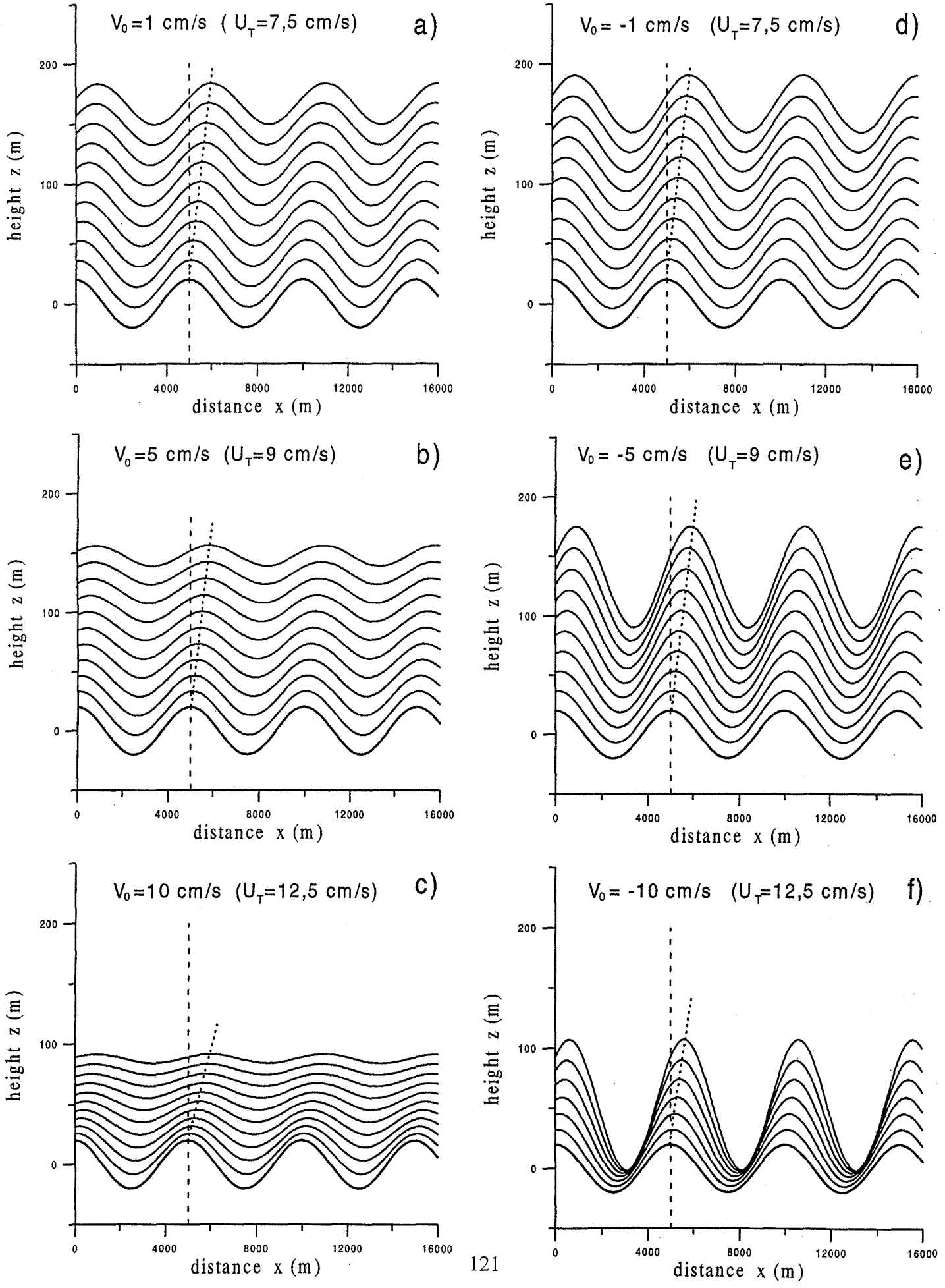
V_0=1 cm/s (U_T=7,5 cm/s)
a)
V_0= -1 cm/s (U_T=7,5 cm/s)
d)
V_0=5 cm/s (U_T=9 cm/s)
b)
V_0= -5 cm/s (U_T=9 cm/s)
e)
V_0=10 cm/s (U_T=12,5 cm/s)
c)
V_0= -10 cm/s (U_T=12,5 cm/s)
f)
height z (m)
distance x (m)
0
100
200
4000
8000
12000
16000

Figure 6

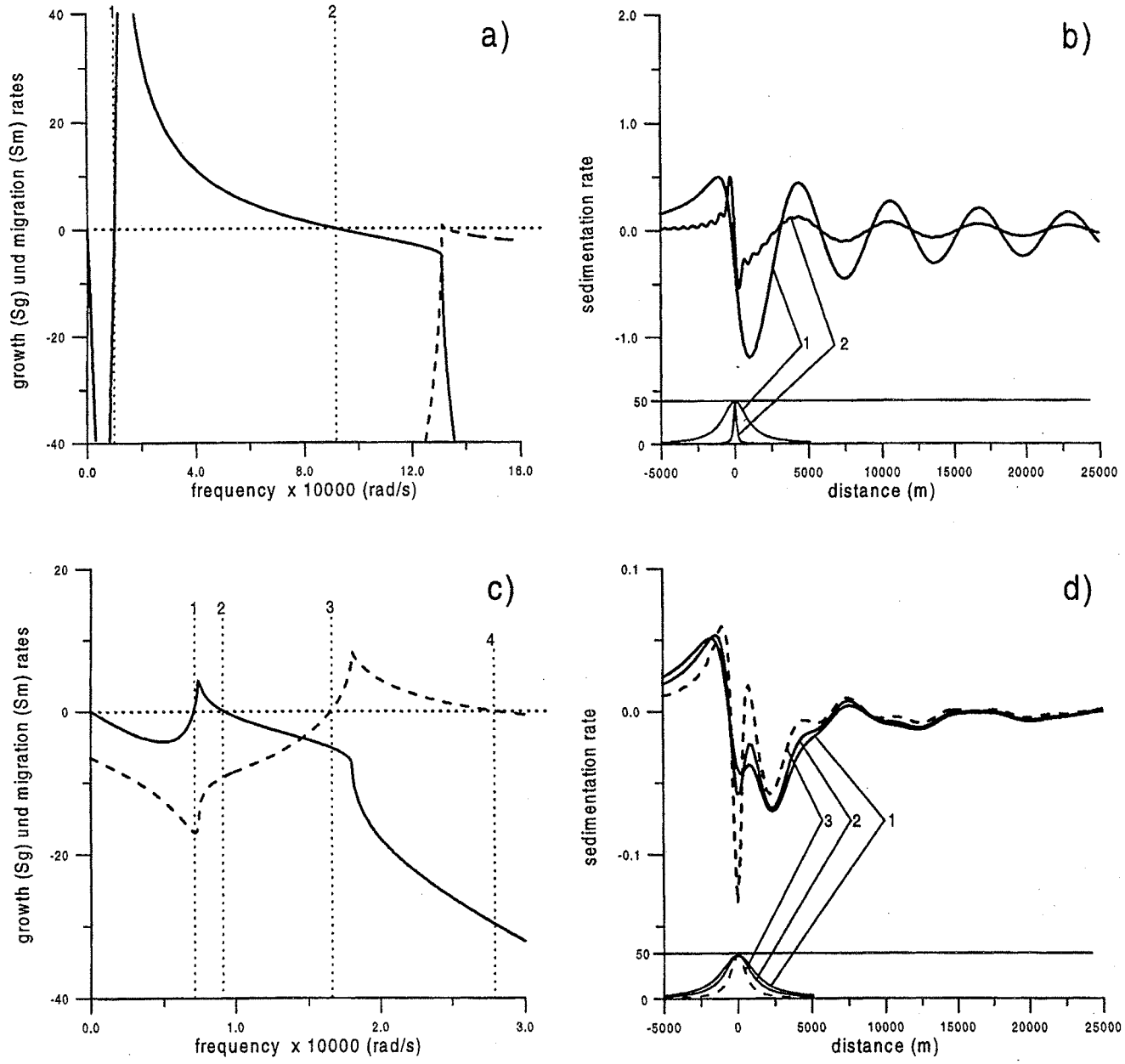
a)
b)
c)
d)
growth (Sg) und migration (Sm) rates
frequency x 10000 (rad/s)
sedimentation rate
distance (m)
1
2
3
4

Figure 7

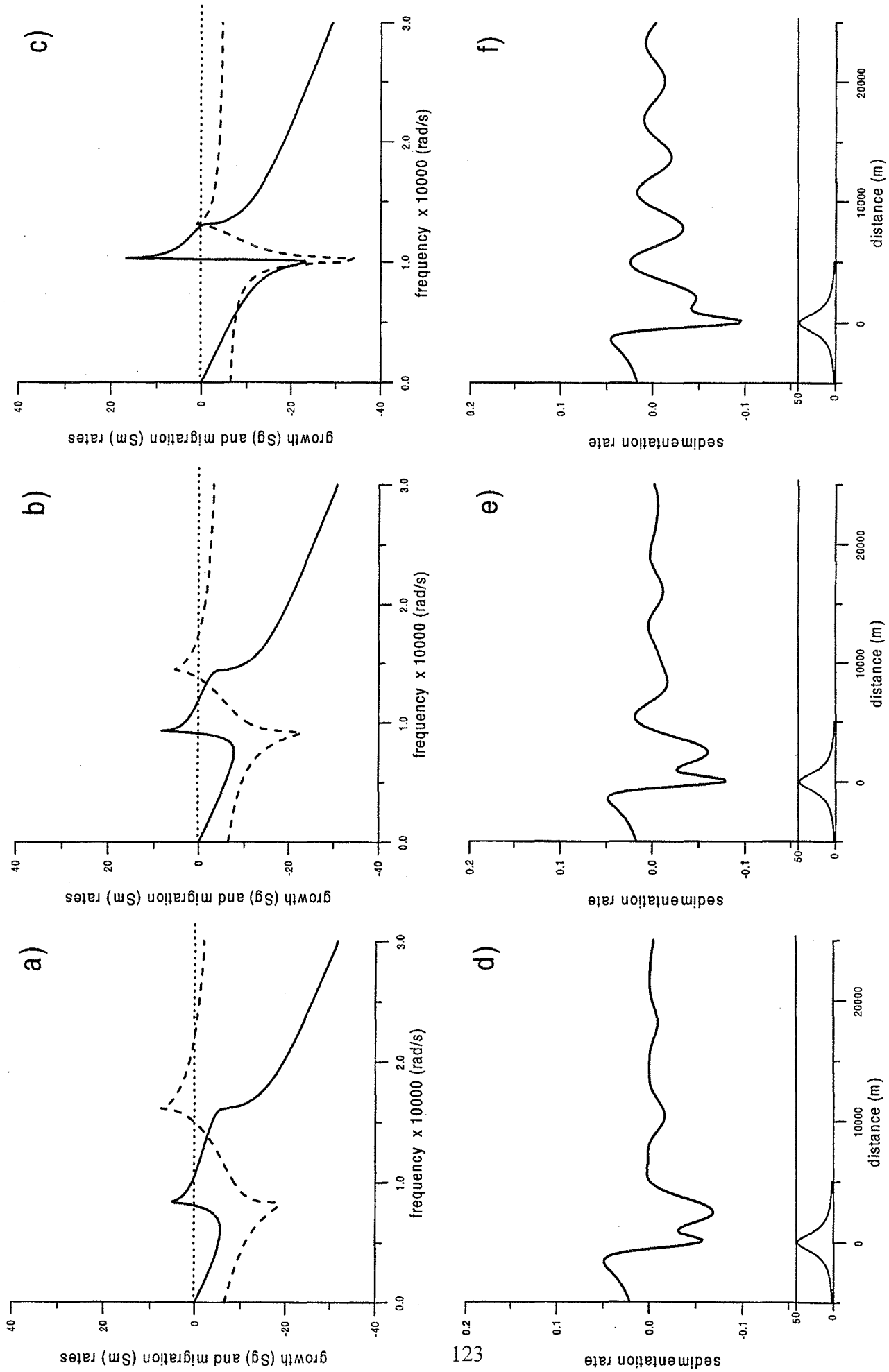
a)
b)
c)
d)
e)
f)
growth (Sg) and migration (Sm) rates
frequency x 10000 (rad/s)
sedimentation rate
distance (m)

Figure 8

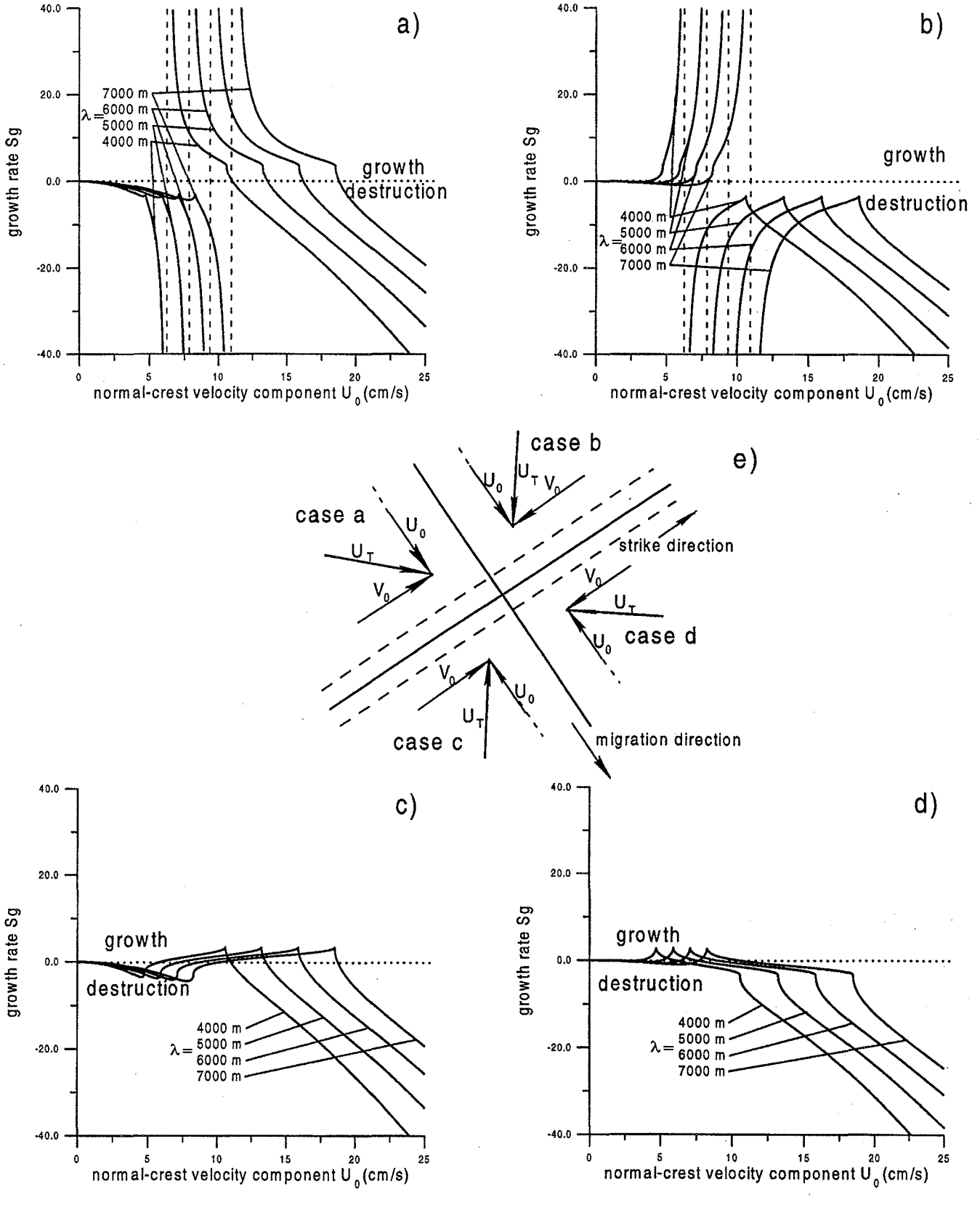
a)
b)
c)
d)
e)
growth rate Sg
normal-crest velocity component U_0 (cm/s)
growth
destruction
λ = 7000 m
6000 m
5000 m
4000 m
case a
case b
case c
case d
U_0
U_T
V_0
strike direction
migration direction

Figure 9

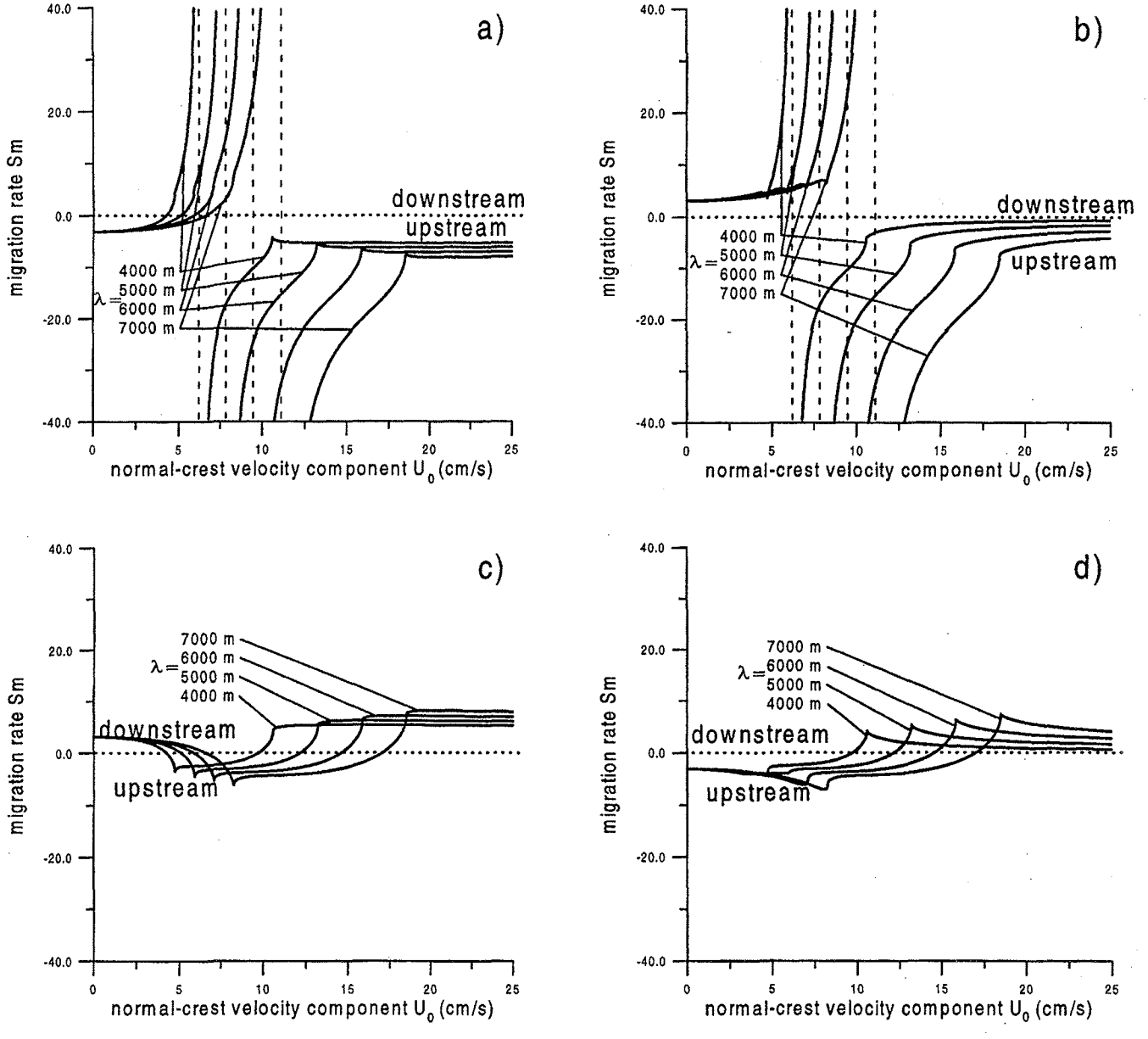
a)
b)
c)
d)
migration rate Sm
normal-crest velocity component U_0 (cm/s)
downstream
upstream
λ=
4000 m
5000 m
6000 m
7000 m
40.0
20.0
0.0
-20.0
-40.0
0
5
10
15
20
25